1970

Structural, magnetic, and spectroscopic study of nickel squarate dihydrate

Michael Habenschuss
Iowa State University

Structural, magnetic, and spectroscopic study of nickel squarate dihydrate

by

Michael Habenschuss

A Dissertation Submitted to the
Graduate Faculty in Partial Fulfillment of
The Requirements for the Degree of
DOCTOR OF PHILOSOPHY

Major Subject: Physical Chemistry

Approved:

Signature was redacted for privacy.

In Charge of Major Work

Signature was redacted for privacy.

Head of Major Department

Signature was redacted for privacy.

Dean of Graduate College

Iowa State University
Ames, Iowa

1970

TABLE OF CONTENTS

LIST OF FIGURES

LIST OF TABLES

INTRODUCTION

Part of the work of Physical and Inorganic Chemistry Group VI has been concerned in recent years with investigating and testing models of magnetic exchange and superexchange. Systems in which magnetic ions interact one-dimensionally most simply test these models. Magnetically one-dimensional systems which have been investigated in this group are $CsCuCl_3$ (Rioux 1969, 1970), $(CH_3)_2NH_2CuCl_3$ and $(CH_3)_4NNiCl_3$ (Gehring, 1969), $CsNiCl_3$ (Smith, Gerstein, Liu and Stucky, 1970) and $KCuCl_3$ (Maass, Gerstein and Willet, 1967, Maass, 1969). All these compounds except $(CH_3)_4NNiCl_3$ appear to exhibit antiferromagnetic, predominantly one-dimensional magnetic interactions. In $(CH_3)_4NNiCl_3$ the magnetic behavior appeared to deviate ferromagnetically from Curie-Weiss behavior.

The impetus for this work on nickel squarate dihydrate came originally from the fact that its structure was proposed to consist of linear chains of Ni^{++} ions linked together by squarate ions (West and Niu,1963a; see Figure 4(b)). The π system of the squarate ion (West and Powell, 1963) was considered to be a likely path for antiferromagnetic superexchange (Anderson, 1963) between neighboring Ni^{++} ions. Although preliminary magnetic susceptibility measurements by Smentowski and

Gerstein[1] gave some evidence of such behavior, those results were found to be in error due to thermal inequilibrium in the sample. It was therefore decided to determine the actual structure of nickel squarate dihydrate and to remeasure the susceptibility of the compound to better define its low and high temperature behavior.

A low temperature peak found in the susceptibility[1] at 1.6°K indicated magnetic ordering at that temperature, and that the magnetic interactions are weak. An ensemble of weakly interacting spin 1 systems is of interest because such systems may order antiferromagnetically with the spins aligned (as is the usual case) or polarized (Mullin, et al., 1966). In the polarized case, the neutron diffraction pattern for the ordered state would be expected to be completely different from that in the aligned, ordered state (Good,[2] private communication), and if detected, such a pattern would be a completely new phenomenon to studies in cooperative magnetism.

In addition to the interest in one dimensionally interacting magnetic systems, and in weakly interacting spin

---

[1]Smentowski, F. J., Department of Chemistry, Texas A&M University, College Station, Texas; and B. C. Gerstein, Department of Chemistry, Iowa State University of Science and Technology, Ames, Iowa. Unpublished susceptibility data for Mn(II), Fe(II), Co(II) and Ni(II) squarates. Private communication. 1968.

[2]Good, R. H. Jr., Department of Physics, Iowa State University, Ames, Iowa. Private communication. 1968.

l systems, magnetic exchange in $NiC_4O_4 \cdot 2H_2O$ is intriguing because of the chemical information inferred from the parameters describing the susceptibility of 3d transition metal ions coordinated with the unique $C_4O_4^{=}$ resonance stabilized ligand. While a substantial amount of structural work has been done on the 3d transition metal croconate ($C_5O_5^{-2}$) complexes none has been done on the 3d transition metal squarate ($C_4O_4^{-2}$) complexes because of the difficulty of obtaining single crystals large enough for single crystal X-ray structure determination. The present work was initiated to elucidate the structure of such complexes, and to glean as much chemical and physical information as possible from the magnetic and spectroscopic behavior of $NiC_4O_4 \cdot 2H_2O$, a representative member of the $M\ C_4O_4 \cdot 2H_2O$ series.

LITERATURE SURVEY

The literature survey will be primarily concerned with studies on squaric acid and croconic acid and their salts with various metal ions. Special emphasis will be placed on structural studies on the metal salts to date, and the geometry of the croconate and squarate ions in these compounds.

The compound diketocyclobutenediol ("squaric acid"),[1] $C_4O_4H_2$ was first synthesized by Cohen, Lacher, and Park (1959). They found it to be a strong acid. They proposed that the anion of squaric acid, $C_4O_4^{-2}$, has resonance stabilization with a symmetrical D_{4h} structure as indicated in Figure 1. From the fact that the potassium salt of squaric acid showed no sharp C=O absorption near 1700cm^{-1}, but showed a broad intense band centered at 1500cm^{-1}, which is within the accepted range of C-O stretching frequencies for carboxylic acid anions, they concluded that the C-O bond in the squarate ion is more like a carbon oxygen bond in a carboxylic acid anion, $[R\text{-}C\lesssim^{O}_{O}]^-$ than a ketonic C=O bond, substantiating their proposal for resonance stabilization in the anion of squaric acid.

---

[1]The terms "squaric acid" and "squarate ion" for diketocyclobutenediol and its dianion were first used by Park, Cohen, and Lacher (1962) and have been adopted by others (West and Niu, 1963a).

Following the suggestion of π-electron delocalization in the croconate ion, $C_5O_5^{-2}$, by Yamada, Mizuno and Hirata (1958), West, Niu, Powell and Evans (1960) measured the Raman spectrum of dilithium croconate, finding two polarized and three depolarized lines in agreement with D_{5h} symmetry for the croconate anion. They also measured the IR spectra of the croconate ion and the rhodizonate anion, $C_6O_6^{-2}$, obtained from rhodizonic acid $H_2C_6O_6$. Neither spectrum showed an absorption in the usual C=O absorption region at 1700cm^{-1}, but, similar to the squarate ion, exhibited broad bands centered at 1570cm^{-1} and 1500cm^{-1}, respectively. They therefore postulated that the three ions $C_4O_4^{-2}$, $C_5O_5^{-2}$, and $C_6O_6^{-2}$ belonged to a new class of monocyclic aromatic anions, $C_nO_n^{-2}$, with the highly symmetric structures demanded by π-electron delocalization. Subsequently West and Niu (1962) prepared the $C_6O_6^{-4}$ anion from tetrahydroxyquinone, and found that the ring configuration in this ion is the chair form with D_{3d} symmetry.

Ito and West (1963) have measured the IR and Raman spectra of the $C_4O_4^{-2}$ and $C_5O_5^{-2}$ ions. Raman spectra were obtained from the potassium salts of the anions in the solid state and from aqueous solutions of the potassium salts. A normal coordinate analysis on the basis of D_{4h} and D_{5h} symmetries allowed assignment of the observed absorption frequencies and a least squares fit yielded force constants

in agreement with the idea of resonance stabilization in the two ions.

West and Powell (1963) have made Hückel LCAO-MO calculations for the π-electron systems of the monocyclic anions $C_nO_n^{-2}$, n=3 to 8, and $C_6O_6^{-4}$, and numerous other polycyclic anions consisting to a large extent, or completely, of oxocarbon groups, many of which are not yet known. The results for the monocyclic anions indicated that the delocalization energy per π-electron decreases sharply for the $C_nO_n^{-2}$ series in going from n=3 to n=4, and slowly with increasing ring size therafter. Carbon-carbon bond orders decrease and carbon-oxygen bond orders increase with increasing ring size. These trends agree with the trends in the force constants derived from a fit to the experimentally observed vibrational absorptions via a normal coordinate analysis for squarate and croconate ions (Ito and West, 1963). In every case the calculated energy levels (in the Hückel approximation) of the π-electron systems have a nondegenerate level, doubly occupied, as the highest occupied level, and a doubly degenerate level as the lowest unoccupied energy level. The energy difference between these two levels decreases with increasing ring size. This is in qualitative agreement with observed spectral transitions in the ions $C_4O_4^{-2}$, 2500Å; $C_5O_5^{-2}$, 3630Å; and $C_6O_6^{-2}$, 4840Å.

In Figure 1 the proposed structures for the squarate,

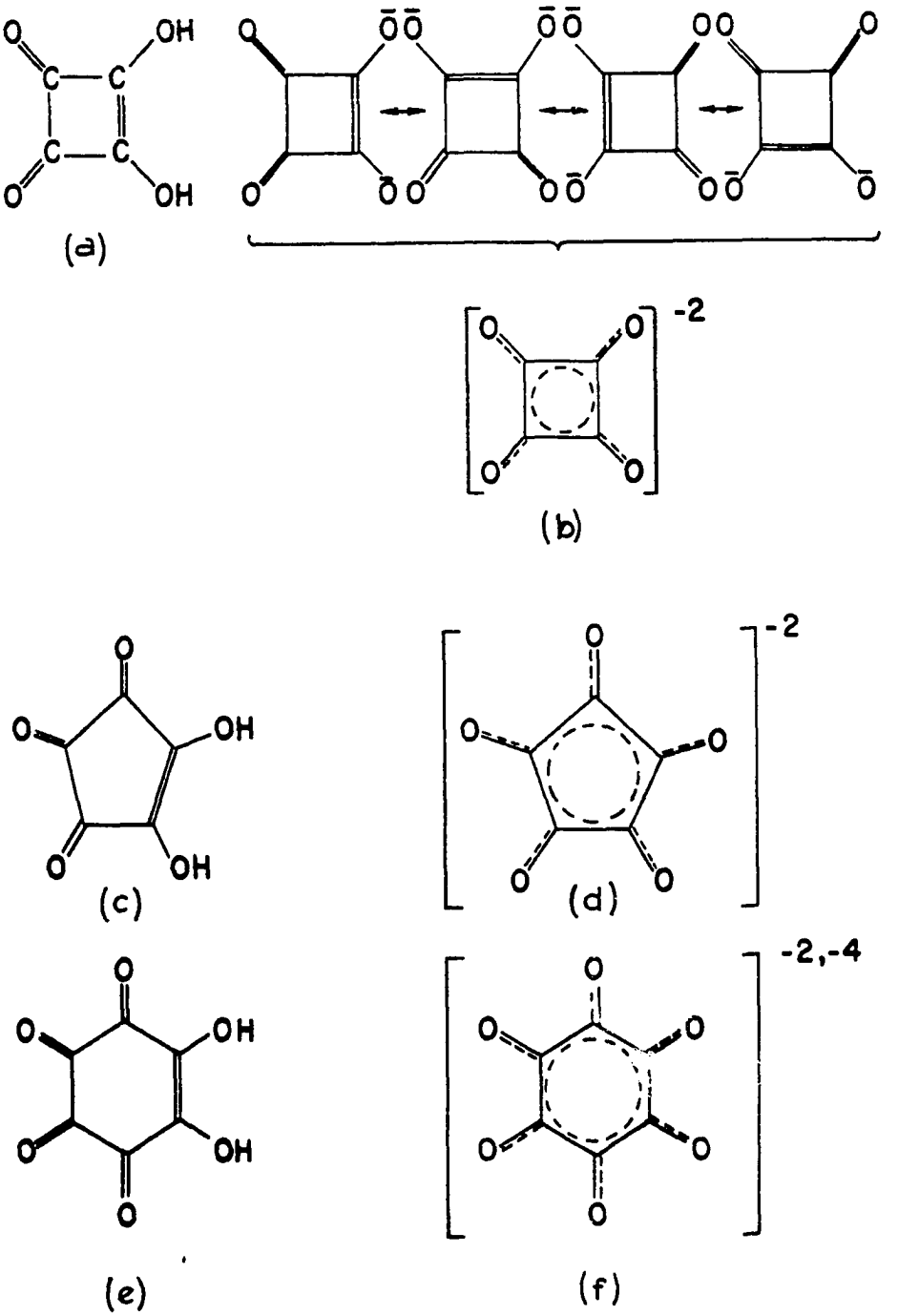

Figure 1. Simple oxocarbon cyclic anions and their parent acids ((a) squaric acid; (b) squarate anion; (c) croconic acid; (d) croconate ion; (e) rhodizonic acid; (f) rhodizonate ion)

croconate and rhodizonate anions and their parent acids are given. Four equivalent valence bond structures are given for the squarate ion to illustrate the possibility of resonance.

West and Niu (1963b) have prepared and characterized complexes of the croconate ion with the divalent ions of Ca, Mn, Fe, Co, Ni, Cu and Zn and the trivalent ions of Al, Cr and Fe. The divalent metal complexes have the general formula $MC_5O_5 \cdot 3H_2O$. All the divalent metal complexes had the same Debye-Scherer x-ray powder pattern, differing only slightly in corresponding d-values, indicating that they all had essentially the same structure. The exception is Ca croconate which had a different powder pattern. The IR spectra of the metal complexes are all similar and showed a band at 1725cm^{-1} which could be assigned as a typical C=O double bond stretching frequency. A very strong broad band from 1300 to 1700cm^{-1} is assigned to a mixture of C-O and C-C stretching modes. Further weak bands were observed at 1230, 1100, 900 and 800cm^{-1}. Gouy measurements of the magnetic susceptibilities at room temperatures showed that all the divalent transition metal complexes are high spin complexes.

The three trivalent metal complexes showed a somewhat variable stoichiometry and include hydroxyl groups as well as water molecules, with probable general formula

$M_5(C_5O_5)_4(OH)_7(H_2O)_{16}$. The three complexes have the same x-ray powder patterns and their structure is concluded to be the same. The compounds exhibit similar infrared spectra: 3250 (s, OH stretch), 1800 (C=O), 1615 (s), 1550-1400 (vs), 1150 (w), 1105 (m), 1090 (m), 1040 (s) and 900 (s)cm^{-1}. West and Niu suggest that both coordinated and noncoordinated carbonyl groups are present in these complexes. The magnetic moments of the Cr(III) and Fe(III) salts are comewhat low for high spin complexes and West and Niu suggest antiferromagnetic spin pairing is reducing the paramagnetism.

The structure of diammonium croconate has been determined by Baenziger, Hegenbarth and Williams (1963), and Baenziger and Hegenbarth (1964). They show that the croconate ion has D_{5h} symmetry with average bond lengths of 1.457Å for the C-C and 1.262Å for C-O bond lengths, respectively. The three crystallographically non equivalent C-C bond lengths are within one estimated standard deviation (e.s.d.=0.014Å) of their average and the three C-O bond lengths are within two e.s.d. (0.011Å) of their average. The C-C-C and C-C-O bond angles are within three e.s.d. of their average of 108.3° and 126.0°, as expected for D_{5h} symmetry . The ion is essentially planar. The bond lengths, bond angles and deviations from the best least squares plane are given in Figure 2. Hydrogen bonding seems to play an important role in holding the structure together via the NH_4^+ ions.

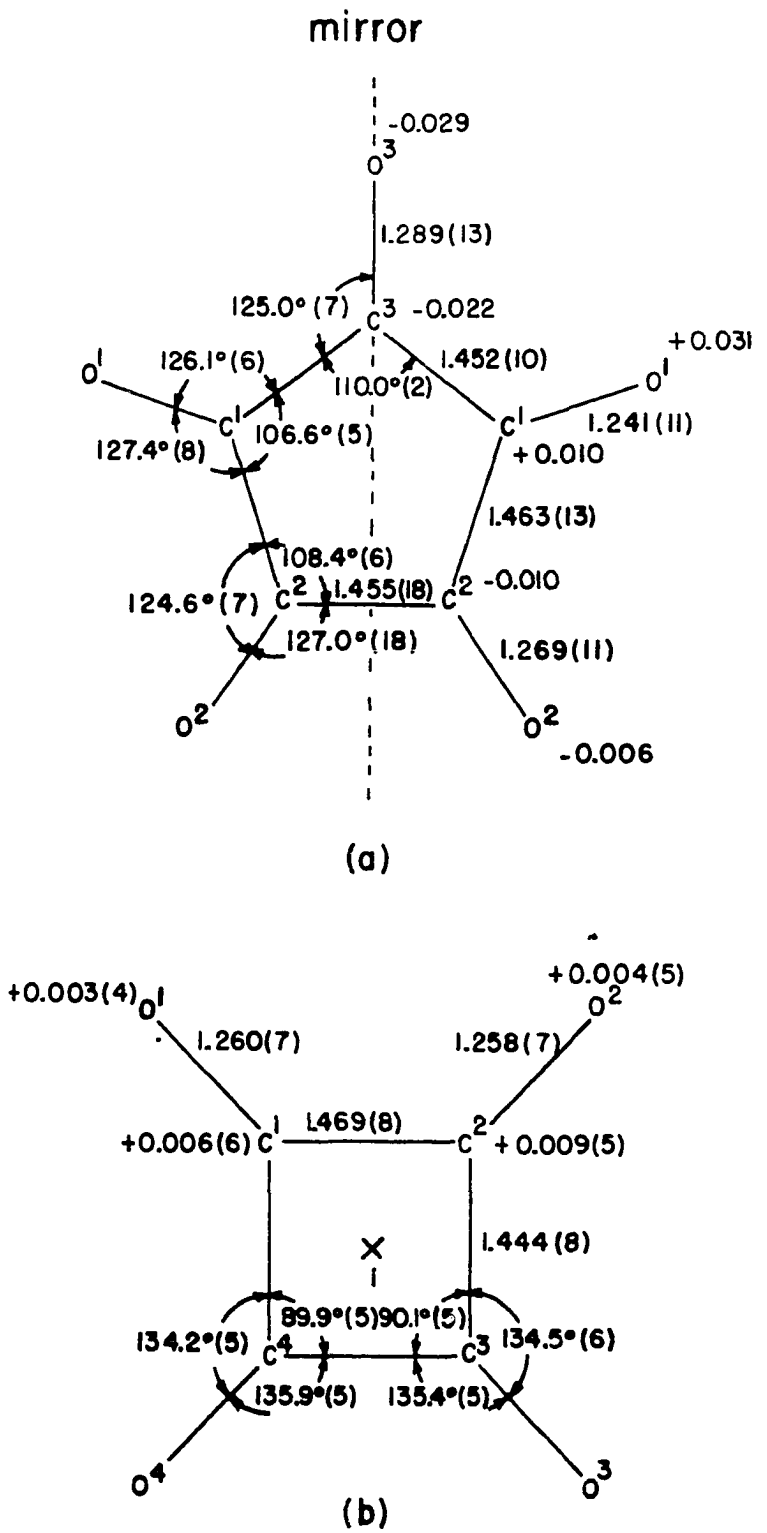

Figure 2. Structure of (a) croconate ion as found in diammonium croconate after Baenziger et al., (1963); and (b) squarate ion found in $K_2C_4O_4 \cdot H_2O$ after Macintyre and Werkema (1964)

Baenziger and Hegenbarth also made further Hückel π-MO calculations for the croconate anion using a large range of values for the oxygen coulomb integrals and the C-O exchange integrals. They evaluate the π-bond orders of the C-C and C-O bonds in the croconate via a bond length vs. bond order plot constructed with values taken from the literature, and use this value to select suitable values for the coulomb and exchange integrals involving the oxygen atoms.

Baenziger, et al. (1963) and Baenziger and Williams (1966) have determined the structure of rubidium hydrogen croconate and ammonium hydrogen croconate. The $HC_5O_5^-$ ion is expected to have mirror symmetry according to the two equivalent valence bond structures:

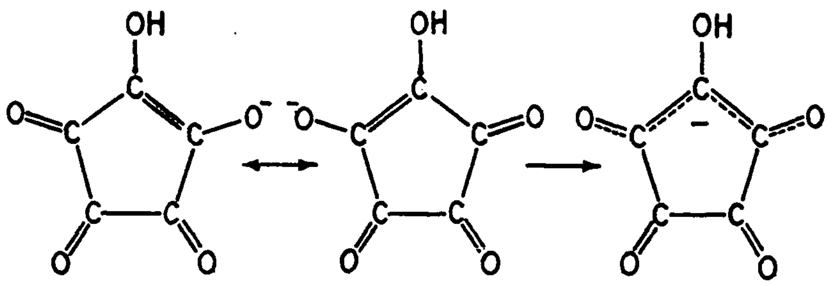

This structure for the ion is not found in either salt. The C-O bond distances vary from 1.21 to 1.34Å (e.s.d. 0.02 to 0.06Å) in the Rb salt and from 1.18 to 1.37Å (e.s.d. 0.01 to 0.02Å) in the NH_4^+ salt. The C-C bond distances vary from 1.40-1.54Å (e.s.d. from 0.02 to 0.06Å) in the Rb^+ salt and from 1.40 to 1.56Å (e.s.d. 0.02 to 0.03Å) in the NH_4^+ salt.

The C-C-C bond angles vary from 102° to 113° (e.s.d. of 2.9° to 4.7°) in the Rb^+ salt and from 102° to 118° (e.s.d. of 1.2° to 2.4°) for the NH_4^+ salt. The C-C-O angles show equally large ranges. The e.s.d.'s in all these parameters are large and make it difficult to make any judgement as to the symmetry of the $HC_5O_5^-$ ion. There is a very short interion O-O distance of 2.50(5)Å[1] and 2.46(2)Å in the Rb^+ and NH_4^+ salts respectively indicative of hydrogen bonding between these two oxygens; the hydrogen involved is the one from the $HC_5O_5^-$ ion.

Glick, Downs and Dahl (1964) have determined the structures of $CuC_5O_5 \cdot 3H_2O$ and $ZnC_5O_5 \cdot 3H_2O$ after preliminary work on the Cu complex had been done by Takehara and Yokoi (1958). The work of Glick, et al. showed that the two complexes are roughly isostructural (in agreement with the studies by West and Niu, 1963b), consisting of chains of metal ions packed parallel to each other in the crystal. The metal ions are linked together within the chain by the croconate anions, each croconate ion acting bidentate towards

---

[1] In this work uncertainties and standard deviations in quoted values will be indicated in parentheses following the quoted value. Values preceded by the ± sign are estimated uncertainties, values without this sign are root mean square standard deviations derived from some least squares procedure. In either case, a decimal point may or may not be included. If the decimal point is not included, the value given for the uncertainty or standard deviation applies to the last significant figures of the actual value of the parameter. That is 2.50(5)Å is equivalent to 2.50(0.05)Å and refers to root mean square standard deviations, whereas 2.50(±5) and 2.50(±0.05) are also equivalent but imply estimated uncertainties.

one metal ion and monodentate towards the next ion. Two croconate oxygens do not bond to any metal ion. In addition to the three croconate oxygens, each metal ion is coordinated by three water oxygens, completing a rough octahedron of oxygen atoms about the metal ion. The structure of the chains is given in Figure 3 for both compounds and various structural parameters are indicated.

The coordination about the Zn^{+2} ion is roughly octahedral with five oxygens at an average distance of 2.13Å and one at a shorter distance of 2.03Å. The O-Zn-O bond angles are close to 90° except for two of 80° and 100°. The coordination about the Cu^{+2} shows the usual Jahn-Teller tetragonal distortion of octahedral coordination about this ion. There are two long Cu-O bonds at an average of 2.33Å, and four shorter bonds at an average of 1.99Å. The long bonds are to two croconate oxygens on different croconate ions, and the four short bonds are to three water oxygens and the remaining croconate oxygen. The O-Cu-O bond angles vary from 81° to 95°. In both the Cu and the Zn salt, the smallest O-M-O angle involves two adjacent oxygens on the same croconate ion.

In the copper complex the croconate ion seems to have generally retained the D_{5h} symmetry it exhibited in diammonium croconate. All C-C and C-O bond lengths are within 3 e.s.d.'s of their average values of 1.46Å and 1.25Å respectively. The

C-C-C and C-C-O bond angles are within 3 e.s.d.'s of their average values of 108° and 126°, respectively, as expected for D_{5h} symmetry. The average values for the C-C and C-O bond lengths are in excellent agreement with those observed in diammonium croconate by Baenziger and Hegenbarth (1964). The small deviations from D_{5h} symmetry seem reasonably related to the asymmetric environment about the croconate ion.

In the Zn salt the croconate ion shows larger deviations from D_{5h} symmetry and seems to exhibit idealized C_{2v} symmetry. The C^1-C^2 bond between the two oxygens chelating the Zn ion is only 1.415Å while the others average 1.485Å (1.480, 1.484, 1.501 and 1.475Å; e.s.d. 0.016Å). The two C-O bond distances which involve the chelating oxygens are 1.25Å while the other C-O bond involved in coordination of the Zn ion is 1.27Å. The other two C-O bond distances are 1.19Å and 1.22Å. These bond lengths suggest essentially ketonic bonds for the two short C-O distances; these bonds involve the non coordinating oxygens. There is also some charge concentration in the short C-C bond relative to the ion as observed in diammonium croconate. The variation of the bond angles agrees with a picture of the ion related to the structure expected for croconic acid. This agrees with the fact that both ketonic and acid salt C-O vibrational modes were observed by West and Niu (1963b).

Glick et al. speculate that the croconate ion structure

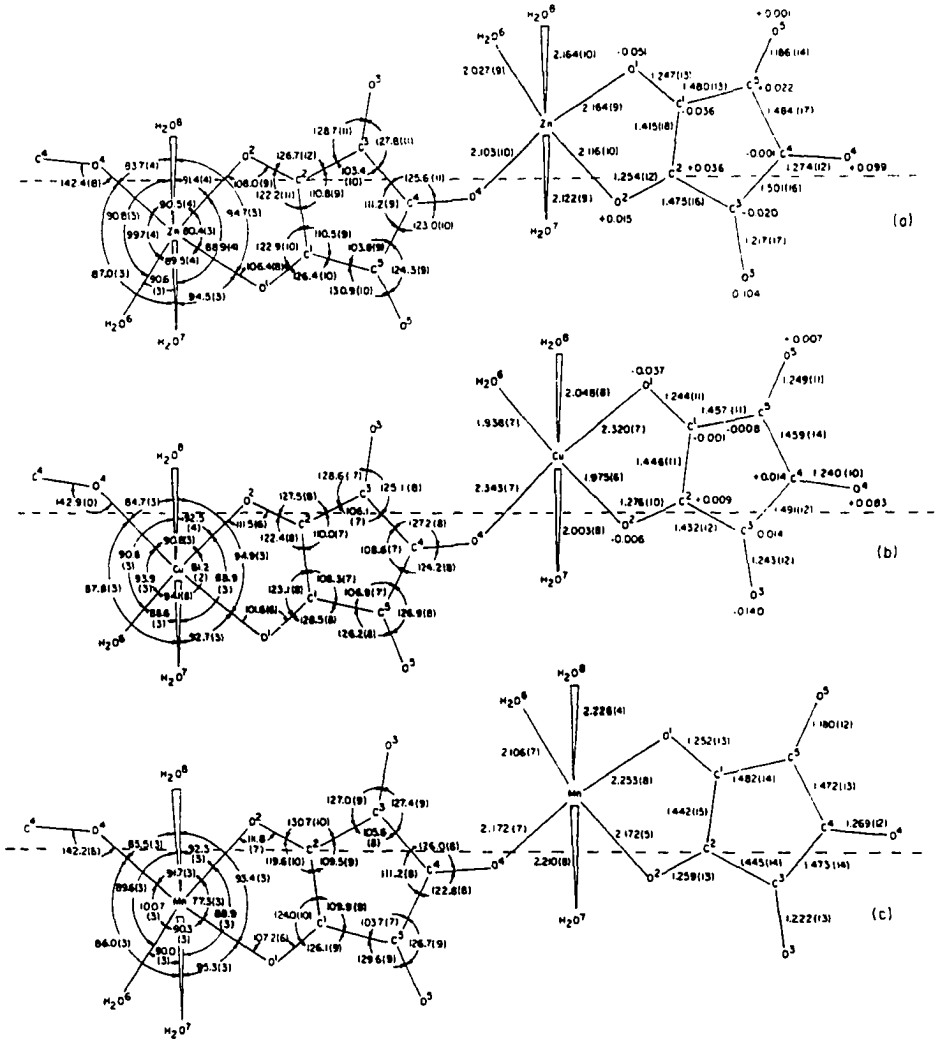

Figure 3. Structures of the (a) Zn(II), (b) Cu(II) and (c) Mn(II) croconates after Glick, Downs and Dahl (1964) and Glick and Dahl (1966)

in these compounds is due to the stereochemical requirements of the cations. Zn^{+2} allows essentially equivalent Zn-O bonds to the croconate oxygens and this equivalency may allow more significant interaction between the Zn^{++} ion and the croconate ion π-system, thus perturbing it more than the Cu^{++} ion, which, due to Jahn-Teller distortions, forms inequivalent Cu-O bonds and thus allows less Cu^{++}-croconate π-system interaction, leaving the π-system essentially unperturbed and the croconate ion with D_{5h} symmetry.

In both compounds O^3 and O^4 are bent out of the plane of the carbon atoms in opposite directions. O^3 is bent in a direction of a water molecule in another chain to which O^3 is hydrogen bonded. Other interchain and intrachain hydrogen bonds also seem to be present and interchain hydrogen bonds seem to be an important mechanism in holding the chains together.

Glick and Dahl (1966) have also determined the structure of manganese croconate, $MnC_5O_5 \cdot 3H_2O$. This compound is not expected to undergo Jahn-Teller distortion and was found to have a structure very similar to that of the zinc croconate. In Figure 3 the structural parameters for this compound are also given.

West and Niu (1963a) have prepared and characterized the complexes of squaric acid with the divalent transition metal ions Mn(II), Fe(II), Co(II), Ni(II) and Cu(II) and with Mg(II), Zn(II) and Ca(II), and with the trivalent ions

Al(III), Cr(III) and Fe(III). The salts containing the divalent metal ions were reported to have the general formula $MC_4O_4 \cdot 2H_2O$. The Debye-Scherer X-ray powder patterns were essentially the same for the divalent Mn, Fe, Co, Ni, Mg and Zn salts, differing only slightly in corresponding d-values, thus indicating that these salts had essentially the same structure. The Ca(II) salt was found to have a different powder pattern and thus a different structure; the Cu(II) salt also seems to have a different powder pattern and structure than the other divalent transition metal ion salts.

The infrared spectra of the divalent squarate complexes show only four bands in the sodium chloride region. There is an extremely broad and strong band extending from 1400 to 1700cm^{-1} which can be assigned to a mixture of C-C and C-O stretching vibrations (Ito and West, 1963); other bands are found at 1150, 1105 and 2210cm^{-1}, the latter being an overtone of the 1105cm^{-1} band. There is no sharp band above 1600cm^{-1} and this indicates that there are no free C=O groups, i.e. all squarate oxygen atoms must be coordinated. The simplicity of the spectra indicates that the symmetry of the squarate ion is not greatly reduced from the D_{4h} symmetry found in potassium squarate by Ito and West (1963).

Copper (II) squarate was found to have additional bands at 1360, 1320, 985 and 900cm^{-1}, indicating a less symmetrical

structure for this compound.

Gouy balance static magnetic susceptibility measurements at room temperature indicated that the transition metal squarates like the croconates are high spin complexes. West and Niu's (1963a) results are given in Table 1.

West and Niu proposed a structure for the isostructural divalent squarates which, in analogy to the croconates, consists of chains of metal ions linked together by squarate ions, each squarate ion acting bidentate to two metal ions and a rough octahedron of oxygens about the metal ion being completed by two water oxygens. All the squarate oxygens are coordinating metal atoms in agreement with the observed IR spectra. The packing of these chains in a three-dimensional crystal is not discussed. A schematic diagram of the proposed structure is given in Figure 4.

The trivalent Al(III), Cr(III) and Fe(III) squarates have the general formula $MC_4O_4(OH)\cdot 3H_2O$ and were found to be isostructural by Debye-Scherer X-ray powder diffraction patterns. The infrared spectra were found to be similar, showing bands at 3250, 1615, 1150, 1105, 1090, 1040 and 900cm^{-1}. The room temperature magnetic moments of the Cr(III) and Fe(III) salts are somewhat lower than expected for high spin compounds, similar to the croconate complexes of these two ions. The results are given in Table 1.

The structure of dipotassium squarate, $K_2C_4O_4\cdot H_2O$, has

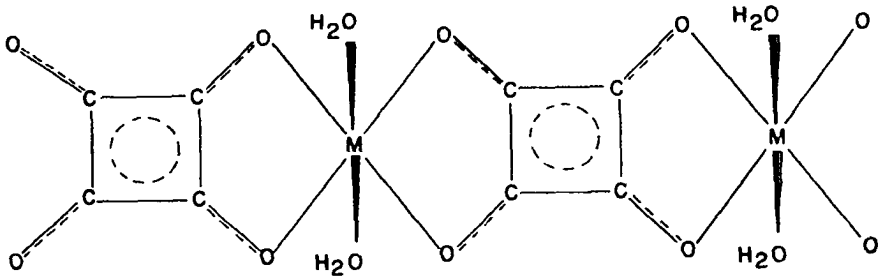

(a)

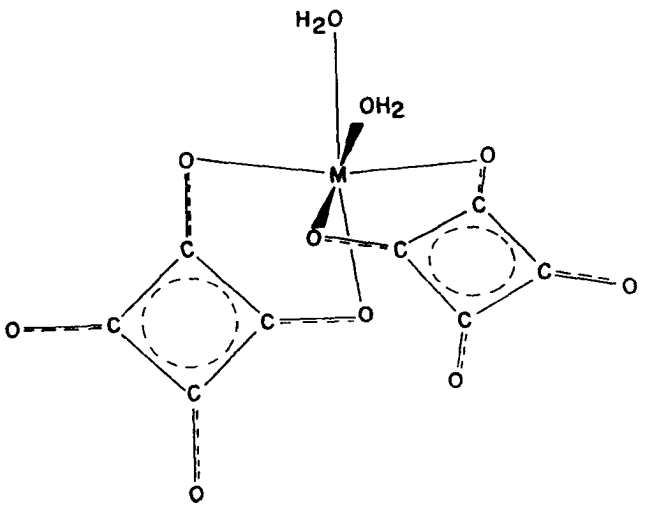

(b)

Figure 4. Proposed structures of divalent transition metal squarates (Mn, Fe, Co, Ni, Zn) after (a) West and Niu (1963a) and (b) Ludi and Schindler (1968)

Table 1. Magnetic moments of squarate complexes at room temperature after West and Niu (1963a)

Squarate	Temp. (°K)	P_{eff} (μ_B)
Cu(II)	295	1.77
Ni(II)	295	3.19
Co(II)	295	5.17
Fe(II)	295	5.43
Mn(II)	295	5.88
Cr(III)	298	3.52
Fe(III)	298	6.26

been determined by Macintyre and Werkema (1964). In this compound the squarate ion was found to have essentially D_{4h} symmetry. In the crystal the center of the squarate ion is at a center of symmetry. The two independent C-C bond distances, 1.469(8)Å and 1.444(8)Å differ by 0.025Å which equals about 3 e.s.d. The two independent C-O distances, 1.260(7)Å and 1.258(7) agree to within less than one e.s.d. The bond angles are within less than one e.s.d. of the required values for D_{4h} symmetry. The center of symmetry requires that the four carbon atoms and the four oxygen atoms be coplanar separately, but does not require the two planes to coincide. The deviations of the atoms from the best least squares plane including all eight atoms is less than two radial e.s.d. of position for all atoms. All these

parameters point to an essentially D_{4h} structure of the squarate anion. The structural parameters are given in Figure 2. The average C-C and C-O bond distances observed in the squarate ion are the same, to within 0.02Å, as those found in diammonium croconate and copper croconate.

The squarate ions are packed on top of each other in stacks, the ions being approximately 3.30Å apart and almost coplanar, but neighboring ions are rotated alternately by $\pm 45°$ with respect to each other about the stack axis. The water molecules form bridges between the squarate ions via symmetrical hydrogen bonds. The potassium ions are packed between the parallel stacks and hold the structure together in the plane perpendicular to the stacks. No such ionic forces hold the structure together in the direction parallel to the stacks, and Macintyre and Werkema propose that the close approach of 3.30Å between the squarate anions is evidence for electron exchange between the anions, since the normal van der Waals equilibrium separation of parallel π-systems is about 3.4Å (graphite), and it would be expected to be larger between negatively charged π-systems. Therefore, they propose that the structure is held together in the direction of the stacks by a molecular selfcomplexing between neighboring squarate anions.

Recently, Ludi and Schindler (1968) have reported that they have derived three different compounds from solutions

of Ni(II) and Co(II) ions and dipotassium squarate, which could be readily distinguished by x-rays. From Guinier powder patterns a pure cubic modification of composition $MC_4O_4 \cdot 2H_2O$ was found to have lattice constants of 8.06Å and 8.16Å for the Ni(II) and Co(II) salts, respectively. The densities were found to be 1.93 and 1.87 g/cm^3 at 20°C, thus implying three formula units of $MC_4O_4 \cdot 2H_2O$ per unit cell. They also measured the reflectance spectra of the powdered compounds and found absorptions at 8600, 13,300, 15,200, 21,500 sh[1] and 25,300cm^{-1} for $NiC_4O_4 \cdot 2H_2O$ and 7800, 11,400 sh, 16,000 sh, 19,600 and 21,500sh cm^{-1} for $CoC_4O_4 \cdot 2H_2O$ leading to values for Dq of 860 and 890cm^{-1} and to values of Racah's parameter, B, of 850 and 860cm^{-1} respectively for the Ni and Co salts, assuming octahedral coordination about the transition metal ions. They assume that each metal ion is chelated by two squarate ions, but due to the large unit cell size, propose that the two water oxygens are in cis positions in contrast to the structure proposed by West and Niu (1963a). The coordination about the metal ions proposed by Ludi and Schindler is given in Figure 4; they do not speculate about the packing of these units in the crystal.

In addition to the work described above, there has been some structural work on ring systems related to cyclobutenedione. In particular the structure of phenylcyclobutenedione

[1]sh: shoulder.

(Wong, Marsh and Schoemaker, 1964) and 1-cyclohexenyl-1-cyclobutenedione (Karle, Britts and Bremmer, 1964) have been determined.

There has also been a mass spectrometric study of squaric acid, croconic acid, rhodizonic acid and several derivatives of these compounds, suggesting that dihydroxy-cyclopropenone, $H_2C_3O_3$ exists as a singly charged ion in the fragmentation schemes of all these compounds (Skujins, Delderfield, and Webb, 1968).

There are also several studies on the synthesis and reactions of squaric acid; a recent review has been written by Maahs and Hegenberg (1966). There is much interest in squaric acid as a starting material for organic dyes, and there are several papers on the conversion of squaric acid, to cyclobutenediylium dyes in which the chromophores are the cyclobutenediyliumdioxide groups (Sprenger and Ziegenbein, 1968)

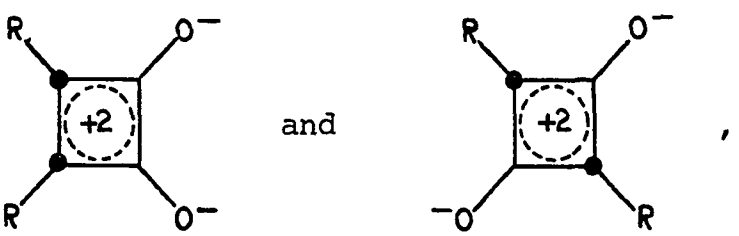

where the R's are various groups such as

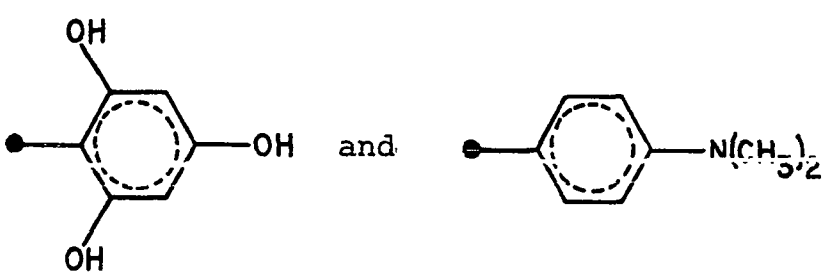

Some work has been done in this laboratory on the magnetic properties of some of the squarates by Smentowski and Gerstein[1]. They measured the magnetic susceptibilities of the Mn(II), Fe(II), Co(II) and Ni(II) squarates using the mutual inductance technique in the 1.3 to 300°K temperature range, finding that all exhibit paramagnetic behavior above 4.2°K. Early indications of one dimensional magnetic ordering in Ni(II) squarate were traced to thermal inequilibrium in the sample. Their experimental points were fit by this author to an equation of the form $\chi_m^{-1} = aT + b$ by a least squares procedure. The results, including the effective magnetic moments in Bohr magnetons are given in Table 2.

Table 2. Susceptibilities and magnetic moments of Mn(II), Fe(II), Co(II) and Ni(II) squarates as determined from data by Smentowski and Gerstein

Squarate	$\chi_m^{-1} = aT + b$	P_{eff} (μ_B)
Mn(II)	0.2362(14)T + 0.258(67)[a]	5.82(2)[a]
Fe(II)	0.2749(10)T + 0.254(62)	5.39(1)
Co(II)	0.3891(26)T + 3.46(28)	4.53(2)
Ni(II)	0.7540(82)T + 4.41(66)	3.26(2)

[a]The uncertainties indicated are root mean square standard deviations (in the parameters) derived from the scatter of the experimental points about the line of best fit. No information about other errors is available.

[1]Smentowski, F. J., Department of Chemistry, Texas A&M University, College Station, Texas; and B. C. Gerstein, Department of Chemistry, Iowa State University of Science and Technology, Ames, Iowa. Unpublished susceptibility data for Mn(II), Fe(II), Co(II) and Ni(II) squarates. Private communication. 1968.

The effective moments are in reasonable agreement with those obtained by West and Niu (1963a), except for the Co(II) squarate which is about 14% low. No immediate explanation for this is available. The data for Ni squarate exhibits scatter on the order of 20% in χ_m at 78°K due to thermal inequilibrium in the sample and between the sample and the thermocouple. Indications of thermal inequilibrium at 4.2°K and above are also observed in the data. A peak in the susceptibility attributed to the onset of long range order is observed at about 1.6°K in Ni squarate.

SAMPLE PREPARATIONS

Samples of nickel squarate ($NiC_4O_4 \cdot 2H_2O$) were prepared using squaric acid obtained from the Aldrich Chemical Co., Milwaukee, Wis., and from "analytical reagent" grade $NiCl_2 \cdot 6H_2O$ obtained from the Mallincrott Chemical Works, St. Louis. The squaric acid was analyzed for carbon and hydrogen by combustion analysis. The results were: calculated for $C_4O_4H_2$, in weight percent: C, 42.12%; H, 1.77%; found: C, 41.95 ($\pm$0.08)%; H, 1.77 ($\pm$0.02)%. All major constituent analyses were performed by Analytical Chemistry Group I of this laboratory except where noted otherwise. (The deviations quoted are average deviations of analytical results from their mean as obtained from several similar analyses performed by Analytical Chemistry Group I.)

Powder Samples

Powder samples were prepared as described by West and Niu (1963a). The preparation consisted of first dissolving the squaric acid in dilute KOH solution and then adding a dilute solution of $NiCl_2 \cdot 6H_2O$. The pH was adjusted to prevent precipitation of $Ni(OH)_2$. A very finely divided green powder precipitated, was filtered off and dried. Samples prepared in this way always were found to be low in Ni content. The analytical results for a typical sample (labeled sample 1) prepared in this way are given in Table 3.

Table 3. Analytical results for various samples of $NiC_4O_4 \cdot 2H_2O$. Results are in weight percent

	% Ni	% C	% H
Calculated for $NiC_4O_4 \cdot 2H_2O$	28.39	23.23	1.950
Sample 1; prepared by method of West and Niu (1963a)	24.83(±0.15)	23.04(±0.15)	2.80(±0.02)
Sample 2; prepared from $C_4O_4H_2$ and $NiCl_2 \cdot 6H_2O$ solutions in 50-50 ETOH/HOH	25.37(±0.15)	24.63(±0.15)	3.00(±0.02)
Sample 3; prepared from $C_4O_4H_2$ and $NiCl_2 \cdot 6H_2O$ solutions in large volumes of water at 60°C	27.79(±0.15)	22.67(±0.15)	2.06(±0.03)

The observed Ni content is 3.5 wt. % too low and the H content is 0.85 wt. % too high. The X-ray powder patterns obtained for these samples, however, are the same as those reported by West and Niu. The yields obtained using the above procedure were on the order of 50%; this was believed due to destruction of the $C_4O_4^=$ ion in basic solution. The unexpected analytical results are believed due to extra water and some unknown carbon containing impurity in the powder.

In an attempt to prepare better samples, squaric acid and $NiCl_2 \cdot 6H_2O$ were dissolved directly in a 50/50 mixture of ethanol and water. The ethanol water mixture was used to aid in the solution of the squaric acid, which is only sparingly soluble in water. This preparation resulted in a powdered sample of the same appearance as sample 1 and the same Debye Scherer pattern. Yields were about 90%. The analytical results for a typical sample are given in Table 3 (labeled sample 2). As can be seen, the Ni analysis is still 3.0 wt. % below the expected concentration. The C and H concentrations are high by 1.6 wt. % and 2.5 wt. % respectively. These results can be explained roughly by assuming about 0.41 moles extra water and about 0.37 moles extra ethanol per mole of $NiC_4O_4 \cdot 2H_2O$. These values were calculated from the experimental Ni and C concentrations and predict a H concentration of 3.08% compared to an experimental

value of 3.00(±0.02)%. Some of the extra solvent molecules might have been adsorbed on the surface of the very small crystals. Others could be occluded in the crystals or clathrated in the loose structure of the crystal (see discussion of structural studies). Susceptibility measurements were made on this sample.

Recently some $NiC_4O_4 \cdot 2H_2O$ was prepared by combining a hot saturated aqueous solution of squaric acid with a hot dilute solution (0.4M) of $NiCl_2 \cdot 6H_2O$. Crystals precipitated on cooling the solution. The yield was 65%. Base was added to the mother liquor to neutralize the liberated HCl and on further reduction of the solution volume a second crop of crystals was obtained. The total yield of the two crops was 90%. The analytical results for Ni, C, and H are given in Table 3 (labeled sample 3). The analytical results for both crops of crystals were the same. As can be seen, these crystals are only 0.69 wt. % low in Ni, 0.55 wt. % low in C and 0.11 wt. % high in hydrogen. If the discrepancy is assumed to be due to extra water, and one assumes that there are about 0.22 moles of extra water, expected concentrations of 27.86 wt. % Ni, 22.79 wt. % C and 2.12 wt. % H are calculated, which are in good agreement with the experimental Ni and C concentrations; the result for H is somewhat high but only slightly outside the estimated limits of error of the experimental results. Some susceptibility measurements were

made on this sample also.

From the above, it seems evident that the disagreement between experimental and expected analytical results based on the chemical formula $NiC_4O_4 \cdot 2H_2O$ for samples 2 and 3 can be explained on the basis of solvent contamination of the samples.

Samples 2 and 3 were analyzed for trace impurities by spark source mass spectrography by the Mass Spectrometry Group of this laboratory. The results are given in Table 4. As can be seen, the impurity atoms detected in higher concentrations are Na, K, Ba and Cl. Mn, Fe, Co, Cu and Zn are also observed. The results may be in error by as much as a factor of 10 in the case of Cl; the results for Na and K may be regarded as upper limits. The results for the rest of the elements are accurate to within a factor of 5.

The X-ray Debye-Scherer powder patterns for all three preparations were the same and corresponded closely to the powder pattern for $CoC_4O_4 \cdot 2H_2O$ given by West and Niu (1963a). The d-values given by West and Niu for $CoC_4O_4 \cdot 2H_2O$ are given in Table 5. They are indexed assuming a cubic crystal lattice; the above authors did not indicate that this was possible, and they do give four lines which do not fit into a cubic indexing scheme. However, all of these are easily identified as Cu Kβ lines. In Table 5 are also given the d-values for the $NiC_4O_4 \cdot 2H_2O$ sample labeled as Sample 2 in

Table 4. Mass spectrometric analysis of $NiC_4O_4 \cdot 2H_2O$ samples. Results in atomic ppm

El.	Sample 2 ppm	Sample 3 ppm	Remarks	El.	Sample 2 ppm	Sample 3 ppm	Remarks
Li				In	ND	ND	
Be	<.05	<.05		Sn	ND	ND	
B	<.05	<.05		Sb	ND	ND	
C				Te	ND	ND	
N				I			
O				Cs			
F				Ba	40	70	
Na	100	30		La	≤.9	≤ 4	Previous sample
Mg				Ce	ND	ND	
Al				Pr	.4	4	
Si				Nd	ND	ND	
P				Sm	ND	ND	
S				Eu	.1	.3	
Cl	300	1000		Gd	.4	.5	
K	3	70		Tb	ND	ND	
Ca	3	10		Dy	ND	ND	
Sc	ND	ND[a]		Ho	ND	ND	
Ti	ND	ND		Er	ND	ND	
V	ND	ND		Tm	ND	ND	
Cr	≤.3	≤.5		Yb	ND	ND	
Mn	40	30		Lu	.3	.3	
Fe	10	10		Hf	ND	ND	
Co	20	8		Ta	ND	ND	
Ni	111,000	111,000	Reference	W	ND	ND	
Cu	1	3		Re	ND	ND	
Zn	4	20		Os	ND	ND	
Ga	ND	ND		Ir	ND	ND	
Ge	ND	ND		Pt	ND	ND	
As	ND	ND		Au	ND	ND	
Se	.2	.8		Hg	ND	ND	
Br	.3	10		Tl	ND	ND	
Rb	ND	ND		Pb	1	ND	
Sr	ND	ND		Bi	ND	ND	
Y	ND	ND		Th	ND	ND	
Zr	ND	ND		U	ND	ND	
Nb			Source				
Mo	ND	ND					
Ru	ND	ND					
Rb	ND	ND					
Pd	ND	ND					
Ag	ND	ND					
Cd	ND	ND					

[a]ND, not detected.

Table 5. Comparison of d-values for $CoC_4O_4 \cdot 2H_2O$ from West and Niu (1963a) with d-values obtained for $NiC_4O_4 \cdot 2H_2O$, sample 2

$h^2+l^2+k^2$	$CoC_4O_4 \cdot 2H_2O$ (West and Niu, 1963a)	$NiC_4O_4 \cdot 2H_2O$ (Sample 2)	$h^2+k^2+l^2$	$CoC_4O_4 \cdot 2H_2O$ (West and Niu, 1963a)	$NiC_4O_4 \cdot 2H_2O$ (Sample 2)
1	8.15	8.06	26	1.591	1.580
	6.32[a]		27	1.562	1.549
2	5.75	5.69	29	1.509	1.496
3	4.69	4.652	30	1.482	1.469
4	4.07	4.026	32	1.434	1.423
5	3.63	3.600	33	1.415	
6	3.31	3.288	34		
	3.18[a]		35	1.372	1.362
	3.00[a]		36	1.354	1.343
8	2.87	2.853	38	1.316	1.285
	2.83[a]		40		1.274
9	2.71	2.683	41		1.285
10	2.55	2.547	43		1.228
11	2.45	2.433	44		1.208
12	2.32	2.324	51		1.128
13	2.25	2.233	56		1.077
14	2.17	2.152	59		1.048
16	2.03	2.015	68		0.9788
17	1.965		72		0.9510
18	1.911	1.901	75		0.9310
19	1.863	1.847	76		0.9255
20	1.815	1.812	80		0.9015
21	1.771	1.766	83		0.8855
22		1.718	84		0.8565
24	1.658	1.644	99		0.8115
25	1.624	1.612	100		0.8070

[a] $K\beta$ lines.

Table 3. A Nelson Riley extrapolation of back reflection lines gives cubic lattice constants of 8.067(2)Å and $8.062_5(21)$Å for samples 2 and 3 respectively. The extrapolations were made with the help of a computer program written by Vogel and Kempter (1959, 1961).

Ito and West (1963) have measured the infrared and Raman spectra of the $C_4O_4^=$ ion. The Raman spectrum was obtained from $K_2C_4O_4 \cdot H_2O$ in aqueous solution. The infrared spectrum was obtained from a $K_2C_4O_4 \cdot H_2O$-Nujol mull. Ito and West carried out a normal coordinate analysis of the $C_4O_4^=$ ion using a Urey-Bradley force field and made vibrational mode assignments on the basis of these calculations. They found that the best agreement between calculated and observed spectra could be obtained by assuming D_{4h} symmetry for the $C_4O_4^=$ ion. The infrared active vibrations are listed in Table 6. There are only five observed absorptions, four of which are fundamentals; there are seven Raman active fundamentals predicted for D_{4h} symmetry and seven are observed.

West and Niu (1963a) also report the following absorptions for $NiC_4O_4 \cdot 2H_2O$: a very broad band in the region of 1400-1700 cm^{-1}, assigned to a mixture of C-O and C-C stretching modes, ν_{12} and ν_{13} in Table 6; sharp bands at 1105 cm^{-1} and 2210 cm^{-1}, the latter being an overtone of the 1105 cm^{-1} band. The band at 1105 cm^{-1} could be identified with ν_{13}

Table 6. Observed IR absorption frequencies and vibrational assignments for the $C_4O_4^=$ ion in $K_2C_4O_4 \cdot H_2O$ assuming D_{4h} symmetry (after Ito and West, 1963)

IR absorption frequency (cm^{-1})	Symmetry of normal mode	Label and type of mode
259 s	A_{2u}	ν_4, out of phase CO bending
350 m	E_u	ν_{14}, in plane CO bending
1090 s	E_u	ν_{13}, CC stretching
1530 vs, v. broad	E_u	ν_{12}, CO stretching
2200 w	E_u	$\nu_{13}+\nu_5$ (B_{1g}, CC stretching R active, 1123 cm^{-1})

in Table 6 and the band at 2210 cm^{-1} with $\nu_{13}+\nu_5$. They also observe a band at 1150 cm^{-1} which cannot be assigned unambiguously.

Samples 2 and 3 in Table 3 were examined for IR absorptions in the region 4000-600 cm^{-1} in both KBr pellet and Nujol mulls using a Beckman IR7 spectrophotometer. Both samples showed the following absorption bands: a very broad band centered at 1520 cm^{-1}; a sharp band at 1105 cm^{-1}; a somewhat weaker band at 2235 cm^{-1}. No absorption was observed around 1150 cm^{-1}. The three absorptions observed agree well with those reported by West and Niu in this region.

There should, however, be some indications of absorptions due to vibrational modes of water molecules, and in the case of sample 2, ethanol molecules. In fact, a very broad absorption was observed in both samples at 3270 cm^{-1}

which could be due to either the water or ethanol O-H stretching mode (Nakomoto, 1963; Rao, 1963). In sample 2, but not in sample 3, additional absorptions were seen at 2960 cm^{-1} and 2900 cm^{-1} due to the CH_3 symmetric and asymmetric stretching modes, and at 1088 cm^{-1} and 1048 cm^{-1} due to the C-C-O stretching modes in ethanol (Silverstein and Bassler, 1967).

Crystals Grown in Silica Gel

Crystals large enough for single crystal X-ray investigations were grown by the silica-gel technique (Henish, Dennis, and Hanoka, 1965). This method was used because $NiC_4O_4 \cdot 2H_2O$ has a low solubility in water and large crystals cannot be grown from aqueous solution. The largest crystals obtained from aqueous solution are on the order of 0.02 mm on a side. The compound decomposes at 300°C and crystals cannot be grown from a melt.

The silica gel technique for growing crystals consists of separating the two reacting species, in this case $C_4O_4^{=}$ and Ni^{++} ions, by silica gel. The two ions diffuse toward each other and form crystals in the gel which grow slowly to reasonably large size. The function of the gel is to provide a growth medium in which turbulence is eliminated and slow growth of crystals can be diffusion controlled; it also seems to act as a catalytic agent in initiating

crystal growth at nucleation sites, such as gel imperfections and dust particles.

The gel is prepared by acidifying an aqueous solution of sodium metasilicate, $Na_2SiO_3 \cdot 9H_2O$. An effective recipe for preparing gels is as follows: to 10 ml of 15% by wt. aqueous solution of sodium metasilicate 2 ml of 50% by volume of acetic acid is added; after intimate mixing of the two solutions, a gel will form within a few hours. Gels obtained in this way are soft and of low density. These are the characteristics needed to grow large crystals (Henish et al., 1965).

Figure 5 illustrates the apparatus used. Silica gel is formed in a half inch diameter glass U tube. Dilute solutions of potassium squarate and $NiCl_2 \cdot 6H_2O$ are placed into the two arms of the U tube over the gel. Ni^{++} and $C_4O_4^{=}$ ions diffuse slowly through the gel toward each other and crystals will start to form in the gel. Instead of potassium squarate solution, one can use solid squaric acid crystals covered by water.

The crystals of $NiC_4O_4 \cdot 2H_2O$ grown in silica gel appear predominantly as transparent green cubes; they are of various sizes with the largest on the order of 0.5 mm on a side. They appear to be of the same form as the solution grown crystals except for their larger size. On examination under a microscope, imperfections inside the crystals in the form

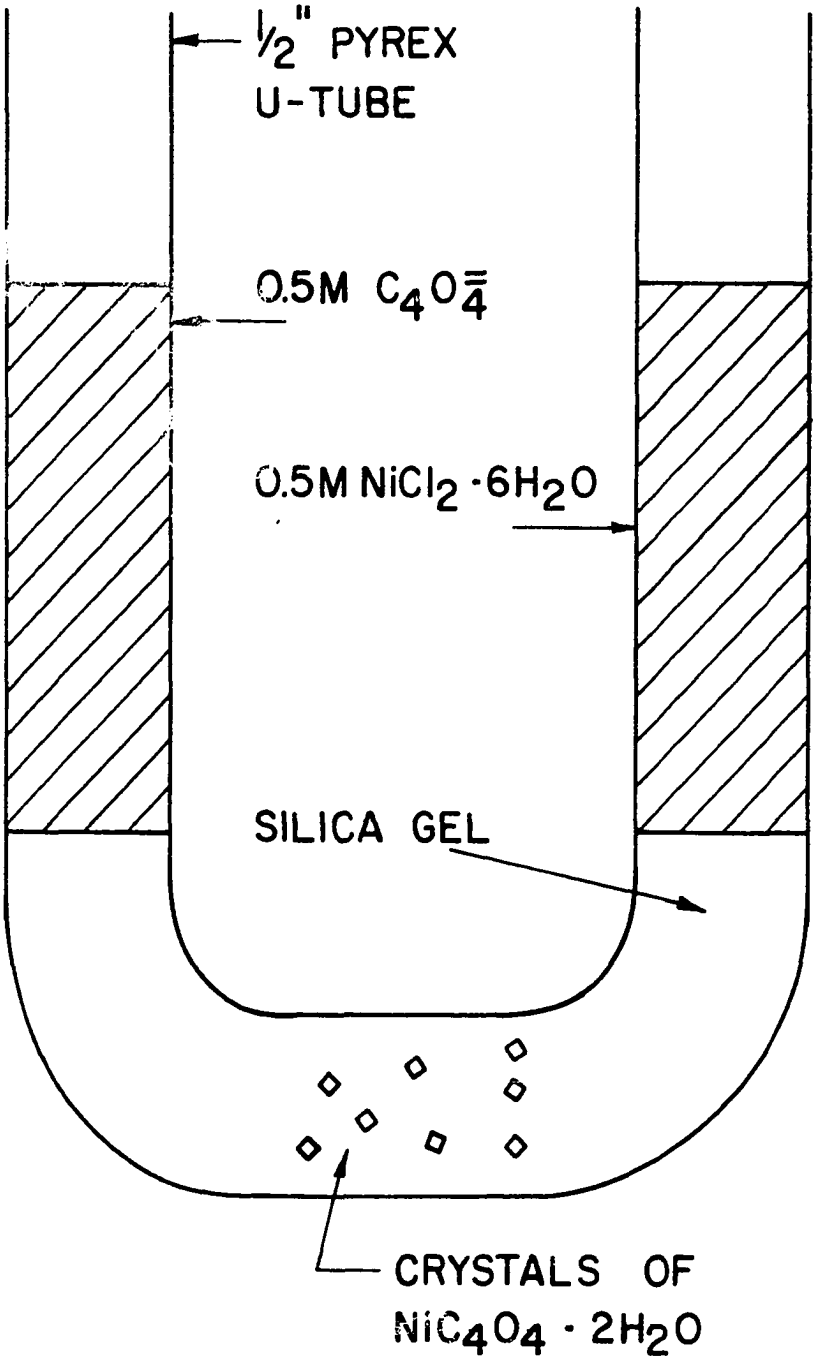

Figure 5. Apparatus used for growing large $NiC_4O_4 \cdot 2H_2O$ crystals

of veils and crack's are visible. In Figure 6 the appearance of the crystals is seen. A view of any face of a crystal cube exhibits faint diagonal lines. These must be due to faults in the crystal; all crystals examined have these faults and many of them also exhibit other faults.

The X-ray powder patterns of the crystals grown in silica gel are the same as those grown from solutions.

Figure 6. Appearance of $NiC_4O_4 \cdot 2H_2O$ in microscope by transmitted light (the smaller crystal is 0.145 mm on edge)

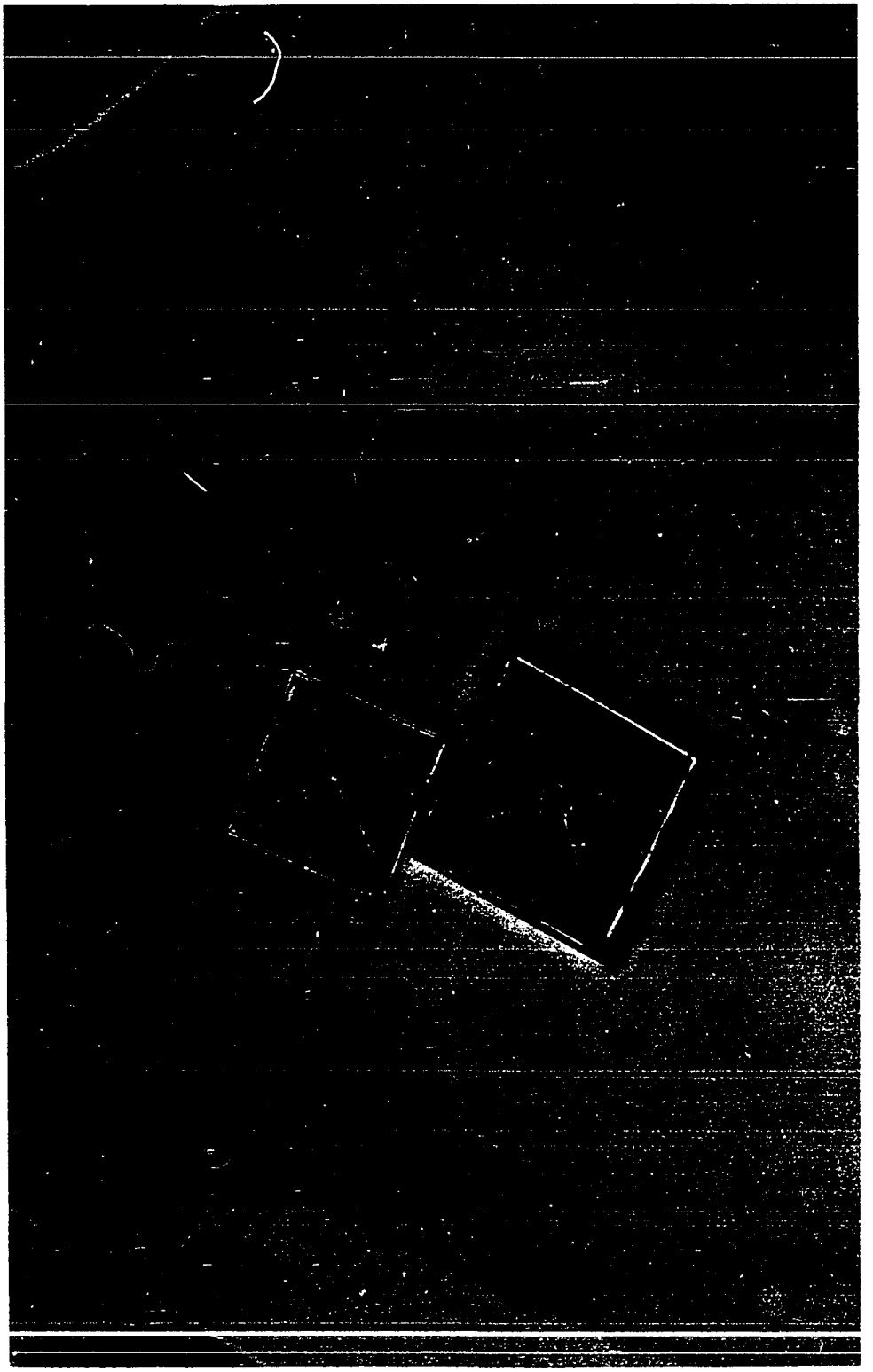

STRUCTURAL INVESTIGATION

As has been discussed previously, the structure of Ni squarate dihydrate has been postulated by West and Niu (1963a) to be as given in Figure 4. Another possibility for the coordination about the Ni(II) ion was proposed by Ludi and Schindler (1968) and is given in Figure 4 also. Both of these structures would require either an extensively distorted oxygen octahedron or a distorted squarate ion, if the Ni-O bond distances are to be close to the expected value of 1.95Å obtained from Slater's radii (Slater, 1964, 1965). A major purpose of this study was to determine the actual structure of nickel squarate in the solid state via single crystal X-ray diffraction techniques. The techniques of X-ray diffraction will not be discussed extensively. They are treated exhaustively by various authors in standard texts. The ones found most helpful in this work are: X-ray Structure Determination by Stout and Jensen (1968); Crystal Structure Analysis by Buerger (1960); International Tables for X-ray Crystallography (1952,1959, 1962), (these will be referred to from now on as ITXRC) and Chemical Crystallography by Bunn (1946).

Preliminary Results

As discussed in the "sample preparation" section, initial attempts to grow sufficiently large crystals from aqueous solution for single crystal X-ray diffraction measurements were unsuccessful. Crystals of a suitable size were grown in silica gel as described in the section on sample preparation. The crystals, identical in appearance to the crystals grown from solution, grew predominantly as green, transparent cubes. Their general appearance is given in Figure 6. The Debye-Scherer X-ray pattern of the crystals grown in silica gel is the same as those for crystals grown in aqueous and aqueous-alcoholic solutions. Since the powder patterns could be indexed on the basis of a cubic crystal lattice, it was considered unlikely that the structure consisted of chains as suggested by West and Niu. The cubic unit cell size as determined from Debye-Scherer powder patterns was found to be 8.068(2)Å for the gel grown crystals, giving a unit cell volume of 5.252×10^{-22} cm^3.

The density of the crystals was measured by the flotation technique in a mixture of bromoform ($d(20°C)=2.89$ g cm^{-3}) and carbon tetrachloride ($d(25°C)=1.585$ g cm^{-3}); the density was found to be $1.99(\pm 1)$ g cm^{-3}. This density, together with the measured unit cell volume, implies $3.04(\pm 2)$ molecular units of $NiC_4O_4 \cdot 2H_2O$ per unit cell.

Under the polarizing microscope nickel squarate crystals grown from solution and from silica gel behave typically as non cubic crystals, however. Cubic crystals are optically isotropic; that is, the speed of light is independent of the transverse vibration direction of the light ray, and consequently of its path through the crystal; the indices of refraction are the same for all possible transverse vibration directions of the light ray. When such a crystal is viewed as it is being rotated between two crossed Nicol prisms it will appear uniformly dark. That is, plane polarized light coming from the lower Nicol passes through a cubic crystal unaffected (for all possible orientations of the crystal) and cannot pass the crossed Nicol analyzer, giving the characteristic dark appearance of the cubic crystal between crossed Nicols.

Uniaxial crystals (hexagonal, tetragonal, trigonal) exhibit two refractive indices, for light vibrating parallel and perpendicular to the unique crystallographic axis. If such a crystal is examined between crossed Nicols with the unique axis perpendicular to the line of sight, the crystal will in general be found to be light except for four orientations 90° apart at which the crystal will become dark, or extinct. These orientations are such that the unique crystallographic axis is parallel or perpendicular to the plane of the polarized light. A complete discussion of

these and related optical phenomena are given by Bunn (1946) and Bloss (1961).

When nickel squarate crystals are viewed between crossed Nicol prisms, extinctions at four distinct orientations 90° apart are observed when any crystal has one of its three pairs of cube faces perpendicular to the direction of view. At other orientations the crystals appear light. This property indicates that the crystal structure is not cubic, and is indicated in the series of pictures of Figure 7 which show the appearance of two nickel squarate crystals between crossed polarizers at various orientations with respect to the Nicols. The planes of polarization are vertical and horizontal for the polarizer and analyzer respectively. The exposures were made at 100X with a Zeiss polarizing photomicroscope kindly made available by Dr. Donald G. Biggs of the Geology Department at Iowa State University. The smaller crystal is 0.145 mm on edge.

In addition, color patterns are observed on the faces of the crystals when viewed between crossed Nicols; these do not appear uniform as expected for a single crystal but show a regular pattern, which has fourfold symmetry about a point in the center of the face; these patterns are the same for all pairs of faces through which the crystal is viewed. Figure 7 gives an indication of this symmetry in the patterns of dark and light observed in the crystal faces.

Figure 7. Appearance of $NiC_4O_4 \cdot 2H_2O$ crystals between crossed nicols. The planes of polarization of the polarizer and analyzer are vertical and horizontal respectively. Successive pictures show the crystals progressively rotated. The smaller crystal is approximately 0.145 mm on edge

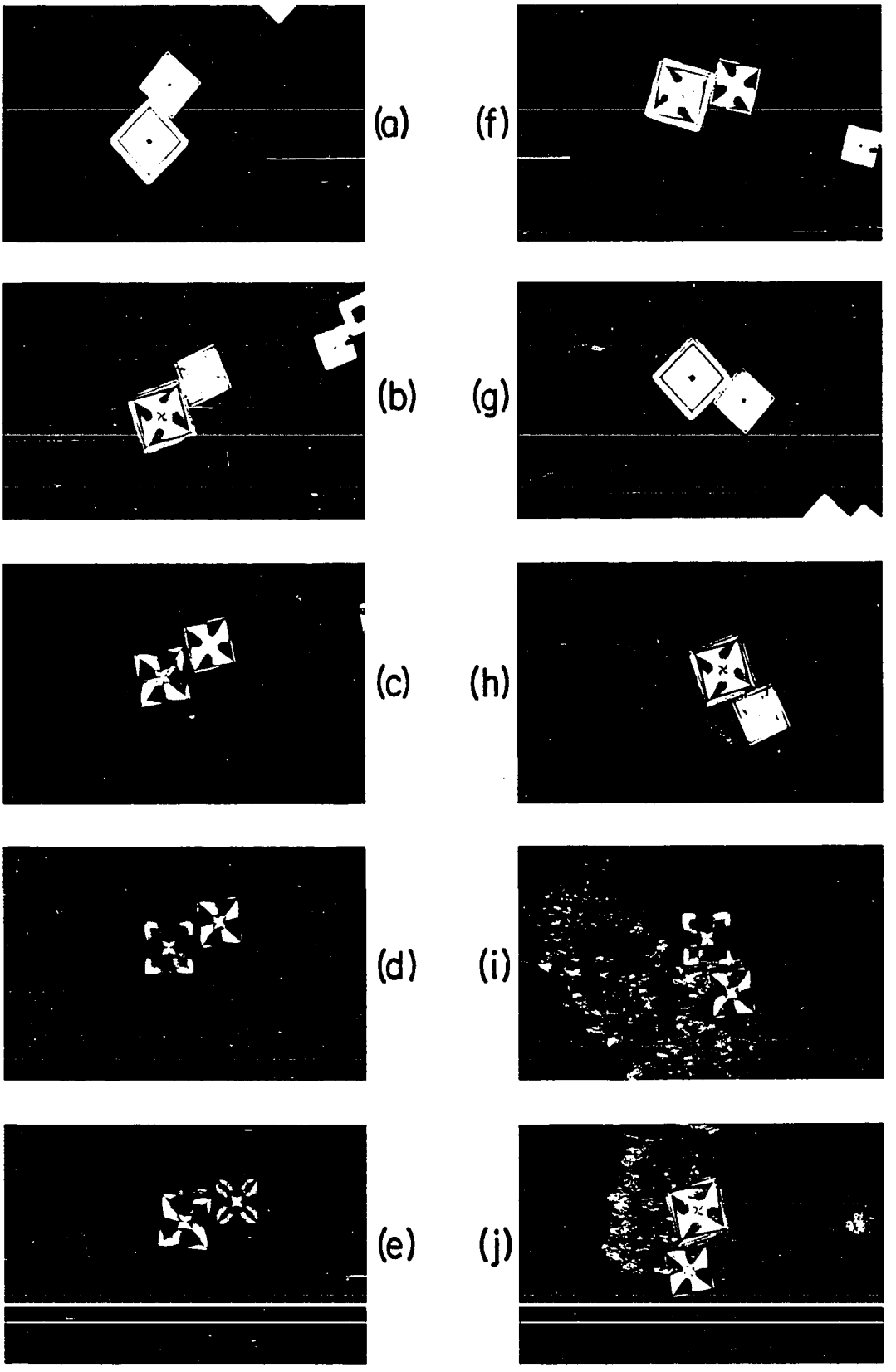
(a)
(f)
(b)
(g)
(c)
(h)
(d)
(i)
(e)
(j)

The diagonal lines separating these patterns are also seen in crystals viewed by transmitted light only, as seen in Figure 6. These observations indicate that the crystals are probably "twinned". Each crystal cube appears to consist of some multiple of six individuals. The appearance of the crystals under the microscope indicates that a crystal cube is made up of six square pyramids, the apexes of which are at the center of the cube and their bases forming the faces of the cube. Further, there are indications that each pyramid is composed of four individuals, bringing the total to twenty-four in a crystal cube.

Since the Debye-Scherer powder pattern of the silica gel grown crystals can be indexed assuming a cubic crystal lattice, however, the question arises as to why this is so, and a study of the "twinned" crystal cubes and single crystal fragments by single crystal X-ray techniques was expected to shed light on the twinning mode and lead to a structure solution.

In order to aid in the selection of a suitable crystal for single crystal X-ray investigation, the linear absorption coefficient was calculated for $NiC_4O_4 \cdot 2H_2O$ from values of mass absorption coefficients tabulated in ITXRC (1962). The values found are:

$$\mu(CuK\bar{\alpha}) = 38.6 \text{ cm}^{-1}$$
$$\mu(MoK\bar{\alpha}) = 27.8 \text{ cm}^{-1} \qquad (1)$$

This would give for the optimum crystal size (Stout and Jensen, 1968) for maximum scattering,

$$t_{opt}(CuK\bar{\alpha}) = 0.52 \text{ mm}$$
$$t_{opt}(MoK\bar{\alpha}) = 0.72 \text{ mm} \qquad (2)$$

Since a crystal of 0.52 mm size would require absorption corrections to the measured diffraction intensities it is desirable to use a smaller crystal of about 0.1 mm in its largest dimensions to permit elimination of absorption corrections. In the case of $NiC_4O_4 \cdot 2H_2O$ crystals, which grow as cubes, a crystal of about 0.1 mm on a side should be suitable for data collection without the use of absorption corrections; larger crystals require absorption corrections to the measured diffraction intensities.

Film Data

A "twinned" crystal cube of about 0.5 mm on a side was selected and mounted in a goniometer on a glass fiber with one face perpendicular to the goniometer axis. The crystal was aligned roughly under the microscope. Rotation photographs obtained on a Weissenberg camera showed a real cell axis parallel to the goniometer axis and perpendicular to two crystal faces, and the final alignment along this axis was performed on the Weissenberg camera. Rotation, hk0,

hk1, hk2 and hk3 reciprocal lattice level Weissenberg photographs were obtained and revealed the axis to be a fourfold rotation axis. The reciprocal lattice unit cell dimensions obtained from the rotation and the 0th level photographs agreed with the unit cell dimensions obtained from the powder patterns. The diffraction symmetry was found to be m3m, and no systematic extinctions were observed. The reciprocal lattice unit vectors are perpendicular to the faces of the crystal; the threefolds of the diffraction symmetry are along the body diagonals of the crystal; that is, the symmetry of the diffraction pattern (symmetry of the intensity weighted reciprocal lattice) coincides with the external shape symmetry of the crystal cube. For m3m diffraction symmetry a unique set of intensity data consists of all reflection intensities such that $h \geq k \geq \ell \geq 0$, which is 1/6 of an octant. The larger set of reflections ($h \geq k \geq 0$; $\ell = 0, 1, 2, 3$) was actually measured. In this set, groups of reflections (h,k,ℓ), (h,ℓ,k), (k,ℓ,h), should have the same diffraction intensities for m3m symmetry. This seemed to be the case on visual examination of the Weissenberg photographs, but was checked by making intensity measurements.

Intensity data was collected using the multiple film Weissenberg technique employing nickel filtered CuK_{α} radiation. Four films each of the 0th to 3rd reciprocal lattice

levels were obtained simultaneously by packing four films at a time into the camera. Diffraction intensities were estimated visually for each film using a calibrated spot density scale prepared with the same crystal. Transmission factors for each set of four films were calculated using an averaging procedure involving all reflections readable on two or more adjacent films. Using these factors, average intensities normalized to the most intense films were calculated for each reflection. Rough uncertainties were assigned to each reflection according to the following criteria:

$$\begin{aligned} \sigma(I^{o}) &= K \qquad \text{if } I^{o}<K \\ &= 0.2I^{o} \quad \text{if } I^{o}>K \end{aligned} \tag{3}$$

where K is 16 times the minimum intensity on the spot density scale and 0.2 is the density increment of the spot density scale. This assignment of uncertainties is similar to the one introduced by Hughes (1941) and often used for film data.

Lorentz-polarization and spot shape corrections to the intensities were made using tables from the ITXRC (1959). Absorption corrections were calculated using a program originally written by Busing and Levy (1957). The calculated transmission factors for the diffraction intensities varied from 0.160 to 0.322 for the (1, 0, 0) and (7, 7, 3) reflections, respectively. The observed relative absolute values

of the structure factors and their uncertainties were obtained using the relations

$$F^{O}(hk\ell) = [I^{O}(hk\ell)/(Lp)(A)]^{1/2}$$

$$\sigma(F^{O}) = \frac{\sigma(I^{O})}{2F^{O}(Lp)A} \qquad (4)$$

189 intensities were measured; of these, 3 were judged to be zero and 33 had $|F^{O}| \leq 2\sigma$; 134 were unique and 55 were related to the unique set by the diffraction symmetry. Even without bringing all intensities to a common scale, symmetry related intensities were within 2σ of their averages.

How to proceed from this point, however, presents a problem. In investigating a true single crystal a space group or several possible space groups are determined at this point from the diffraction symmetry and any observed extinction conditions. However, in this case, the optical observations indicate a non cubic crystal structure, with the crystal under investigation being a "twinned" crystal consisting of some multiple of six individuals. The observed m3m diffraction symmetry requires that the orientations of these individuals be related to each other in such a way that all diffraction maxima of one individual coincide with some diffraction maximum of every other individual. Further, the sum of the diffraction intensities

from all individuals must yield the observed m3m diffraction symmetry. This condition also requires that the dimensions and shape of the non-cubic unit cell of the true structure be very close to the cubic case, $a=b=c$, $\alpha=\beta=\gamma$. In none of the Debye-Scherer powder patterns and diffractometer powder pattern tracings are splittings of the lines observed. Some indications of splittings are observed in Weissenberg photographs of a "twinned" crystal at $2\theta \geq 140°$, where a splitting into three spots is observed with separations of about 1.0° in 2θ for the (10,0,0) reflection, for example. The splitting is in the direction of the reciprocal lattice line and can be interpreted as a combination of $K_{\alpha_1}-K_{\alpha_2}$ splitting which is about of the same magnitude, and a splitting of about 0.016Å in the lattice constant of 8.068(2)Å. The splitting is not found at smaller 2θ values, being smaller than the spot size, if it is real.

Since the twinning mode is not known one can only proceed with the analysis of the structure by ignoring the fact that the crystal is twinned and deriving a view of the "twinned" crystal as seen by the X-rays. This view will contain additional symmetry elements, introduced by the twinning, in addition to those of the true structure. It is hoped that these two types of symmetry can be separated and allow a structure for the compound to be deduced.

Accordingly, from the m3m diffraction symmetry and the

fact that no extinctions are observed, three possible space groups were found to be $P_{432}(O^1$, no. 207), P_{43m} $(T_d^1$, no. 215) and $P_{m3m}(O_h^1$, no. 221) (ITXRC, 1952). Since these space groups have 24, 24 and 48 general positions respectively, and there are only 3 $NiC_4O_4 \cdot 2H_2O$ units per unit cell, it follows that the Ni atoms and the centers of the $C_4O_4^=$ ions must be located at special positions. The special threefold positions in all three space groups are the same, (1/2,0,0; 0,1/2,0; 0,0,1/2) and (0,1/2,1/2; 1/2,0,1/2; 1/2,1/2,0). These positions correspond to the centers of the faces and the centers of the edges of the unit cell. One may put the nickels into either set of threefold positions and the squarate ions into the others; the two arrangements are equivalent. If the nickel atoms are placed in the positions (1/2,1/2,0; 1/2,0,1/2; 0,1/2,1/2) it is possible to calculate the diffraction intensities from the nickel atoms alone; since on the average the nickel atom contributes more than 30% of the diffraction intensity to each reflection, one would expect the experimental intensities to parallel the calculated intensities. For the nickel positions only, the structure factors can be derived from the general expression

$$F(hk\ell) = \sum_r f_r(hk\ell) \exp[2\pi i(hx_r + ky_r + \ell z_r)] \qquad (5)$$

This sum can be separated into a sum over equivalent positions, and a sum over atoms within an asymmetric unit:

$$F(hk\ell) = \sum_n f_r \left[\sum_m \exp[2\pi i(hx_{m,n}+ky_{m,n}+\ell z_{m,n})]\right] \qquad (6)$$

where the sum over n is over all unique atoms in an asymmetric unit and the sum over m is over the symmetry related atoms. The term in the square brackets can be written as

$$T(hk\ell)_n = \sum_m \cos 2\pi(hx_{m,n}+ky_{m,n}+\ell z_{m,n})$$

$$+ i \sum_m \sin 2\pi(hx_{m,n}+ky_{m,n}+\ell z_{m,n}) \qquad (7)$$

$$= A_n + iB_n$$

A_n and B_n are simplified by substituting the general positions of the space group under consideration. If the space group has a center of symmetry, then to every atomic position (x,y,z) there will correspond a position $(\bar{x},\bar{y},\bar{z})$ and therefore $B_n=0$. The simplified form of A_n for the space group P_{m3m}, which has 48 equivalent positions and is centrosymmetric is given in the ITXRC (1952) as

$$\begin{aligned} A = 8 \{&\cos(2\pi hx)[\cos(2\pi ky)\cos(2\pi\ell z)+\cos(2\pi\ell y)\cos(2\pi kz)] \\ &+\cos(2\pi hy)[\cos(2\pi kz)\cos(2\pi\ell x)+\cos(2\pi\ell z)\cos(2\pi kx)] \\ &+\cos(2\pi hz)[\cos(2\pi kx)\cos(2\pi\ell y)+\cos(2\pi\ell x)\cos(2\pi ky)]\} \\ B = 0 \end{aligned} \qquad (8)$$

The asymmetric unit contains only one nickel atom at (1/2, 1/2,0). The symmetry operations generate 48 other atoms at the same or different positions. Since there are only three Ni atoms per unit cell, expression (8) must be multiplied by 1/16. The structure factor expression for three nickel atoms in positions (1/2,1/2,0; 1/2,0,1/2; 0,1/2,1/2) in space group P_{m3m} then reduces to

$$\begin{aligned} F(hk\ell) &= \frac{1}{16} \times 8\ [2\cos(\pi h)\cos(\pi k)+2\cos(\pi h)\cos(\pi \ell) \\ &\quad + 2\cos(\pi k)\cos(\pi \ell)]f_{Ni}(hk\ell) \\ &= [(-1)^h(-1)^k+(-1)^\ell+(-1)^k(-1)^\ell]f_{Ni}(hk\ell) \qquad (9) \\ &= 3f_{Ni}(hk\ell), \text{ if h, k, } \ell \text{ are all even or all odd} \\ &= -f_{Ni}(hk\ell), \text{ otherwise} \end{aligned}$$

Or, the calculated diffraction intensities are

$$\begin{aligned} I(hk\ell) &= 9f_{Ni}^2(hk\ell), \text{ if h, k, } \ell \text{ are all even or all odd} \\ &= f_{Ni}^2(hk\ell), \text{ otherwise.} \qquad (10) \end{aligned}$$

The observed diffraction intensities do roughly follow these rules, although the other atoms in the unit cell are expected to modify this result somewhat. If either space group P_{432} or $P_{\bar{4}3m}$ had been used, the results would have been the same. Although neither space group is centric, a center is added by the Ni atoms if they are in the special positions discussed.

The position of the Ni atoms was confirmed by calculating a Patterson (Patterson, 1935; Buerger, 1959) function which is functionally the same as a Fourier electron density function but uses $|F(hk\ell)|^2$ as the coefficient of the exponential terms instead of $F(hk\ell)$.

$$\rho(xyz) = \frac{1}{V} \sum_{\substack{hk\ell \\ -\infty}}^{\infty} F(hk\ell)\exp[-2\pi i(hx+ky+\ell z) \quad \text{(electron density)} \tag{11}$$

$$P(uvw) = \frac{1}{V} \sum_{\substack{hk\ell \\ -\infty}}^{\infty} |F(hk\ell)|^2 \exp[-2\pi i(hu+kv+\ell w) \quad \text{(Patterson)} \tag{12}$$

This function, instead of giving the electron density distribution in the unit cell obtained if a conventional electron density Fourier synthesis were made, exhibits peaks at all points which are end points of vectors between atoms in the actual structure. All these vectors originate at the origin of the Patterson map. The intensities of the peaks are proportional to the product of the atomic scattering factors of the atoms to which the interatomic vector belongs. If, as in nickel squarate, there are heavy atoms such as Ni(Z=28) and light atoms such as O(Z=8) and C(Z=6) then the intensities of peaks due to Ni-Ni, Ni-O, Ni-C, O-O, C-C and O-C peaks should be proportional to the product of the atomic numbers of the two atoms involved, that is in the ratios of 784:224:168:64:36:48. There is an intense origin peak proportional to $\sum_r Z_r^2$. Although one has to contend with

multiplicities, it is usually simple to differentiate between heavy-heavy, heavy-light and light-light peaks. The heavy-heavy interatomic vectors are then used to determine the positions of the heavy atoms by inspection or by superposition techniques. The heavy atom positions are used to calculate phases which are assigned to the observed moduli of the structure factors $|F(hk\ell)|$. This procedure is called the heavy atom method for determining the phases of the observed $|F(hk\ell)|$'s. With these phases an electron density map can be calculated which will show additional atoms besides the heavy atoms.

In the case of $NiC_4O_4 \cdot 2H_2O$, the Patterson map was used to confirm the tentative placement of the nickel atoms in the special positions as discussed previously. For space group P_{m3m}, expression (12) simplifies to (ITXRC, 1952)

$$P(uvw) = \frac{8}{V} \sum_{\substack{uvw \\ 0}}^{\infty} |F(hk\ell)|^2 \cos(2\pi hu)\cos(2\pi kv)\cos(2\pi \ell w) \qquad (13)$$

A program written by D. E. Williams[1] was used to calculate the Patterson map using the observed $|F(hk\ell)|^2$'s obtained from films as discussed previously. It was assumed that the scale factors for the four reciprocal lattice levels were approximately the same since the films from which they were

---

[1]Williams, D. E., Iowa State University of Science and Technology, Ames, Iowa. A FORTRAN IV program to calculate electron density and Patterson maps for orthorhombic and cubic space groups. Private communication. 1966.

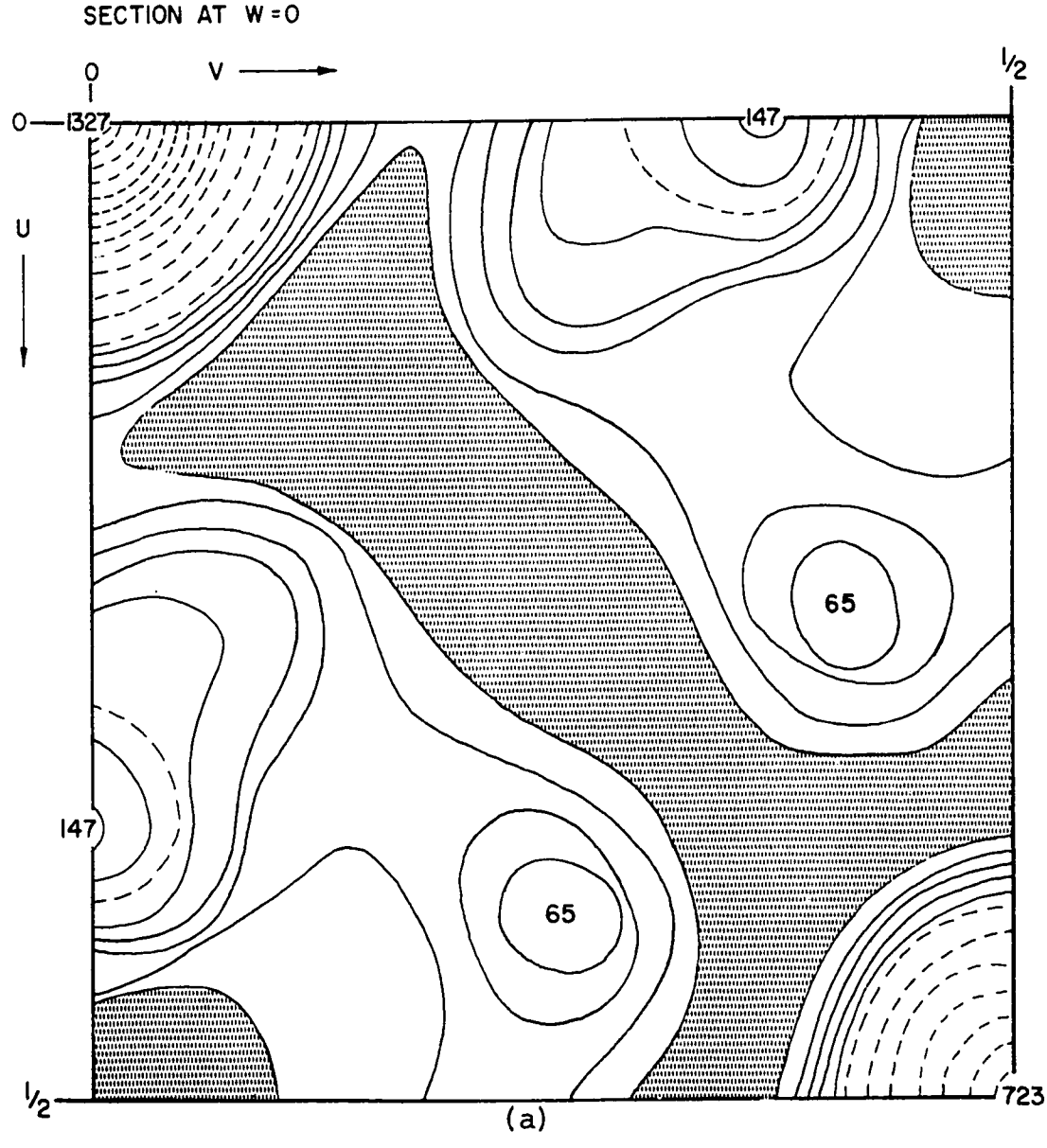

Figure 8. Patterson map calculated from film data. The scale is arbitrary. Solid contours are drawn at intervals of 20, starting at 0. Dashed contours are drawn at intervals of 100 starting at 100. Negative areas are stippled ((a) One quarter of section at w=0; the rest of the section is obtained by rotating the map about a fourfold rotation axis perpendicular to the section at the origin, (b) Patterson map section at w=1/2)

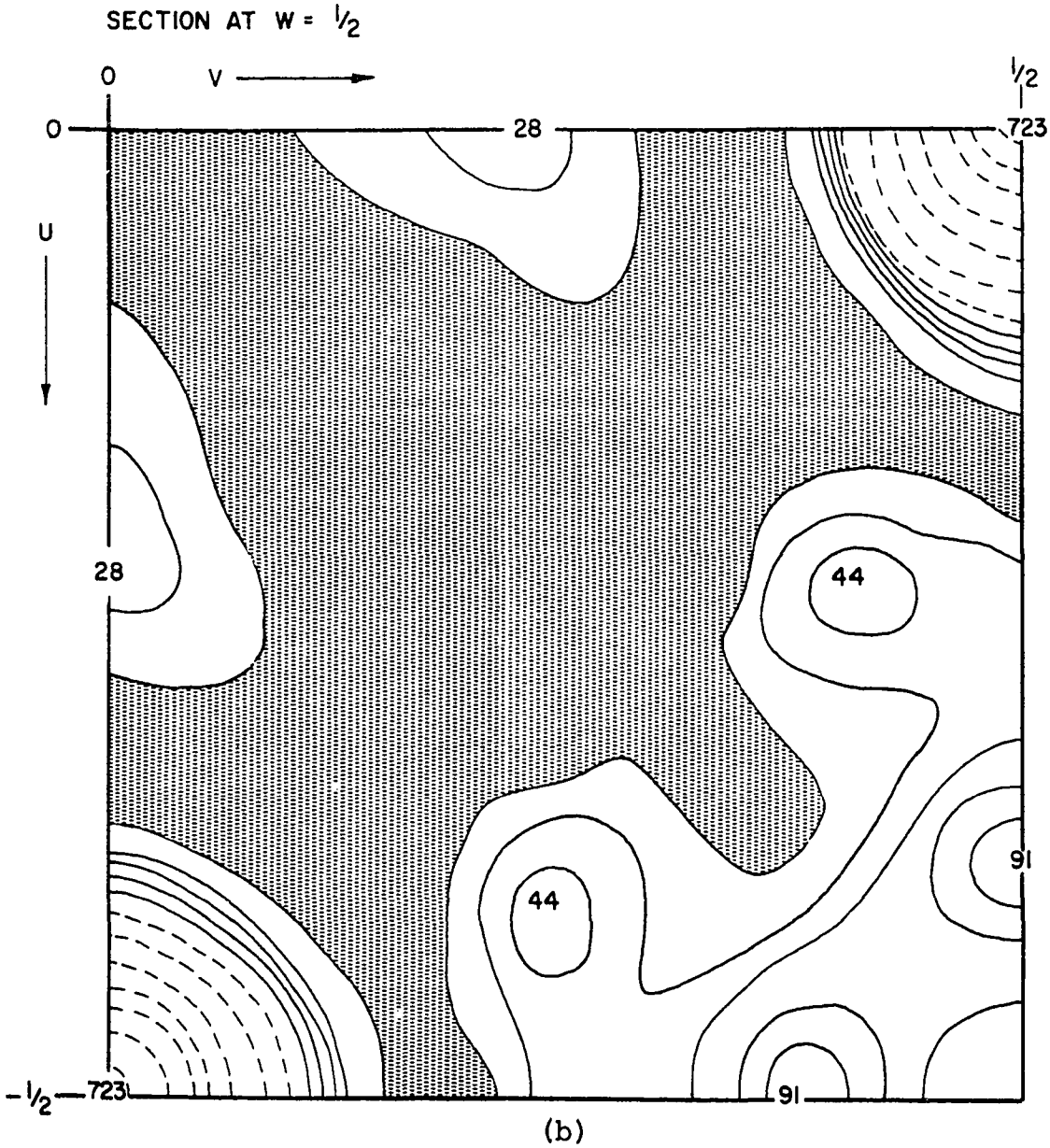

(b)

Figure 8 (Continued)

derived were taken under identical conditions as far as possible. The w=0 and 1/2 sections of the calculated Patterson map are given in Figure 8. The Ni-Ni peaks are observed at (1/2,1/2,0; 0,1/2,1/2; 1/2,0,1/2). These are exactly the interatomic vectors obtained from the positions assumed for the Ni atoms in the previous discussion.

Since $(\Sigma Z_{Ni}^2)/\Sigma Z_{O,C}^2 = 784/532 \simeq 1.4$, the phases derived from the nickel positions should be very good, but in any subsequent least squares refinement the R factor will be somewhat insensitive to the positions of the light atoms and the refinement will yield large uncertainties in the positional parameters of the light atoms (Stout and Jensen, 1968, p. 278). Phases were assigned to the measured $|F(hk\ell)|$'s and the same program used in the Patterson synthesis was used to calculate an electron density map. The result is given in Figure 9. Figure 9(b) shows the electron density in one quarter of the z=1/2 unit cell face; Figure 9(a) shows the whole face. The outlines of two squarate ions can be seen, related to each other by mirror planes parallel to the z-axis. The skeleton of a squarate ion of dimensions as found in $K_2C_4O_4 \cdot 2H_2O$ (Macintyre and Werkema, 1964) has been superimposed on one set of peaks. The oxygen peaks fit the assumed geometry well. The carbon peaks of the two ions are not well resolved. The intensities of the squarate oxygen peaks relative to the intensities of

the Ni peaks are such as to suggest only half an oxygen atom for each of the eight oxygen peaks in the face, the total being four squarate oxygens per face, or one squarate ion per face. The only significant electron density observed inside the unit cell is exemplified by the peaks seen in Figure 9(c) and 9(d) which show sections at z=0.433 and z=0.233; the peaks are those with peak heights of 22 and can be identified as water oxygens (the peaks with peak heights of 17 in the z=0.434 section are part of the squarate oxygen peaks in the z=1/2 section, and the ones with peak heights of 30 in the z=0.233 section are squarate oxygens in the yz and xz faces). The intensities of the water oxygen peaks relative to the intensities of the Ni peaks are such as to suggest only one quarter of an oxygen atom at each of the positions indicated in the sections at z=0.433 and z=0.233. There are twenty-four such peaks in the unit cell while there should only be six water oxygens per unit cell. It seems that the total electron density for the six water oxygen atoms is distributed over twenty-four peaks, each of them of intensity equivalent to 1/4 of an oxygen atom.

Since two squarate ions cannot simultaneously occupy the same face of the unit cell and since the total electron density in the face represents only one squarate ion it follows that the observed electron density map is due to the

Figure 9. Electron density map of $NiC_4O_4 \cdot 2H_2O$ calculated from film data collected on a "twinned" crystal. The scale is in $0.1e\text{Å}^{-3}$. Solid contours are drawn at intervals of $1e\text{Å}^{-3}$ and dashed contours are drawn at intervals of $10e\text{Å}^{-3}$ starting at $10e\text{Å}^{-3}$, ((a) Section at z=0.5; the whole face. Areas where $\rho(xyz) < 1e\text{Å}^{-3}$ are stippled. (b) Section at z=0.5; 1/4 of the face. (c) Section at z=0.433; 1/2 of the section. (d) Section at z=0.233, 1/4 of the section)

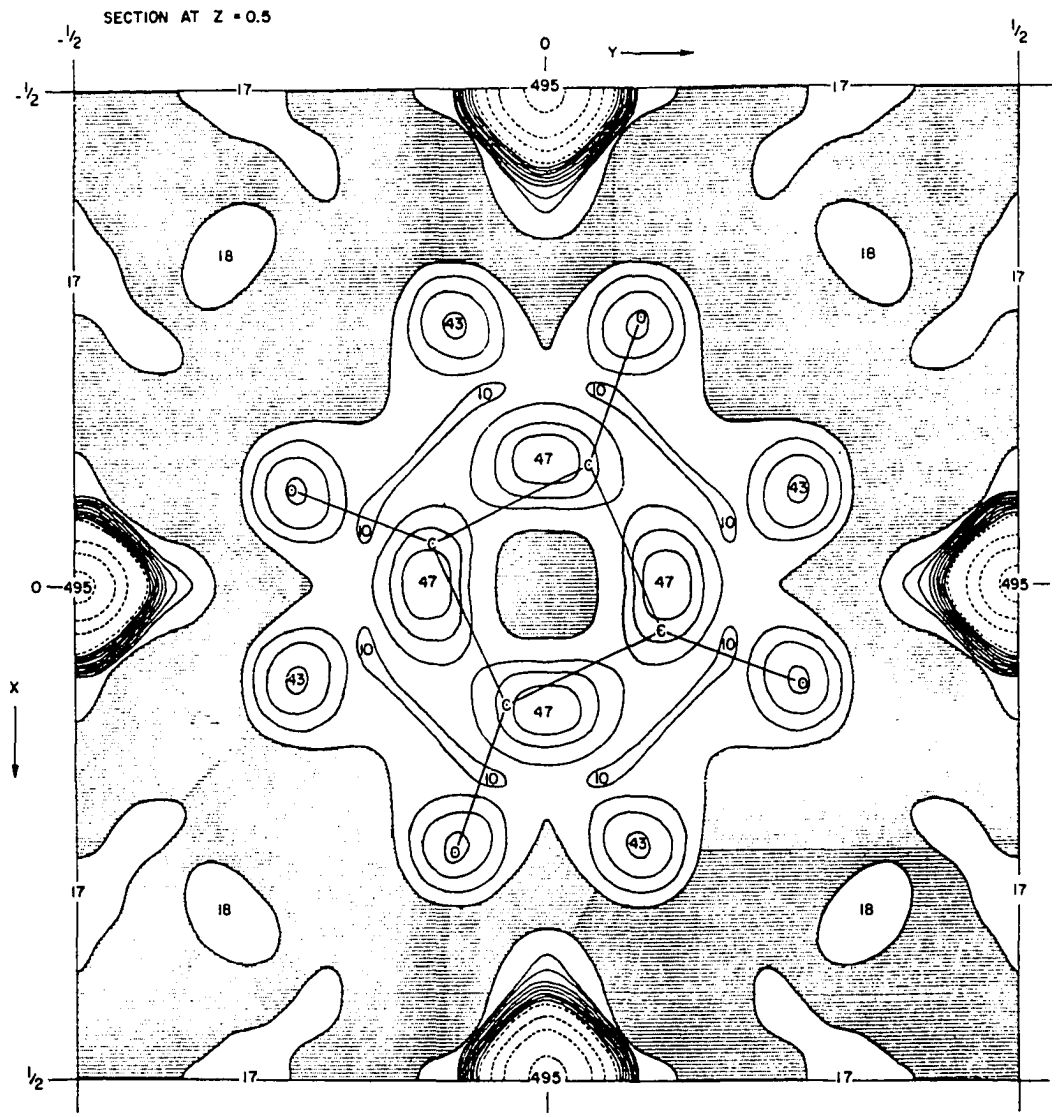
SECTION AT Z = 0.5
-½
0
Y
½
-½
17
495
17
18
18
17
17
43
0
10
10
47
C
0
10
10
43
0
495
495
X
10
10
47
47
C
10
43
C
47
0
10
10
0
43
17
18
18
17
½
17
495
17

(a)

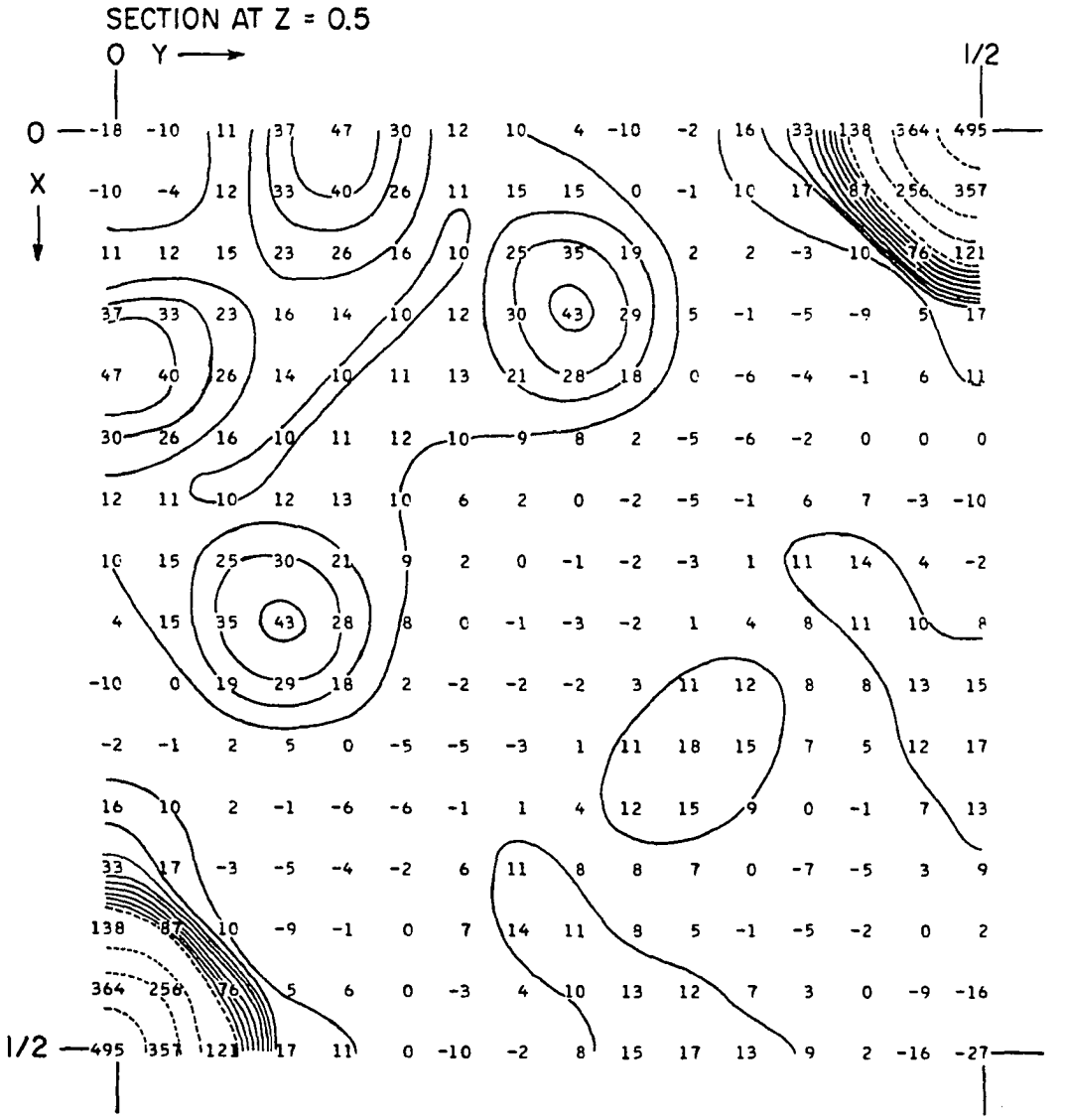

(b)

Figure 9 (Continued)

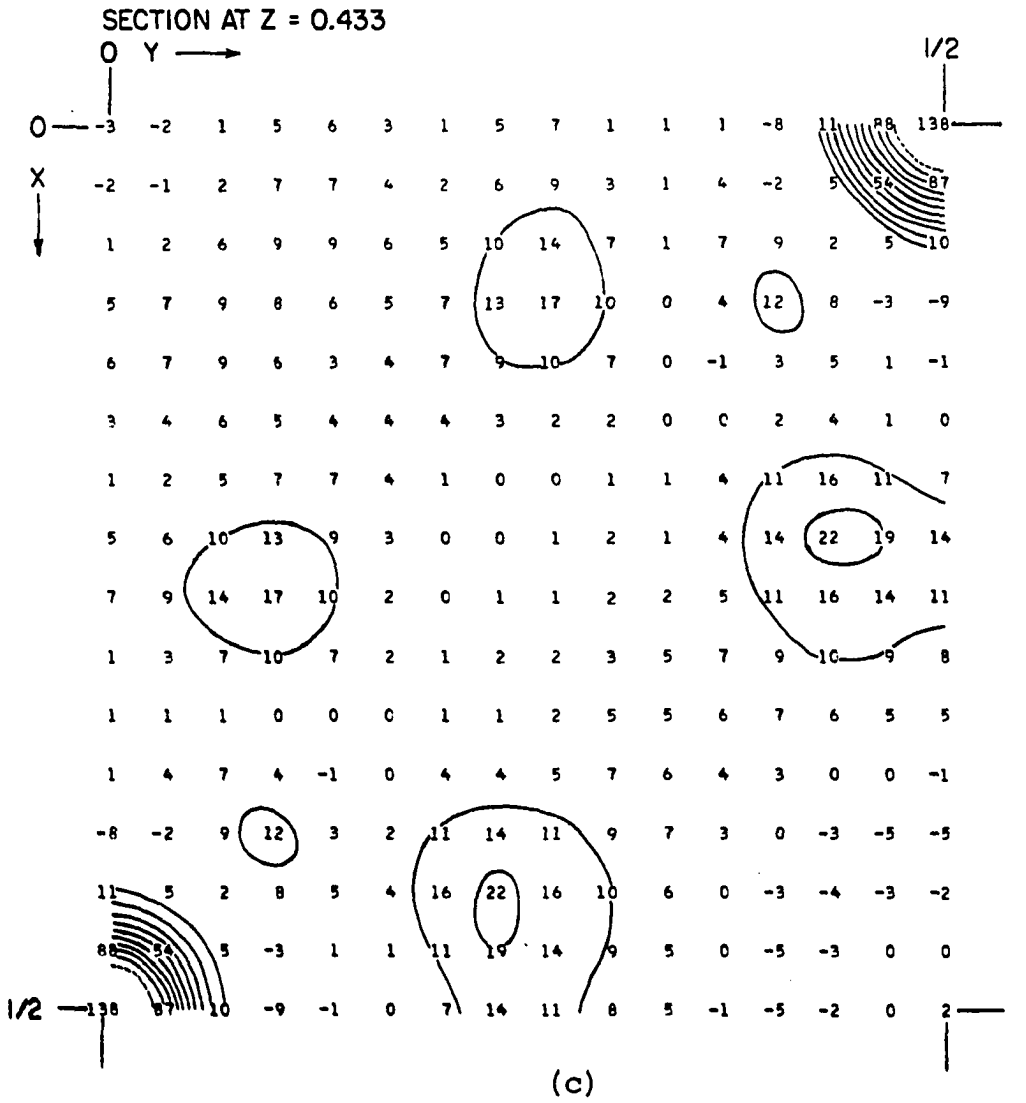

Figure 9 (Continued)

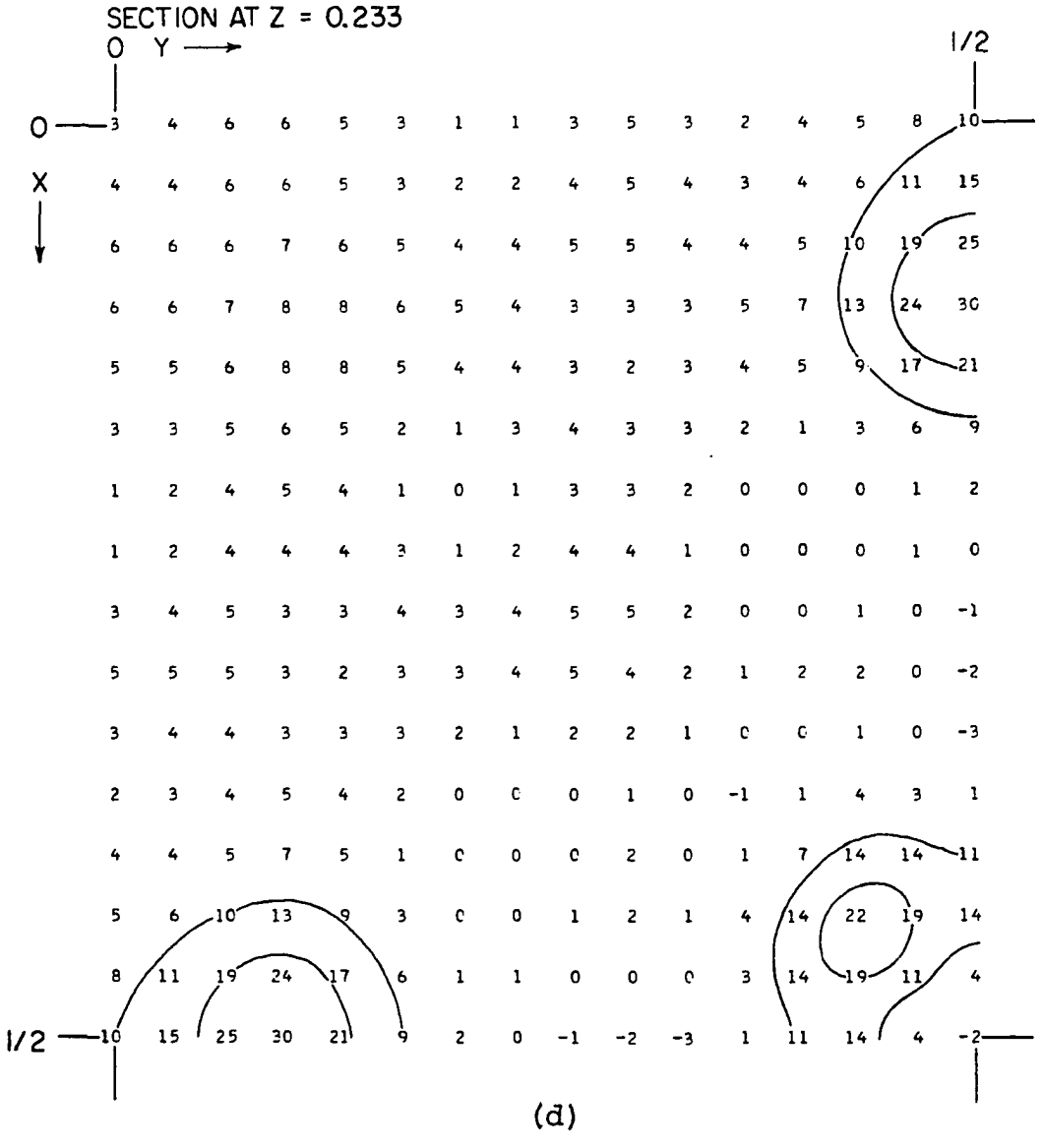

(d)

Figure 9 (Continued)

fact that the crystal under investigation is multiply twinned, and the observed image results from superposition of the images from two or more individuals in which the squarate ions are in different orientations. As seen by the X-rays, the arrangement of the Ni atoms appears the same in all individuals of the "twinned" crystal and only the orientation of the squarate ions and the positions of the water molecules differ for different individuals.

The structure of the unit cell of an untwinned crystal could be that shown in Figure 10. The Ni atoms are in the middle of the unit cell edges and the squarate ion is in the unit cell faces, with each squarate O atom bonded to a different Ni atom. The squarate ion is oriented so that a line through the O-C-C-O atoms of the squarate ion makes an angle of $\simeq 20°$ with a line through two Ni atoms on opposite edges of the unit cell face. The three squarate ions are arranged so that there is a threefold axis of rotation along the (1,1,1) direction in the unit cell. The water O atoms are placed around the Ni atoms to complete O octahedra about the Ni atoms. In order to produce a "twinned" crystal with m3m diffraction symmetry one would need some multiple of eight individuals with their threefold axes pointing along both directions of the body diagonals of the unit cell of the "twinned" crystal. In Figure 10 the water oxygens are drawn for only one Ni atom in order

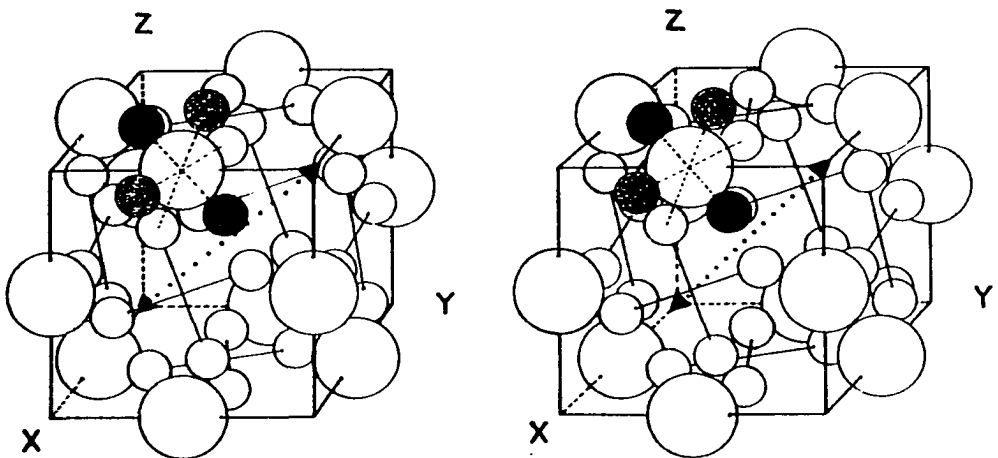

Figure 10. Proposed structure for $NiC_4O_4 \cdot 2H_2O$. Schematic stereo pair. The large spheres represent Ni atoms (Slater radius=1.35A); the smaller spheres represent oxygen atoms (Slater radius=0.60Å). The squarate ion is represented by the squarate oxygens only. The octahedral coordination about one Ni atom is indicated. The stippled circles represent squarate oxygen atoms from different unit cells and the solid black circles represent water oxygens. The rest of the water oxygen atoms have been omitted to avoid undue complication in the diagram. There is a C_3 rotation axis along the body diagonal indicated as a dotted line

to avoid undue complexity, and to show the octahedral coordination about the Ni atom.

In this proposed structure, there is no reason why the angles between the (1,0,0), (0,1,0) and (0,0,1) axes should be 90°. The threefold rotation axis along the (1,1,1) direction only requires that they be equal, and in general, one would expect the structure as depicted in Figure 10 to be elongated or compressed along the (1,1,1) direction.

If the actual structure is in fact as proposed above, the observed cubic diffraction symmetry and unit cell dimensions (including unit cell angles) for the twinned crystal indicate that such a distortion is very small. The squarate ions need not be exactly in the plane of the unit cell face. In fact it is considered most likely that they are tipped slightly out of the faces in order to render the coordination about the Ni atoms more closely octahedral, the threefold symmetry along the (1,1,1) direction being maintained. In this proposed structure it is possible for each water molecule to form two hydrogen bonds to two squarate oxygens on different squarate ions which have a lone pair of electrons situated in a favorable position. In fact it is these hydrogen bonds which might in large measure stabilize the structure as it is proposed. If, however, one admits the possibility that the squarate ions are not

strictly coplanar with the Ni atoms to which they are bonded, then one must recognize that the peaks observed in the electron density map are really the sum of peaks slightly above and below the apparent common plane observed. Such a possibility would be reflected in electron density peaks elongated in the direction perpendicular to the apparent squarate ion plane; it would also cast some uncertainty on bond lengths and bond angles derived from the average positions of the squarate ions.

To obtain rough C-C, C-O and Ni-O bond distances, a least squares refinement of all atomic positions as seen in the Fourier map was performed, although it was recognized that the bond distances obtained in this manner would not be very accurate because the assumed structure in the refinement would be incorrect. The space group P_{m3m} was assumed and the nickel atoms were placed in the special positions found from the Patterson. The squarate oxygen and carbon atoms were placed in the positions obtained from the Fourier map with occupation factors of 1/2. The water oxygen was placed in the observed position with an occupation factor of 1/4. Isotropic temperature factors were used and only the (x,y) coordinates of the squarate oxygen and carbon atoms, the (x,y,z) coordinates of the water oxygen atom, all isotropic temperature factors and four scale factors (for the hk0, hkl, hk2 and hk3 reflections respectively) were allowed

to vary. The refinement was carried out using a full matrix least squares program (Busing, Martin and Levy, 1962). Atomic scattering factor tables used were those of Hansen, Herman, Lea and Skillman (1964) and those in ITXRC (1962). Weights for each reflection were taken as $w(h,k,\ell) = [\sigma(h,k,\ell)]^{-2}$ where $\sigma(h,k,\ell)$ is the estimated uncertainty in $F^{o}(h,k,\ell)$ as described previously. All data were used in the refinement. Four cycles of refinement led to a discrepancy factor,

$$R = \Sigma \, ||F^{o}| - |F^{c}|| / \Sigma \, |F^{o}| \qquad (14)$$

of 15.2%, and a weighted discrepancy factor,

$$R_{w} = (\Sigma w(F^{o} - F^{c})^{2})^{1/2} / (\Sigma w(F^{o})^{2})^{1/2} \qquad (15)$$

of 20.6%. The positional parameters and temperature factors are given in Table 7. The uncertainties in the positional parameters are 0.015-0.025Å and will result in bond distances with large uncertainties. Ni-O, C-O, and C-C bond distances obtained from the positional parameters in Table 7 are given in Table 8 (Busing, Martin and Levi, 1964). The geometry of the squarate ion and the coordination about the nickel atom deduced from these results consistent with the proposed structure given in Figure 10 is shown in Figure 11. The Ni-O bond distances are within the accepted range of 1.95-2.17Å observed in various compounds (Slater, 1965;

Table 7. Positional and thermal parameters derived from the film data

Atom	x	y	z	B
Ni	0.0[a]	0.5[a]	0.5[a]	3.76(14)
Os	0.1041(18)	0.2629(19)	0.5[a]	5.12(30)
C	0.0412(26)	0.1228(25)	0.5[a]	5.35(54)
Ow	0.2343(23)	0.4075(28)	0.4421(32)	2.01(44)

[a]Parameter not varied.

ITXRC, 1962). The C-O and C-C bond distances are within their e.s.d.'s of the values found for the squarate ion in $K_2C_4O_4 \cdot H_2O$ by Macintyre and Werkema (1964, see Figure 2(b)). The C-C-O bond angles of the squarate ion are found to be 140.6(2.1)° and 129.4(2.1)° which deviate considerably from the 135° expected for the ion with D_{4h} symmetry. The various O-Ni-O bond angles given in Table 8 and Figure 11

Table 8. Bond distances and angles derived from the film data

bond distances		bond angles	
$Ni-O_s$	2.089(15) Å	O_s-C-C	140.6(2.1)°
$Ni-O_w$	2.085(19) Å	$C-O_s-Ni$	132.1(1.3)°
$C-O_s$	1.239(24) Å	O_s-Ni-O_w	92.1(0.6)°
C-C	1.478(30) Å	O_s-Ni-O_s'''	80.7(0.3)°
		$O_w-N_i-O_s'''$	99.2(0.3)°

angle of cocking of squarate ion in the face: 21.6°

Figure 11. Bond distances and bond angles derived from film data assuming "twinning" and actual structure as given in Figure 10. The complete coordination about only one Ni atom is shown. All atoms except the water O atoms and the two squarate O atoms indicated are at z=0.5. The z coordinates of two squarate O atoms and two water O atoms are given. The z coordinates of the rest of the water O atoms depend on the choice of orientation of the squarate ion in the xz and yz face. The circles indicating the atoms are drawn to correspond to Slater atomic radii (Ni-1.35Å, O-0.60Å, C-0.70Å)

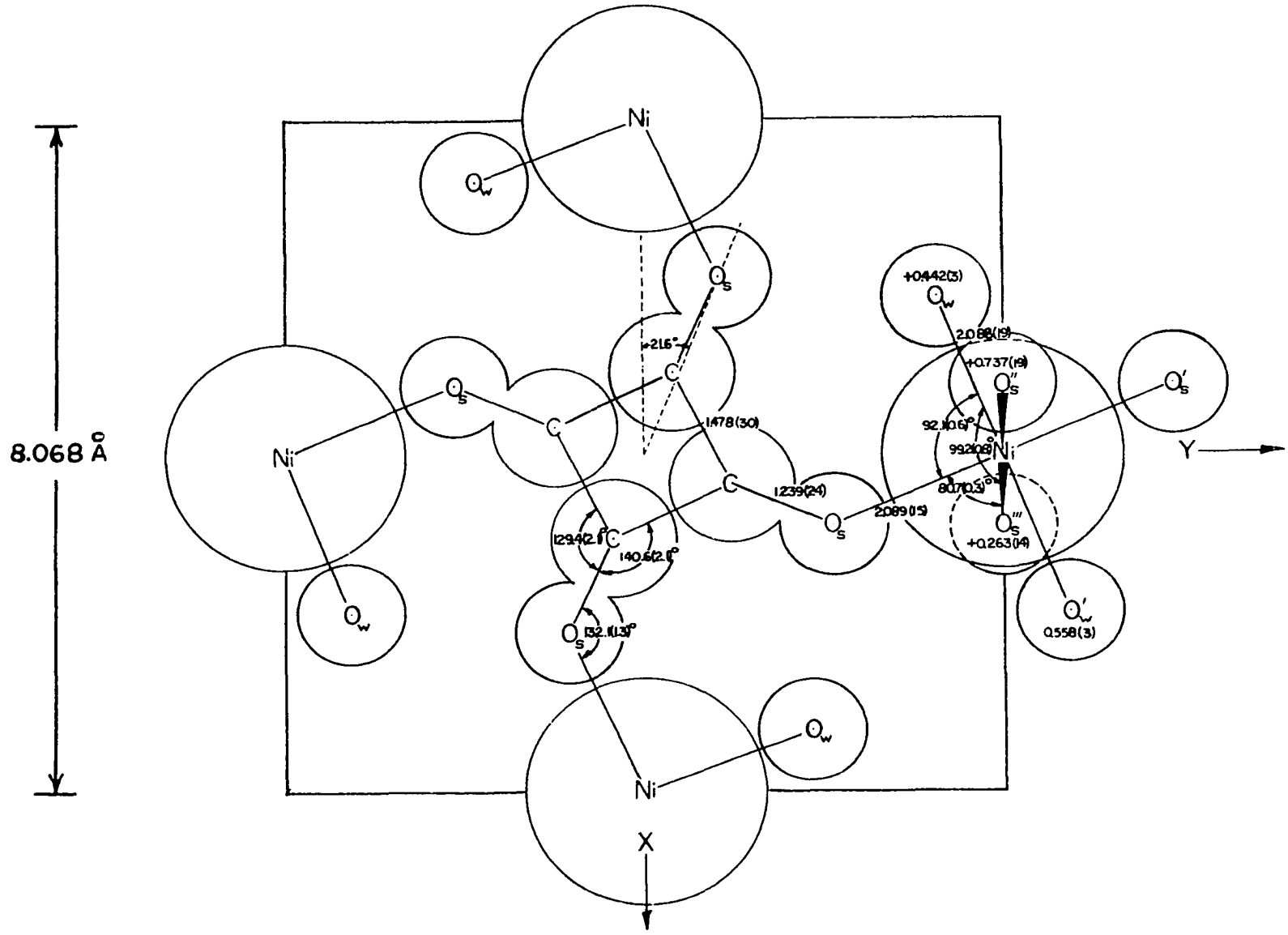
8.068 Å
Ni
O_w
O_s
+21.6°
1.478(30)
C
1.239(24)
O_s
2.089(15)
+0.442(3)
O_w
2.088(19)
+0.737(19)
O''_s
92.1(0.6)°
99.2(0.8)°
Ni
80.7(0.5)°
O'''_s
+0.263(14)
O'_s
Y
O'_w
0.558(3)
129.4(2.1)°
C
140.6(2.1)°
O_s
132.1(1.3)°
O_w
Ni
X

vary from 80.7 to 99.2°. These angles could be closer to 90° if the squarate ion were allowed to tilt slightly out of the plane, without altering the Ni-O bond distances significantly.

The large temperature factor found for the Ni atom could be due to generally inaccurate data, or it could be due to the possibility that in the real structure the shape of the unit cell deviates sufficiently from the cubic case, so that Ni atoms in different individuals in the "twinned" crystal are not on lattices strictly commensurate, thus yielding a diffraction pattern which is characteristic of an enlarged atom. The least squares program can only accommodate the trial structure to this situation by increasing the temperature factor of the nickel atom. This same type of effect might be operating with respect to the squarate ion atoms if the ion is in fact tilted slightly out of the face.

A list of observed and calculated structure factors is given in Table 9.

Counter Data

In order to determine the cause of the large estimated standard deviations in the atomic positions and the large temperature factor obtained for Ni, intensity data was collected for a second crystal on a General Electric single crystal orienter using Zr filtered MoK_{α} radiation. The

Table 9. Observed and calculated structure factors for the "twinned" crystal. Film data. R=15.2%

L = 0			
H	K	FO	FC
1	0	287	-428
2	0	762	1049
3	0	511	-589
4	0	658	654
5	0	395	-324
6	0	85	120
7	0	58	-70
8	0	219	205
9	0	24	-22
10	0	66	61
1	1	358	-561
2	1	114	51
3	1	398	-276
4	1	35	-18
5	1	194	-195
6	1	70	76
7	1	95	-93
8	1	36	-31
9	1	82	-69
10	1	23	-4
2	2	377	364
3	2	156	-147
4	2	487	430
5	2	170	-135
6	2	209	169
7	2	52	-50
8	2	181	153
9	2	32	-22
10	2	37	40
3	3	197	-167
4	3	164	-157
5	3	84	-64
6	3	33	-3
7	3	100	-59
8	3	55	-47
9	3	22	-15
4	4	163	132
5	4	154	-123
6	4	129	115
7	4	27	-13
8	4	118	93
5	5	78	58
6	5	54	-67
7	5	27	-13
8	5	66	-57
6	6	152	126
7	6	28	-23
8	6	65	56
7	7	47	-37

L = 1			
H	K	FO	FC
1	0	377	-561
2	0	101	51
3	0	327	-276
4	0	37	-18
5	0	166	-195
6	0	61	76
7	0	83	-93
8	0	15	-31
9	0	70	-69
10	0	15	-4
1	1	466	341
2	1	88	-122
3	1	451	376
4	1	87	-82
5	1	342	344
6	1	0	-37
7	1	110	98
8	1	55	-36
9	1	104	92
10	1	0	-11
2	2	89	-92
3	2	151	-110
4	2	195	-210
5	2	118	-100
6	2	138	-128
7	2	36	-8
8	2	63	-54
9	2	34	-25
10	2	17	-12
3	3	370	411
4	3	64	-60
5	3	293	293
6	3	58	-58
7	3	139	124
8	3	59	-49
9	3	62	63
4	4	50	59
5	4	80	-87
6	4	59	-44
7	4	44	-54
8	4	20	-5
9	4	45	-36
5	5	154	160
6	5	49	-35
7	5	105	98
8	5	33	-35
9	5	34	40
6	6	91	-90
7	7	66	65

L = 2			
H	K	FO	FC
1	0	117	51
2	0	382	364
3	0	152	-147
4	0	478	430
5	0	168	-135
6	0	189	169
7	0	52	-50
8	0	174	153
9	0	28	-22
10	0	32	40
1	1	126	-122
2	1	99	-92
3	1	163	-110
4	1	191	-210
5	1	119	-100
6	1	144	-128
7	1	36	-8
8	1	59	-54
9	1	35	-25
10	1	14	-12
2	2	233	262
3	2	84	-92
4	2	419	422
5	2	83	-70
6	2	222	237
7	2	43	-51
8	2	134	119
9	2	34	-24
3	3	153	-165
4	3	170	-178
5	3	118	-108
6	3	74	-63
7	3	66	-51
8	3	32	-25
4	4	168	188
5	4	76	-79
6	4	143	153
7	4	24	-17
8	4	85	72
5	5	46	-54
6	5	25	-29
7	5	54	-55
8	5	26	-11
6	6	109	120
7	6	0	-12
8	6	32	38
7	7	33	-44

L = 3			
H	K	FO	FC
1	0	339	-276
2	0	175	-147
3	0	175	-167
4	0	158	-157
5	0	89	-64
6	0	39	-3
7	0	93	-59
8	0	46	-47
9	0	14	-15
1	1	478	376
2	1	166	-110
3	1	385	411
4	1	70	-60
5	1	305	293
6	1	62	-58
7	1	143	124
8	1	63	-49
9	1	65	63
2	2	86	-92
3	2	150	-165
4	2	171	-178
5	2	111	-108
6	2	78	-63
7	2	70	-51
8	2	33	-25
3	3	339	420
4	3	25	-35
5	3	231	256
6	3	69	-72
7	3	122	123
8	3	48	-44
9	3	36	44
4	4	75	-61
5	4	36	-25
6	4	62	-63
7	4	29	-17
8	4	28	-33
5	5	128	139
6	5	47	-47
7	5	76	83
8	5	18	-23
6	6	50	-47
7	6	17	-16
7	7	28	46

crystal used was a cube 0.114 mm on a side; it was oriented in the same way as the one used in collecting the film data, the fourfolds of the apparent m3m diffraction symmetry again being perpendicular to pairs of crystal faces. The crystal was oriented in the spectrogoniometer (single crystal orienter) using the procedures of Furnas (1957) who gives a comprehensive description of the use of the spectrogoniometer. Three reflections, (8,0,0), (0,8,0) and (0,0,8) were used as standard reflections, and were used throughout the data taking procedure to check the stability of the X-ray source and crystal alignment. No systematic variations in the diffraction intensities of these standard reflections was observed during the period of intensity measurements.

From the instrumental orienter settings for these three reflections a value of $a = 8.068_5 \text{Å}$ for the cubic lattice constant was calculated, in excellent agreement with the value of 8.068(2) obtained from Debye-Scherer powder patterns. The orienter settings for these three reflections were used also to generate the settings for all reflections with $2\theta \leq 100°$, using a program written by Williams[1].

The intensities of the reflections were measured using

---

[1]Williams, D. E., Department of Chemistry, Iowa State University of Science and Technology, Ames, Iowa. Generation of single crystal orienter angles. Private communication. 1966.

a θ-2θ coupled scan with a 5° takeoff angle. Forty second stationary-counter background counts were made before and after the scan across the reflection. The scan across the reflection was at an angular velocity of 2°/minute in 2θ for 100 seconds, or a total scan of 3.32°. The scan was started 1.6° in 2θ before the calculated position of the reflection, placing the reflection approximately at the mid-point of the scan. A ratemeter output of the count rate on a chart recorder was monitored to insure that all of a particular reflection was included in the scan.

The integrated count for each reflection was corrected for background by subtracting an average integrated background count (=1.25(BGRD1+BGRD2)). Lorentz and polarization corrections were made. Absorption corrections were made in the same manner as discussed for the film data. The linear absorption coefficient used was 27.8 cm^{-1} and the calculated transmission factors varied from 0.758 to 0.788 for the (1,0,0) and (6,6,6) reflections respectively. Standard deviations were assigned to the intensities according to the formula:

$$\sigma(I_o) = (C + C_b + (0.05C)^2 + (0.05C_b)^2 + (0.05A)^2)^{1/2} \quad (16)$$

where C, C_b, and A are the total counts, the background counts, and the absorption correction respectively. The quadratic terms correspond to estimated systematic errors in

the total counts and background counts due to X-ray tube instability and estimated errors in the absorption correction of 5%. The standard deviations of the observed structural factors were calculated using Equation 4.

All 481 possible reflections with $h \geq k \geq \ell \geq 0$ and with $2\theta<90°$ ($\sin \theta/\lambda < 0.996$) were scanned. Of these, 288 reflections were found to have intensities above background; an additional 25 were found to have $F^o \leq 2\sigma$ and were taken to be unobserved. This resulted in a unique set of 263 reflections. Many of these were measured twice and some more often; duplicate measurements were averaged. In addition, 44 reflections which are related to the unique set by the diffraction symmetry were also measured (to check the diffraction symmetry); two of these had $F^o<2\sigma$. It was found that the intensities of 39 of these were within σ, and the rest were within 2σ of the average of the symmetry related reflection intensities.

An electron density map was calculated from this data using phases determined from assumed Ni positions as discussed previously for the film data. The results are given in Figure 12. Figure 12(a) shows a section through the whole face at $z=1/2$. As can be seen the carbon atom peaks of the two superimposed squarate ions are now resolved. The squarate ion skeleton superimposed on one set of peaks has the dimensions found for the ion in $K_2C_4O_4 \cdot H_2O$. A more

Figure 12. Electron density map calculated from counter data collected on a "twinned" crystal. The scale is in $0.1e\text{Å}^{-3}$. Solid contours are drawn at intervals of $1e\text{Å}^{-3}$, starting at $1e\text{Å}^{-3}$, and dashed contours are drawn at intervals of $10e\text{Å}^{-3}$ starting at $10e\text{Å}^{-3}$ ((a) Section at z=0.5; the whole face. Areas where $\rho(xyz)<1e\text{Å}^{-3}$ are stippled. (b) Section at z=0.5; 1/4 of the face. (c) Section at z=0.438; 1/4 of the section. (d) Section at z=0.219; 1/4 of the section)

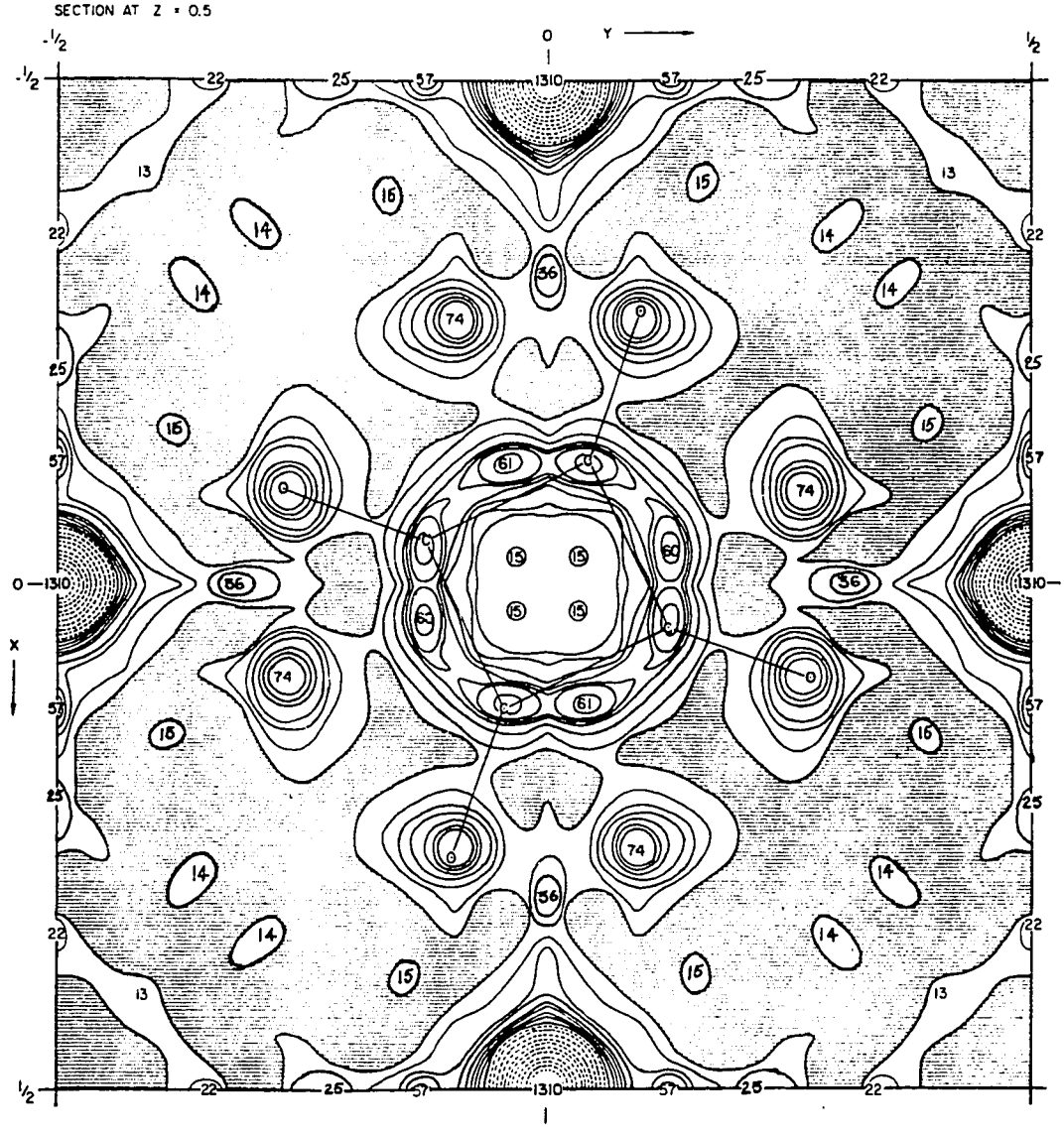

(a)

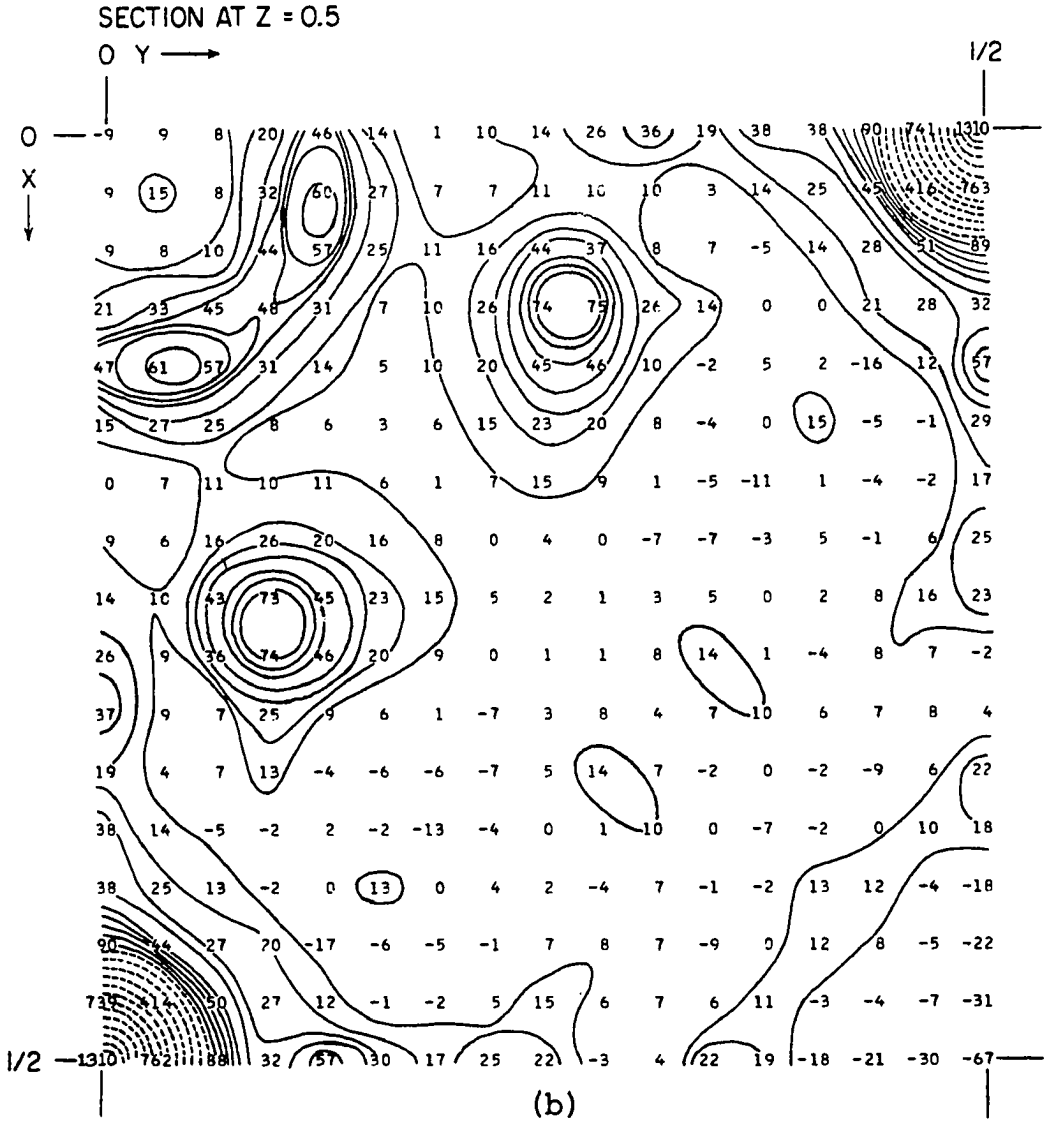

Figure 12 (Continued)

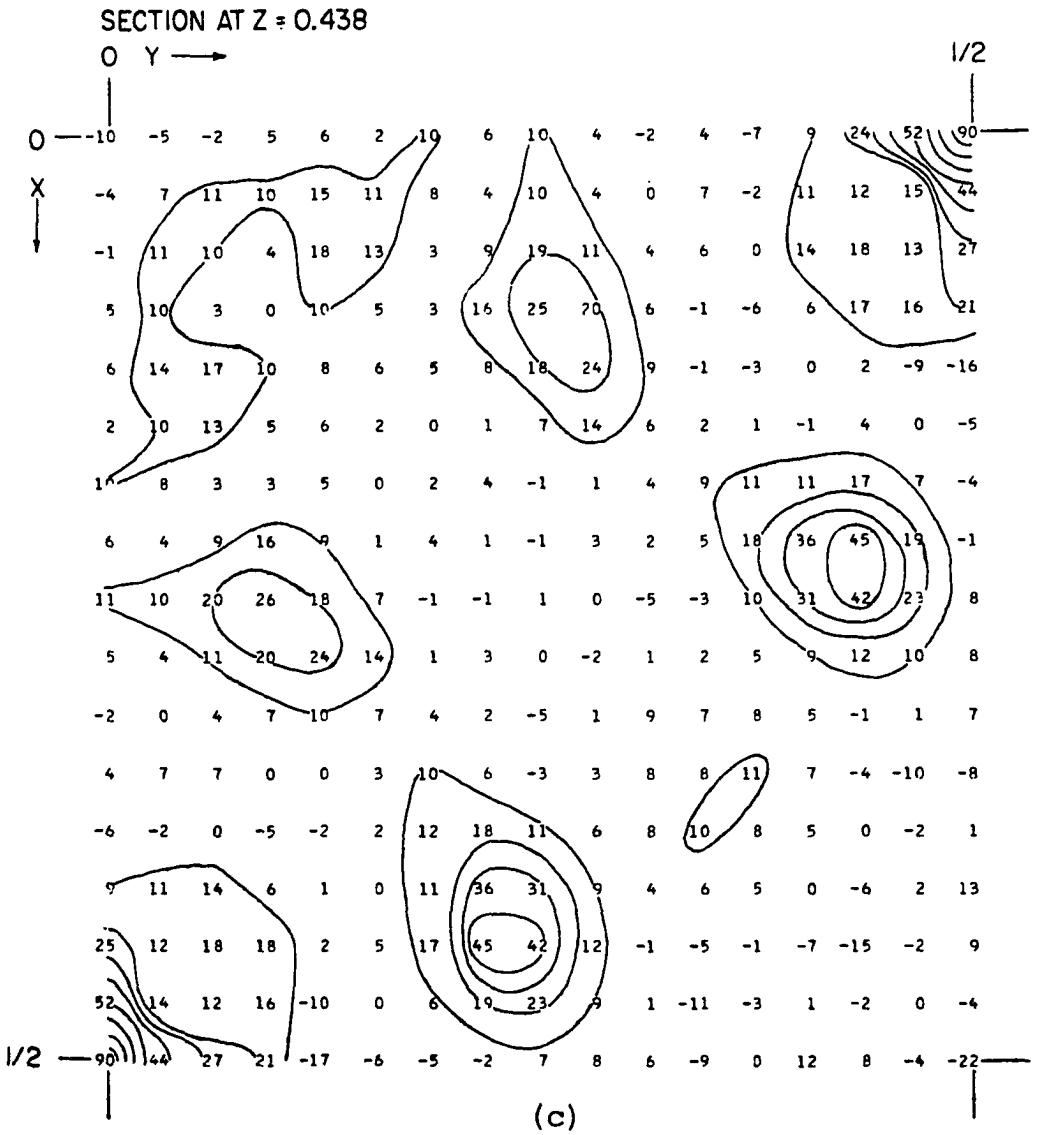

Figure 12 (Continued)

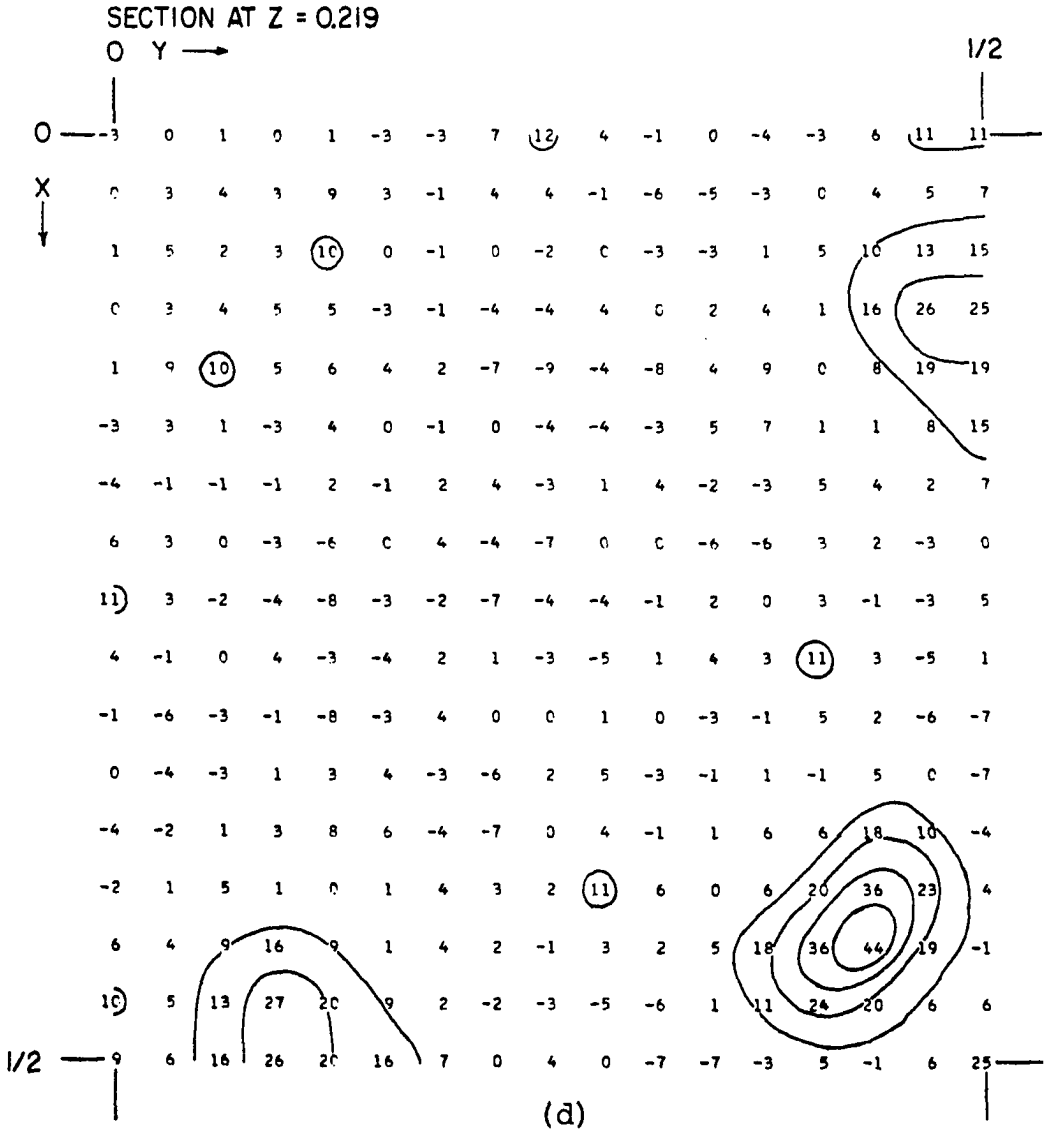

Figure 12 (Continued)

detailed map is given in Figure 12(b) where only one quarter of the section at z=1/2 is shown. Figures 12(c) and 12(d) show sections at z=0.438 and z=0.219. These sections show the water oxygen peaks in the positive octant of the unit cell. The conclusions reached from consideration of the electron density map calculated from the film data also hold for the counter data map. In addition one can see that the squarate oxygen peak as seen in Figure 12(d) is elongated in the direction perpendicular to the face it is in. This could be an indication that the squarate ion is tilted out of the plane of the nickel atoms.

A least squares refinement using the above 307 observed reflections and using the positional and isotropic-thermal parameters obtained from the film data led, after four cycles of full matrix least squares refinement, to an unweighted R factor of 10.1% and a weighted R factor of 10.4%. The resulting positional and thermal parameters are given in Table 10. The calculated bond distances and bond angles, assuming the structure to be as given in Figure 10, are given in Table 11. As can be seen, the thermal parameters for the Ni, O_S and C atoms have been reduced, compared to the film data, by 57%, 40% and 38% respectively. The thermal parameter of the O_W atom has increased slightly. The positional parameters have changed somewhat, the changes ranging from one to five times the e.s.d.'s in the film data

Table 10. Positional and isotropic thermal parameters derived from counter data for a "twinned" crystal

Atom	x	y	z	B
N_i	0.0[a]	0.5[a]	0.5[a]	1.60(44)
O_s	0.0979(13)	0.2647(13)	0.5[a]	3.07(18)
C	0.0457(17)	0.1222(18)	0.5[a]	3.33(31)
O_w	0.2366(20)	0.4202(58)	0.4336(62)	2.09(39)

[a]Parameters not varied.

Table 11. Bond distances and bond angles derived from counter data for a "twinned" crystal assuming isotropic thermal parameters

bond distances		bond angles	
$Ni-O_s$	2.056(10)Å	O_s-C-C	134.6(1.4)°
$Ni-O_w$	2.084(16)Å	$C-O_s-Ni$	140.6(2.1)°
O_s-C	1.224(16)Å	$O -Ni-O_w$	93.8(1.3)°
C-C	1.489(20)Å	O_s-Ni-O_s'''	81.5(0.2)°
		O_w-Ni-O_s'''	96.6(1.3)°

Squarate ion orientation: angle between O-C-C-O vector of squarate ion and across face Ni-Ni vector:

from O position, $\theta = 20.3\ (\pm 0.4)$

from C position, $\theta = 20.5\ (\pm 1.0)$

positional parameters. For the O_s and C atoms the e.s.d.'s decreased by about 30%. For the O atom the e.s.d. in the x coordinate remained the same, while the e.s.d.'s in the y and z coordinates doubled. The decreases in the thermal parameters and in some e.s.d.'s of the positional parameters were expected because of the greater accuracy of the counter data and the larger number of reflections measured; the increase in the e.s.d.'s of the O_w positional parameters is not explained.

Since the electron density map calculated from the counter data gave indications that the O_s atoms had a non-spherical electron peak distribution it was decided to carry out a least squares refinement using anisotropic thermal parameters. Because of symmetry the Ni atom had to be considered to vibrate isotropically, while for the O_s and C atoms one principle vibration direction had to be assumed perpendicular to the unit cell face. This attempt was unsuccessful because the thermal parameter matrix of the O_w atom was not positive definite after one cycle of refinement. Therefore a least squares refinement was performed in which the Ni and O_w atoms were assumed to have isotropic temperature factors and the O_s and C atoms were considered to have anisotropic temperature factors; after two cycles of least squares refinement an unweighted R factor of 8.8% and a weighted R factor of 9.4% were obtained. The resulting

Table 12. Positional and thermal parameters derived from counter data for a "twinned" crystal, assuming anisotropic thermal parameters[a] for O_s and C

	Atom			
	Ni	O_s	C	O_w
x	0.0[b]	0.0981(11)	0.0460(14)	0.2363(19)
y	0.5[b]	0.2642(10)	0.1220(14)	0.4189(37)
z	0.5[b]	0.5[b]	0.5[b]	0.4339(39)
β_{11}x10^3	5.84(0.30)	8.21(1.31)	9.05(1.69)	9.53(2.11)
β_{22}	5.84[b]	7.57(1.24)	7.41(1.36)	9.53[b]
β_{23}	5.84[b]	20.96(2.16)	17.00(2.27)	9.53[b]
β_{12}	0[b]	-1.86(1.09)	1.48(1.23)	0[b]
β_{13}	0[b]	0[b]	0[b]	0[b]
β_{23}	0[b]	0[b]	0[b]	0[b]

[a]Thermal parameters are defined by $\exp[-(\beta_{11}h^2+\beta_{22}k^2+\beta_{33}\ell^2+2\beta_{12}hk+2\beta_{13}h\ell+2\beta_{23}k\ell)]$.

[b]Parameters not varied.

positional and thermal parameters are given in Table 12 and the resulting bond distances, assuming a structure as given in Figure 10 are given in Table 13 and Figure 13. The changes in the positional parameters in going from isotropic thermal parameters to anisotropic thermal parameters for O_s and C are all less than the e.s.d.'s of either set of the positional parameters. The e.s.d.'s themselves have all decreased somewhat. The derived bond distances and bond angles are also within their e.s.d.'s of each other in the two cases. A list of observed and calculated structure factors resulting from the counter data taken on the "twinned" crystal is given in Table 14.

Table 13. Bond distances and bond angles derived from counter data for a "twinned" crystal, assuming anisotropic thermal parameters for O_s and C

bond distances		bond angles	
$Ni-O_s$	2.060(9)Å	$C-O_s-Ni$	137.3(0.8)°
$Ni-O_w$	2.085(16)Å	O_s-C-C	134.4(1.2)°
O_s-C	1.222(14)Å	O_s-Ni-O_w	93.5(1.1)°
C-C	1.487(16)Å	O_s-Ni-O_s'''	81.5(0.2)°
		O_w-Ni-O_s'''	96.6(1.1)°

Squarate ion orientation: angle between O-C-C-O vector of squarate ion and across face Ni-Ni vector

from O position θ = 20.3(0.4)°

from C position θ = 20.5(1.0)°

Table 14. Observed and calculated structure factors for the "twinned" crystal. Counter data. R=8.8%

L = 0

H	K	FO	FC
1	0	399	-459
2	0	1307	1195
3	0	575	-623
4	0	821	806
5	0	453	-457
6	0	186	196
7	0	114	-105
8	0	374	377
9	0	65	-68
10	0	199	184
11	0	64	-62
12	0	121	130
13	0	102	-82
14	0	80	65
0	1	403	-459
1	1	511	-605
3	1	411	-336
4	1	61	-61
5	1	242	-234
6	1	62	55
7	1	144	-150
8	1	76	-71
9	1	128	-127
10	1	61	-52
11	1	65	-58
12	1	57	-48
13	1	51	-32
0	2	1309	1195
2	2	514	497
3	2	195	-198
4	2	646	608
5	2	222	-230
6	2	335	319
7	2	97	-84
8	2	335	337
9	2	79	-77
10	2	152	152
11	2	69	-55
12	2	79	98
0	3	603	-623
1	3	404	-336
2	3	194	-198
3	3	221	-222
4	3	216	-220
5	3	116	-103
6	3	7	-27*
7	3	140	-116
8	3	98	-96
9	3	63	-52
10	3	49	-34
11	3	58	-43
0	4	821	806
1	4	66	-61
2	4	668	608
3	4	218	-220
4	4	295	279
5	4	225	-215
6	4	247	248
7	4	52	-63
8	4	243	242
9	4	42	-17
10	4	181	186
11	4	37	-27
12	4	115	101
0	5	450	-457
1	5	245	-234
2	5	225	-230
3	5	114	-103
4	5	228	-215
5	5	52	54
6	5	100	-97
7	5	54	-50
8	5	136	-122
9	5	24	-13*
10	5	64	-47
11	5	49	-52
12	5	62	-27
0	6	192	196
6	6	286	281
7	6	66	-79
8	6	179	177
9	6	49	-59
10	6	125	123
11	6	31	-29*
12	6	76	67
6	7	57	-79
7	7	104	-97
8	7	67	-70
9	7	49	-38
11	7	66	-40
0	8	383	377
7	8	69	-70
8	8	135	140
9	8	63	-52
10	8	112	101
12	8	46	67
8	9	77	-52
9	9	62	-45
8	10	110	101
10	10	69	61
0	14	66	65

L = 1

H	K	FO	FC
0	1	462	-605
1	1	632	457
2	1	131	-152
3	1	596	520
4	1	140	-136
5	1	553	538
6	1	37	-58
7	1	232	235
8	1	111	-112
9	1	247	241
10	1	19	-27*
11	1	128	142
12	1	14	-10*
13	1	152	128
15	1	13	45*
1	2	132	-152
2	2	134	-124
3	2	191	-161
4	2	264	-271
5	2	174	-173
6	2	217	-213
7	2	75	-68
8	2	100	-111
9	2	70	-68
10	2	65	-54
11	2	42	-40
12	2	25	-34*
0	3	378	-336
1	3	585	520
2	3	195	-161
3	3	595	567
4	3	103	-106
5	3	492	485
6	3	113	-101
7	3	280	271
8	3	116	-116
9	3	177	191
10	3	66	-59
11	3	122	131
13	3	115	99
3	4	117	-106
4	4	34	25
5	4	140	-142
6	4	101	-103
7	4	83	-94
8	4	54	-45
9	4	118	-113
10	4	103	-98
11	4	76	-53
12	4	48	-49
13	4	39	-39
3	5	486	485
4	5	134	-142
5	5	308	331
6	5	106	-108
7	5	243	244
8	5	77	-87
9	5	154	154
10	5	42	-47
11	5	146	133
12	5	25	-25*
13	5	65	78
5	6	88	-108
6	6	169	-175
7	6	52	-36
8	6	45	-37
9	6	46	-38
10	6	51	-56
6	7	66	-36
7	7	212	209
8	7	76	-56
9	7	134	128
10	7	55	-26*
11	7	97	96
1	8	97	-112
6	8	18	-37*
9	9	118	113
10	9	59	-9

L = 2

H	K	FO	FC
0	2	524	497
1	2	125	-124
2	2	384	348
3	2	121	-124
4	2	579	587
5	2	89	-113
6	2	373	424
7	2	88	-71
8	2	290	306
9	2	65	-86
10	2	138	133
11	2	65	-61
12	2	96	82
3	3	234	-219
4	3	254	-246
5	3	190	-178
7	3	126	-114
8	3	91	-84
9	3	49	-39
10	3	42	-24
3	4	256	-246
4	4	333	341
5	4	147	-141
6	4	305	312
7	4	63	-53
8	4	219	224
10	4	19	169*
4	5	125	-141*
5	5	104	-104
6	5	58	-61
7	5	118	-117
8	5	75	-68
9	5	62	-36
10	5	14	-27
5	6	74	-61
6	6	282	288
7	6	39	-56
8	6	163	158
9	6	73	-54
10	6	122	117
7	7	135	-127
8	7	44	-44
9	7	59	-49
10	7	29	-29
8	8	100	121
10	8	100	94
9	9	29	-46*

L = 3

H	K	FO	FC
0	3	214	-222
3	3	525	578
4	3	77	-72
5	3	397	440
6	3	122	-127
7	3	252	271
8	3	100	-105
9	3	137	154
10	3	30	-82*
11	3	115	118
4	4	123	-118
5	4	73	-70
6	4	115	-117
7	4	62	-58
8	4	65	-77
9	4	57	-65
10	4	19	-70*
11	4	49	-40
5	5	267	301
6	5	110	-119
7	5	190	224
8	5	74	-69
9	5	129	129
10	5	62	-64
11	5	119	113
6	6	111	-112
7	6	40	-48
8	6	47	-37
5	7	211	224
7	7	150	181
8	7	27	-39*
9	7	88	110
8	8	37	-29
9	9	81	97

L = 4

H	K	FO	FC
0	4	271	279
4	4	119	153
6	4	212	237
7	4	44	-69
8	4	190	195
9	4	48	13
10	4	165	174
11	4	40	-17
12	4	97	87
5	5	49	-28
6	5	68	-77
7	5	57	-45
8	5	91	-84
9	5	36	-51*
10	5	64	-55
11	5	56	-42
6	6	220	237
7	6	75	-81
8	6	146	156
9	6	61	-27
10	6	117	122
11	6	29	-32*
7	7	26	-51*
8	7	81	-72
9	7	51	-49
10	7	25	-43*
8	8	114	129
9	9	47	-57

L = 5

H	K	FO	FC
5	5	170	221
6	5	102	-118
7	5	144	186
8	5	58	-45
9	5	86	116
10	5	47	-53
11	5	86	96
6	6	52	-28
7	6	63	-68
8	6	52	-28
9	6	48	-45
8	7	24	-27*
9	7	65	104
10	7	36	-37*
11	7	85	75
8	8	43	-39
9	8	29	-29*
10	8	21	-21*
9	9	81	88
11	9	79	57

L = 6

H	K	FO	FC
0	6	273	281
6	6	147	174
7	6	55	-54
8	6	100	110
10	6	89	87
12	6	48	70
7	7	47	-45
8	7	63	-45
9	7	25	-36*
8	8	84	91
9	8	26	-25*
10	8	62	67
11	8	69	-23

L = 7

H	K	FO	FC
0	7	112	-97
7	7	107	124
9	7	80	92
10	7	26	-30*
11	7	69	63
8	8	39	-45
9	9	79	76

L = 8

H	K	FO	FC
8	8	119	140
8	8	67	79
10	8	64	53

L = 9

H	K	FO	FC
9	9	73	62

Figure 13. Bond distances and bond angles derived from counter data assuming "twinning" and actual structure as given in Figure 10. The complete coordination about only one Ni atom is shown. All atoms except the water O atoms and two squarate O atoms, as indicated, are at z=0.5. The z coordinates of two O atoms and two squarate O atoms are given. The z coordinates of the rest of the water O atoms depend on the assumed orientations of the squarate ions in the xz and yz faces

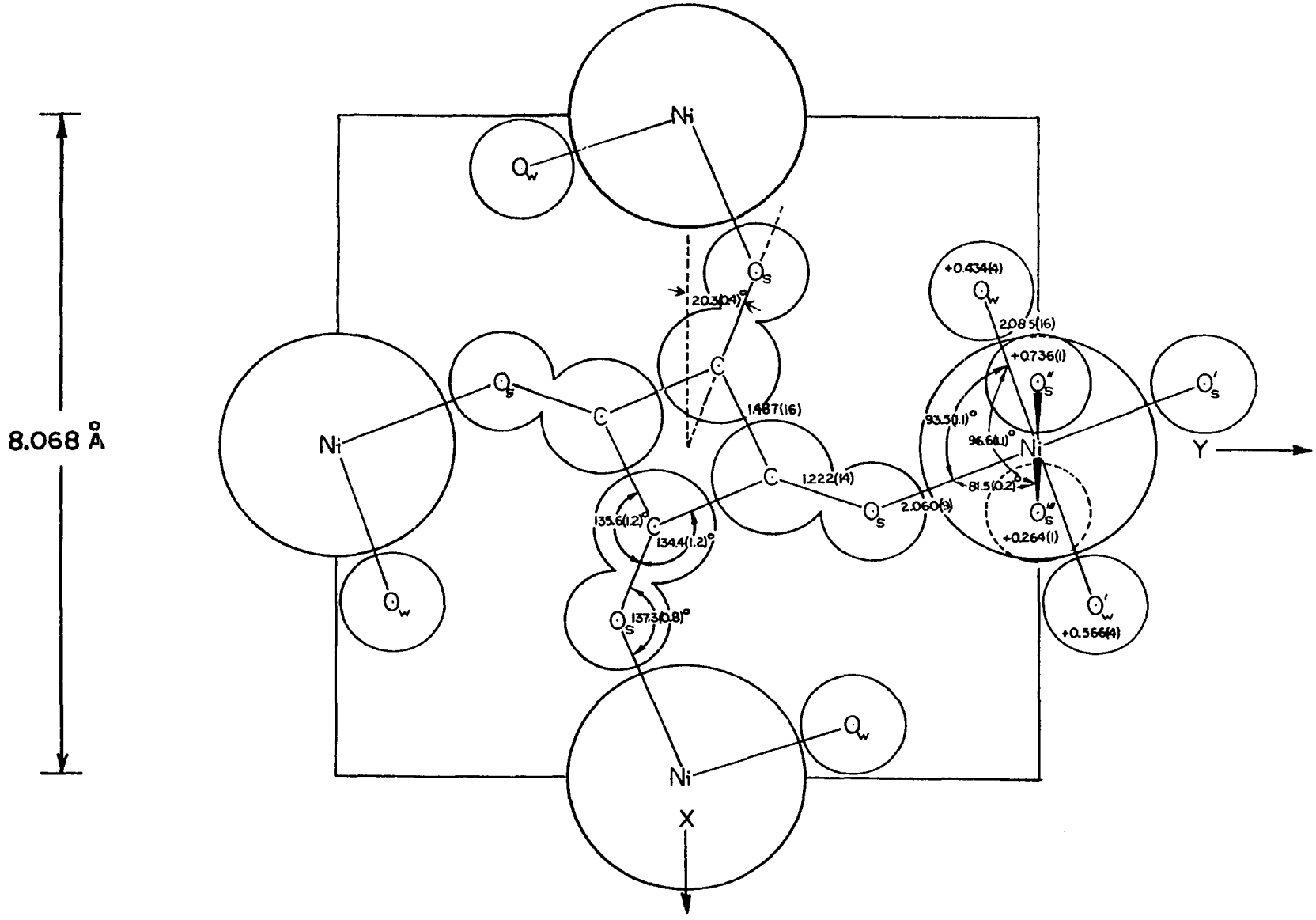
8.068 Å
Ni
O_w
O_s
120.3(0.4)°
C
1.487(16)
1.222(14)
O_s
2.060(3)
135.6(1.2)°
134.4(1.2)°
137.3(0.8)°
+0.434(4)
2.085(16)
+0.736(1)
O''_s
O'_s
93.5(1.1)°
96.6(1.1)°
81.5(0.2)°
Y
O''_s
+0.264(1)
O'_w
+0.566(4)
X

Crystal Fragments

Attempts were made to obtain a single crystal fragment by breaking the "twinned" crystal cubes according to the ideas discussed in the sections on the appearance of the crystals under the polarizing microscope. The general plan was to first isolate one of the square pyramids and then break a fragment from it. It was found that the square pyramids could not simply be broken from a "twinned" crystal cube since the crystal did not cleave naturally along the triangular faces of the square pyramids, but broke irregularly, and the pyramids had to be isolated by trimming irregular fragments obtained from breaking the "twinned" crystal cube. One result of this procedure was the loss of knowledge of the exact location of the final fragment in the original "twinned" crystal cube.

Thirteen different fragments were investigated by single crystal X-ray techniques. Three fragments were examined on Weissenberg cameras and the rest were examined on Buerger Precession cameras (Buerger, 1964). Of the thirteen fragments, six showed a diffraction symmetry different from the m3m diffraction symmetry observed for the "twinned" crystals. None of the crystals examined on the Weissenberg camera showed a recognizable reduction in m3m diffraction symmetry. The deviation from m3m diffraction symmetry was most pronounced for fragment #8, and it was selected for closer

examination. (0,k,ℓ), (1,k,ℓ), ($\bar{1}$,k,ℓ), (2,k,ℓ) and (h,k,0), (h,k,1,), (h,k,$\bar{1}$), (h,k,2) reciprocal lattice level Buerger precession photographs were obtained for this fragment. In addition, zero level exposures such as (h,k,h) ($\bar{h}$,k,h), (2h,k,h) and (2$\bar{h}$,k,h) were also taken. The exposures were made using Zr filtered MoK_{α} (0.7107Å) radiation.

The (0,k,ℓ) and (h,k,0) photographs showed only four-fold rotation symmetry along the h and ℓ axes respectively. No mirror symmetry is found in either photograph; the (h,k,0) section deviates more strongly from m3m diffraction symmetry in that reflections which are related in the "twinned" crystals by mirrors show larger differences in intensity in the (h,k,0) section than in the (0,k,ℓ) section. The upper level photographs show no symmetry at all. Careful examination of all the photographs revealed no overall diffraction symmetry except the center introduced by Friedel's Law. Therefore it was decided to treat the fragment and the data derived from it as belonging to space group P_1.

Crude intensities were estimated visually from the available (0,k,ℓ), (1,k,ℓ), (2,k,ℓ), (h,k,0), (h,k,1) and (h,k,2) photographs using a calibrated spot intensity scale. The exposures consisted of one film for each reciprocal lattice section, each film of different exposure time. Since there was only one spot to measure for each reflection, no averaging procedure could be employed as discussed for the

film data obtained for the "twinned" crystal, and the measured intensities are subject to large errors (40%) especially if the reflection was very intense or very faint (50%). The relative intensity scales also differ from film to film. Information regarding the reflections measured on each film is given in Table 15.

Table 15. Number of reflection intensities measured for fragment #8 from precession photographs and scaling factors

Reciprocal lattice section	No. of reflections measured	No. of reflections found to be zero	Relative scaling factors obtained from cross scaling
(hk0)	132	19	1.0
(hk1)	323	25	1.66(22)
(hk2)	217	28	0.78(9)
(0kℓ)	125	31	0.76(12)
($\bar{1}$kℓ)	309	37	1.56(22)
(2kℓ)	220	41	1.07(9)
Total	1326	181	

Some tables of Lorentz-polarization correction factors for Buerger precession exposures were available, but were found to be for special instrument settings and directly applicable to only some of the data obtained in this work

(Buerger, 1964; ITXRC, 1959). Therefore a computer program was written to calculate Lorentz and polarization corrections for every reflection. The applicable formulas were taken from Buerger (1964), Waser (1951a, 1951b), Burbank, (1952) and Grenville-Wells and Abrahams (1952). The Lorentz and polarization correction factors are given by:

$$L = \frac{1}{\Omega\xi\sin\bar{\mu}\,\sin\eta}\left[\frac{1}{1+\tan^2\bar{\mu}\,\sin^2(\phi+\eta)} + \frac{1}{1+\tan^2\bar{\mu}\,\sin^2(\phi-\eta)}\right]$$

$$p = \frac{1+\cos^2 2\theta}{2} \qquad (17)$$

where

$$\cos\eta = \frac{\sin^2\bar{\mu} + \xi^2 - \sin^2\bar{\nu}}{2\xi\sin\bar{\mu}}$$

and

$$\sin\bar{\nu} = [1-(\cos\bar{\mu}-\zeta)^2]^{1/2} \qquad (18)$$

L is the Lorentz correction factor and p is the polarization correction factor. θ is the diffraction angle of a particular reflection and $\bar{\mu}$ is the precession angle at which a particular reciprocal lattice level has been photographed. ζ, ξ and ϕ are the coordinates of a particular reflection in the reciprocal lattice as indicated in Figure 14. ζ and ξ are

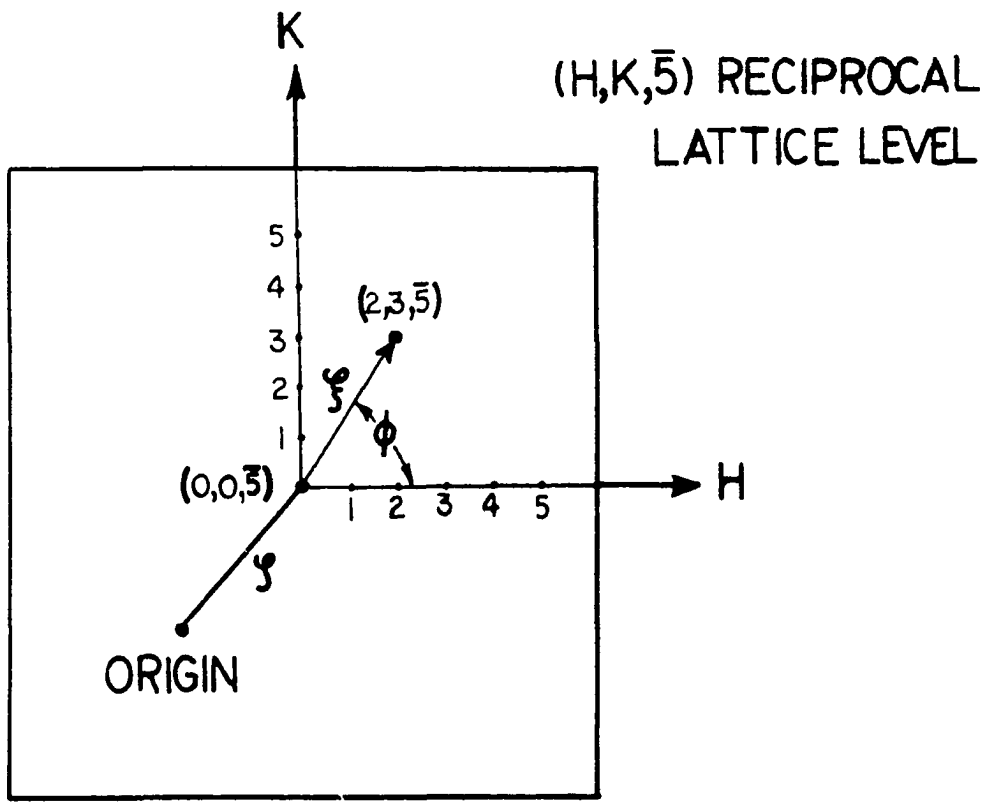

Figure 14. Reciprocal lattice coordinates used in the calculation of Lorentz-polarization correction factors for precession photographs

in reciprocal lattice units, RLU = λ/a = 0.7107Å/8.068Å = 0.08885. Ω is the constant angular velocity of the precession and can be regarded as a scale factor. The program was checked by calculating some of the tables given by Buerger (1964), and was then used to calculate the Lorentz-polarization correction factor for each reflection.

The corrected intensities were brought to a common scale by comparing intensities measured on two films. The resulting relative scale factors are given in Table 15. Although absorption corrections should have been applied to the estimated intensities since fragment #8 was about 0.3 mm in its largest dimensions (see Figure 15), such corrections were not made because of the large uncertainty in the data, estimated to be 40% for most reflections and as much as 50-100% for the most intense and the weakest reflections.

The 132 estimated $|F(hk0)|$ and 125 estimated $|F(0k\ell)|$ values were then used to calculate electron density projections of the structure down the z and x axes using a program written by Rodgers and Jacobson (1969). Phases were calculated using the least squares program (Busing, Martin and Levy, 1964) by assuming the Ni atoms to be in the (1/2,0,0), (0,1/2,0), (0,0,1/2) positions and the space group P_1. The two electron density projections are given in Figure 16. As can be seen, only one squarate ion is evident in the (yx) and (yz) projections. The electron density projection maps do exhibit small residual peaks

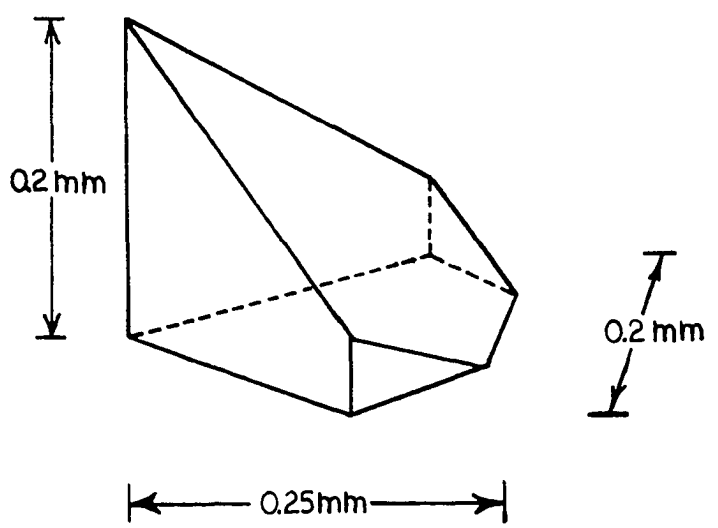

Figure 15. Approximate shape and dimensions of crystal fragment #8. All planes indicated are only approximations to the irregular surfaces of the fragment

Figure 16. Electron density projections on the (xy) and (yz) faces calculated from (h,k,0) and (0,k,ℓ) intensities, respectively. Data from fragment #8. The map unit is $1.54e\text{Å}^{-2}$. The numbers given for the electron density maxima are in terms of these units. Areas where the electron density values are less than zero are stippled. The map is distorted in the vertical or y direction by a factor of 1.08 relative to the horizontal direction due to limitations of the computer printer. ((a) $\rho(xy)$. Solid contours are drawn at intervals of 2 map units starting at zero; dashed contours are at intervals of 10 map units starting at 10. (b) $\rho(yz)$. Solid contours are drawn at intervals of 1 map unit starting at zero; dashed contours are at intervals of 10 map units starting at 10)

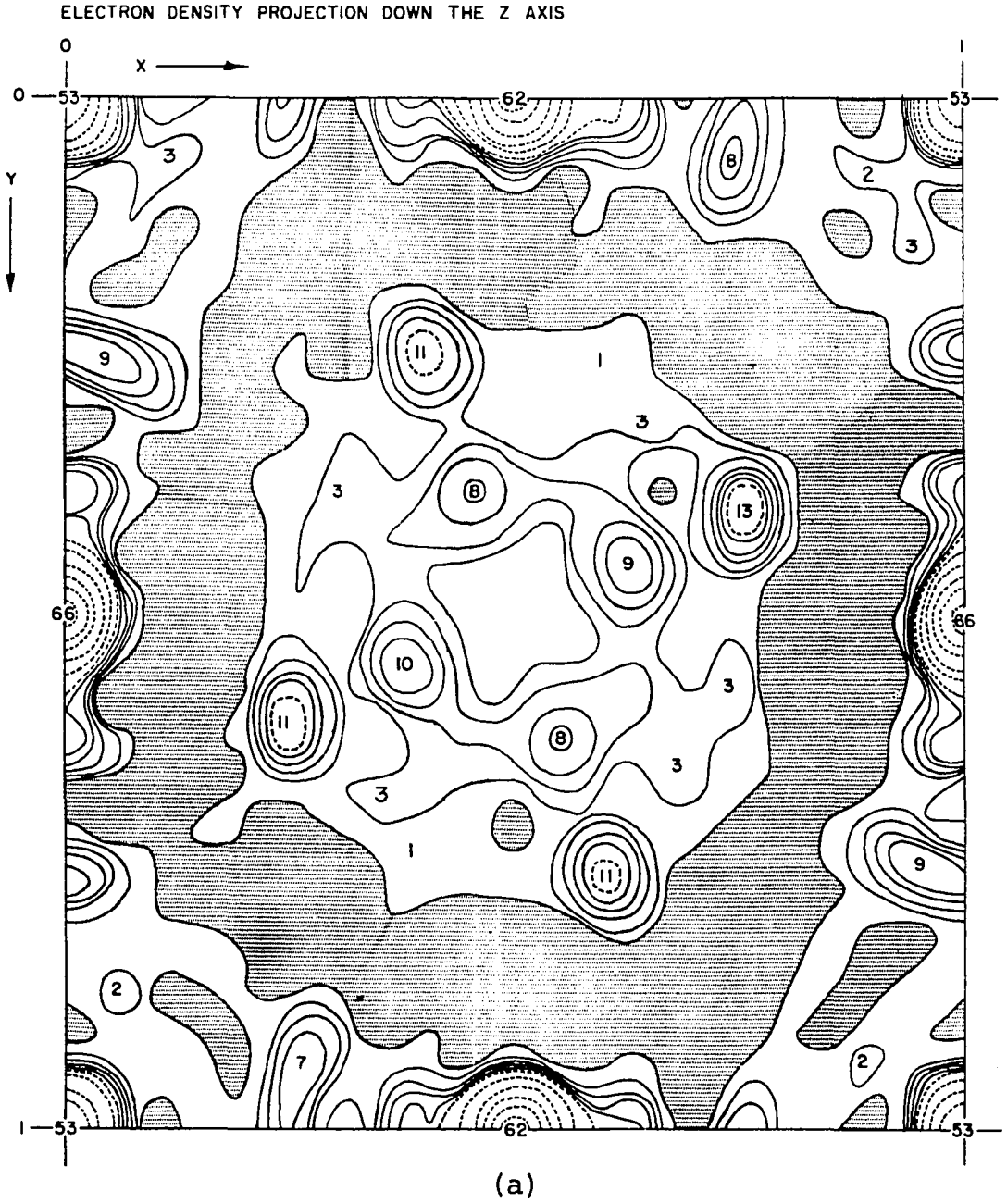
ELECTRON DENSITY PROJECTION DOWN THE Z AXIS
0
X
Y
0
1
0—53
62
53
1—53
62
53
66
66
3
8
2
3
9
11
1
3
3
8
13
9
10
11
8
3
3
3
1
11
9
2
7
2

(a)

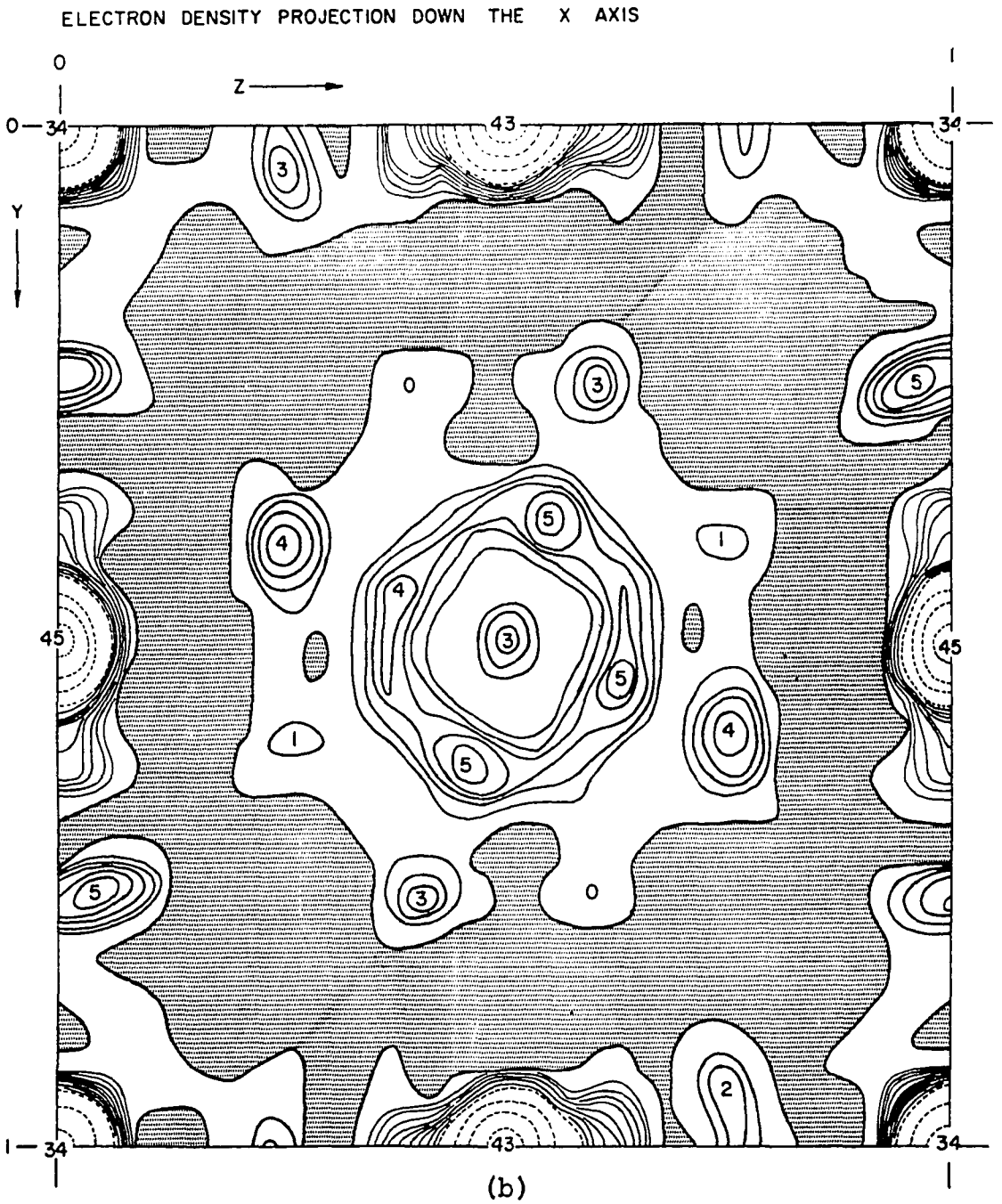

(b)

Figure 16 (Continued)

attributable to the second, superimposed squarate ion. The oxygen peak ratios are 11:1 and 13:3 in the (yz) projection and 4:1 and 3:0 in the (yz) projection; the C atom peak ratios are 8:3 and 9:3 in the (yx) projection and 5:3 in the (yz) projection.

Recalculation of the (yx) electron density projection using the observed squarate ion in the (yx) face and four water O atoms (peaks labeled 8,9,7 and 9 close to the edges in Figure 16(a)) in addition to the Ni atoms to determine phases increased the O and C atom peak ratios only slightly. The recalculated (yx) projection is given in Figure 17.

An electron density map was calculated using all available unique data (1236 reflections) and phases as determined by the Ni positions at the middle of the cell edges. The (x,y,0), (0,y,z) and (x,0,z) sections of the electron density map are given in Figure 18. The only significant electron density inside the unit cell are peaks identifiable as due to water O atoms. The (x,y,0) section clearly shows a squarate ion in the face, although there are strong indications of peaks attributable to a second squarate ion related to the clearly outlined squarate ion by mirror planes as seen for the "twinned" crystal. These features agree with the (xy) electron density projection. In section (0,y,z) the mirroring is much stronger, especially for the carbon atoms which show peak ratios of 31:20 and 21:13. The oxygen

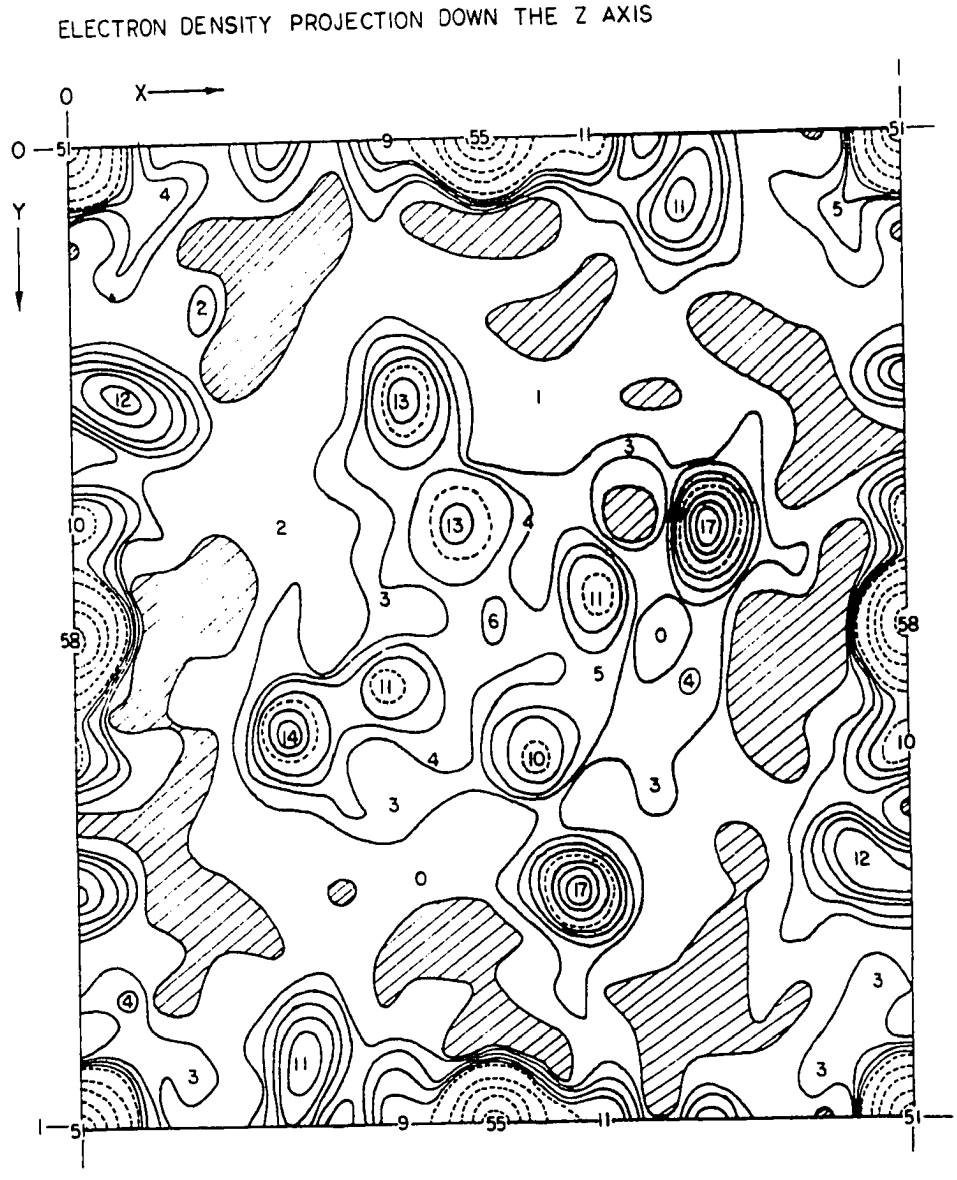

Figure 17. Electron density projection down the z-axis. In addition to the Ni atoms; one squarate ion and four water O atoms observed in Figure 16(a) were used to calculate the phases. Details of scale and contouring are the same as in Figure 16(a). Areas where $\rho(xy) \leq 0$ are cross hatched

Figure 18. Electron density sections calculated from data obtained for fragment #8. Phases were determined by Ni atoms of the center of unit cell edges. The map unit is $0.254 e\text{A}^{-3}$. Solid contours are at intervals of 10 map units starting at 10; dashed contours are at intervals of 50 map units starting at 50. The areas left blank have $\rho(xyz) < 1.3 e\text{A}^{-3}$ ((a) $\rho(x,y,0)$, (b) $\rho(0,y,z)$, (c) $\rho(x,0,z)$)

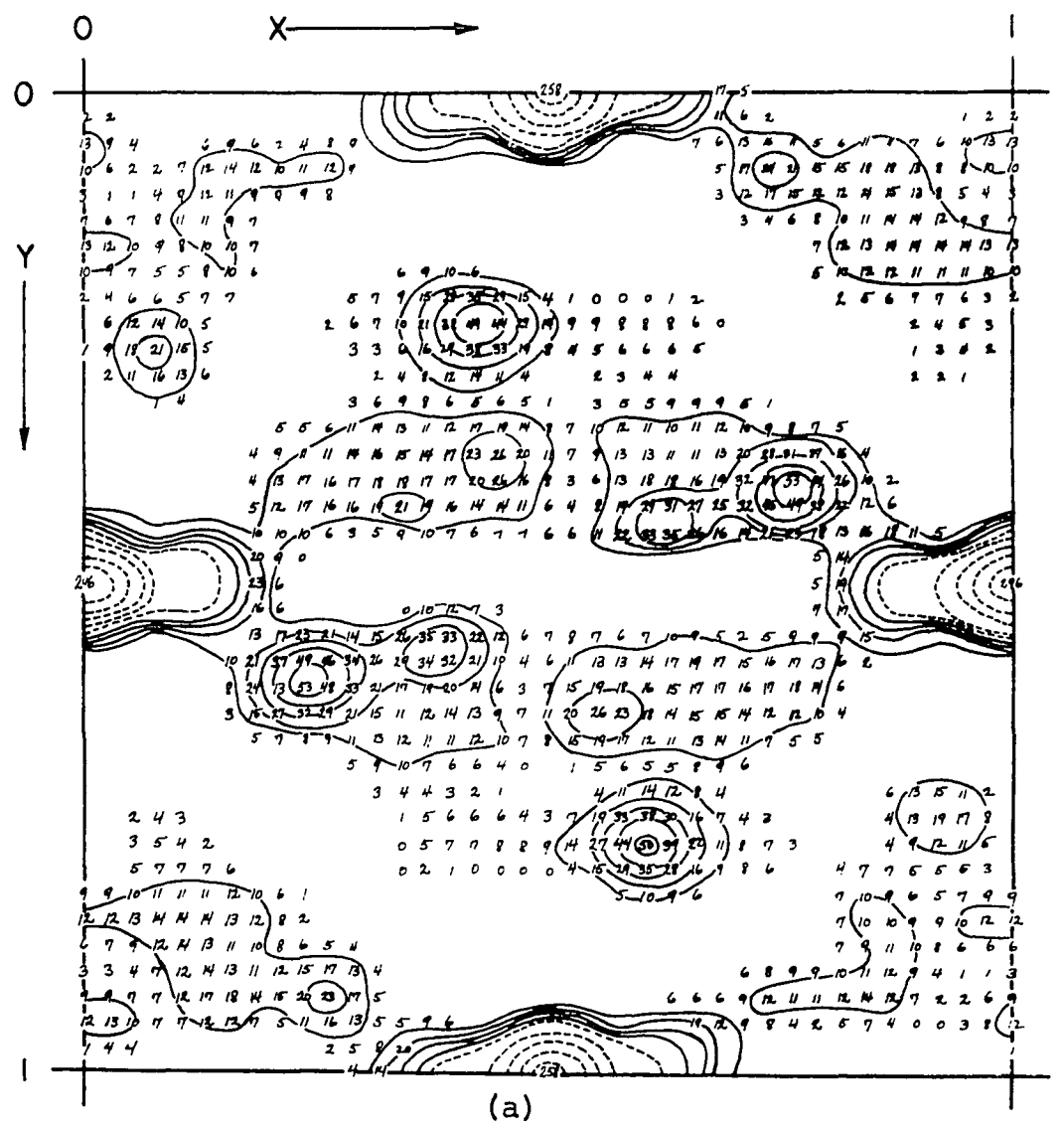
ρ(XYZ) SECTION AT Z = 0
0
X
1
0
Y
1
258
246
(a)

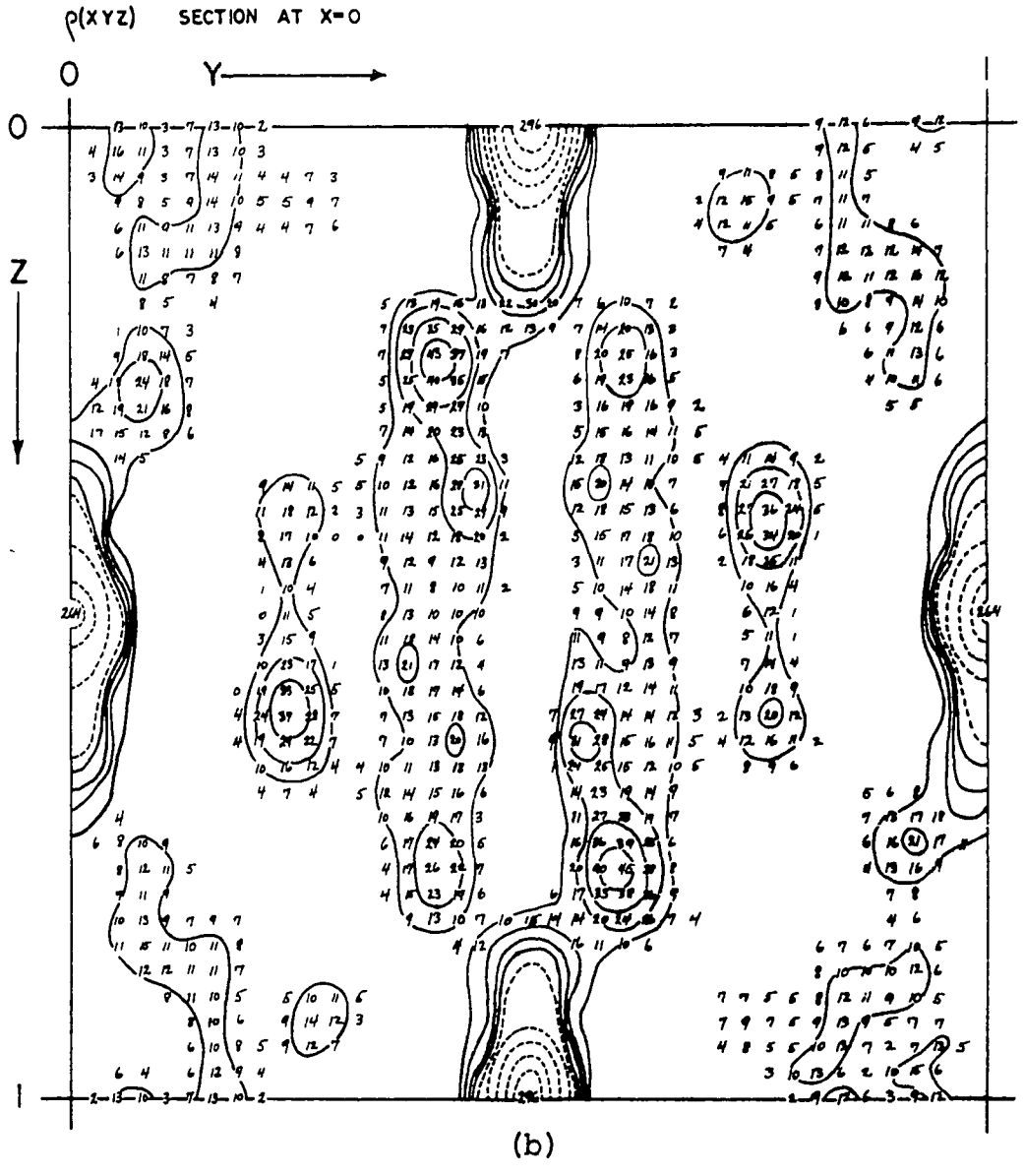

Figure 18 (Continued)

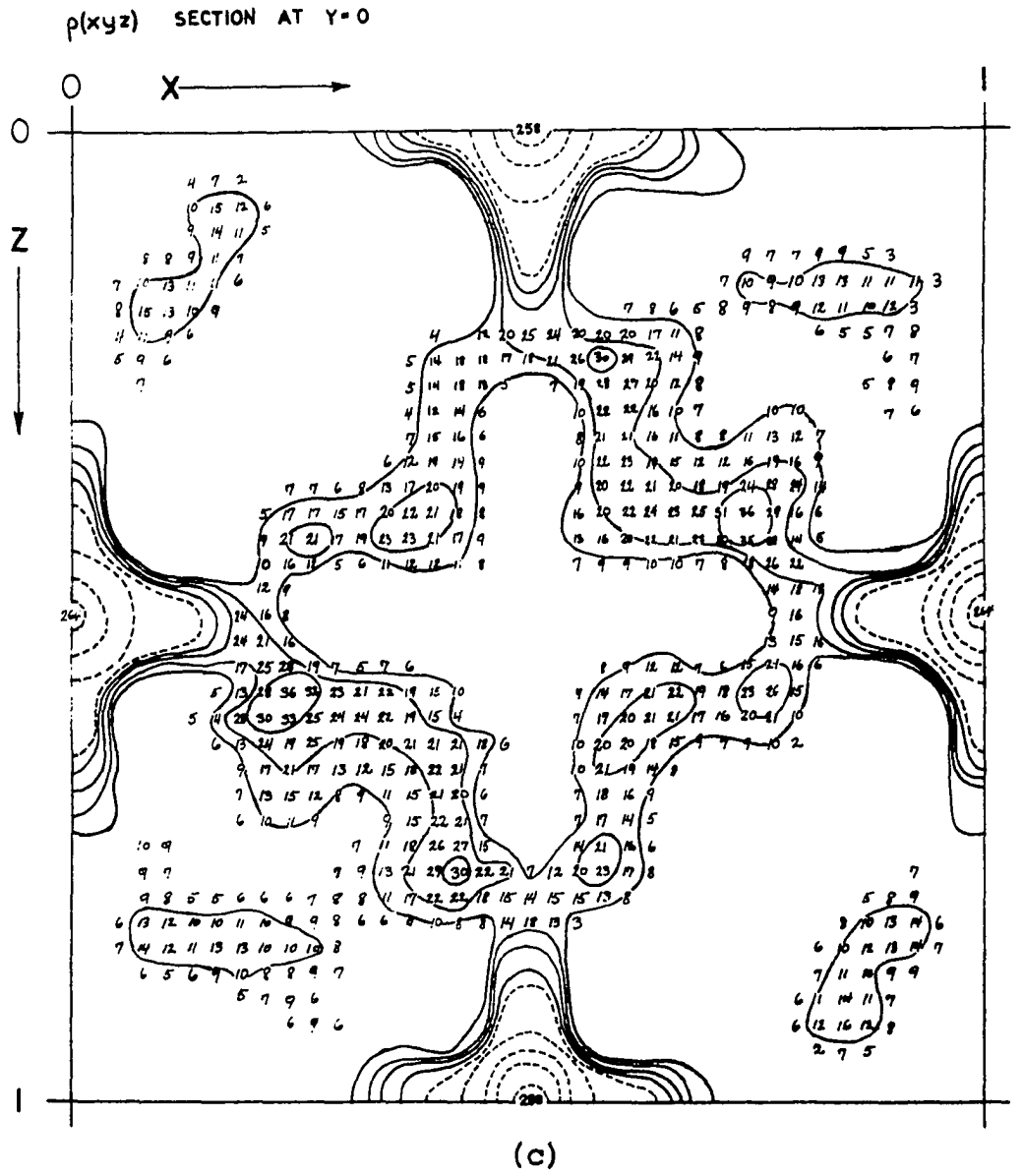

(c)

Figure 18 (Continued)

peak ratios are 43:35 and 36:20. These features agree in general with the (yz) electron density projection.

The (x,0,z) section does not show a clearly recognizable squarate ion. The peculiar elongation of the Ni atom electron density peaks in the z and x directions is most likely due to the limited reciprocal lattice intensity data set available. To calculate an accurate electron density map it is necessary to have a complete set of intensity data, without missing sections. Therefore conclusions in this section are based mainly on the (yx) and (yz) electron density projections for which a complete set of data is available.

From the appearance of the electron density projections and sections (especially the (yz) projection and (0,y,z) section) it seemed that the fragment #8 was still not a single crystal but was composed of several individuals present in unequal amounts. Therefore further work on fragment #8 was discontinued.

Structural Investigations: Summary and Conclusions

Although X-ray powder patterns of $NiC_4O_4 \cdot 2H_2O$ crystals grown from solution and in silica gel can be indexed assuming a cubic crystal lattice, optical examination of these crystals under a polarizing microscope indicate that the crystals do not have a cubic crystal structure, and that

the characteristic crystal cubes obtained both from solution and silica gel are "twinned", consisting of some multiple of six individuals. The appearance of the crystal cubes suggest that they are composed of six square pyramids with their apexes at the center and their bases forming the faces of the "twinned" crystal. There are also indications that each of the pyramids is further composed of four individuals.

From the measured density of the crystals and the apparent cubic unit cell size it is concluded that there are three $NiC_4O_4 \cdot 2H_2O$ units per unit cell.

The diffraction pattern of the "twinned" crystal cubes was found to have m3m diffraction symmetry. A Patterson synthesis located the Ni atoms at the center of the edges of a unit cell with $a=b=c=8.068(2)\text{Å}$ and $\alpha=\beta=\gamma=90°$. An electron density synthesis using the observed structure factors for the "twinned" crystal and the Ni positions for determining the phases revealed the squarate ions to be in the faces. However, two squarate ions were seen to occupy the same position in each face, the two ions being related to each other by mirror planes perpendicular to the face diagonals. Since the actual structure could not contain two squarate ions in the same face, and in view of the optical data, it was concluded that the two superimposed squarate ion images were due to "twinning" in the crystal,

an equal number of individuals having the squarate ion in the two positions observed.

If one assumes the Ni skeleton to be the same for all individuals, namely in the center of the cube edges, and then places the squarate ions in the face, one has a choice of two orientations for each of three faces, or a total of eight different choices of orienting the three squarate ions. Each of these possible arrangements will have a three-fold rotation axis along one body diagonal of the unit cell, and if all eight structures are oriented such that their threefold rotation axes are parallel they will appear identical. That is, only one structure results from all eight possible ways of placing the three squarate ions in the faces. The water O atoms are then placed around the Ni atoms to complete approximate O atom octahedra about the Ni atoms. Such peaks are observed in the electron density map. No other significant peaks were observed in the electron density map inside the unit cell. The resulting structure is the one shown in Figure 10. From a scale model of this structure it was evident that each water molecule could participate in two hydrogen bonds to squarate O atoms, which have a lone pair pointing toward the hydrogen atoms. This hydrogen bonding might in large part be responsible for the stability of this structure.

Support for the above view of the structure was obtained

from a crystal fragment broken from a "twinned" crystal in an attempt to isolate a single crystal. X-Ray intensities obtained for the fragment showed a reduced diffraction symmetry, although a threefold axis could not be located unambigously and the data was treated assuming the lowest symmetry space group P_1. Electron density projections and sections showed the images of only one squarate ion in the (xy) and (yz) faces, although residual electron density attributable to the mirror image of this squarate ion was still present, indicating that the fragment still was not a single crystal but was composed of unequal amounts of one or more individuals.

A least squares refinement of the atomic positions of the squarate ion atoms and the water oxygen atoms (as discussed in the section on the counter data) led to bond distances for the squarate ion and the Ni-O bonds in reasonable agreement with the corresponding values found in the literature.

The structure of $NiC_4O_4 \cdot 2H_2O$ as proposed above has a void inside the unit cell. The size of this void is approximately 4.7Å x 4.7Å x 4.7Å if one assumes the van der Waals thickness of the squarate ion π-system is approximately 3.4Å, the value found in graphite and other aromatic compounds (Robertson, 1953). (Since the squarate ion is negatively charged one expects its π-system to be larger).

This void is large enough to accommodate one or two solvent molecules (H_2O, CH_3CH_2OH) and might be the explanation for the extra solvent molecules found in the solution grown samples discussed in the chapter on sample preparation.

The measured density of the silica grown crystals is 1.99($\pm$1)g/cc, while the calculated density, assuming three $NiC_4O_4 \cdot 2H_2O$ units per unit cell and the measured unit cell volume (5.252×10^{-22} cm^3) is 1.96 g/cm^3. If one assumes that each unit cell has at least one water molecule clathrated in it, then the calculated density would be 2.01 g/cm^3 which is much closer to the measured value. Therefore the density measurement lends further support to the probability of solvent molecules being clathrated in the structure.

A possible twinning mode which would produce a "twinned" crystal with m3m diffraction symmetry would require 8 individuals of equal size (with the structure discussed above) oriented with respect to each other in such a way that the threefold rotation axis of an individual is pointed along both directions of all four body diagonals of a ("twinned" crystal) cube.

In conclusion, the available evidence supports the proposed structure for $NiC_4O_4 \cdot 2H_2O$ discussed above. However, it would be desirable to make further attempts to isolate a single crystal fragment by breaking a "twinned" crystal cube,

so that the structure of $NiC_4O_4 \cdot 2H_2O$ may be determined unambiguously. Of special interest are the dimensions, configuration, and exact orientation of the squarate ion, the coordination geometry about the Ni ion, and the possibility of hydrogen bonding. It would also be desirable to retain knowledge of the location and orientation of the single crystal fragment in the "twinned" crystal cube from which it is broken, in order to shed light on the twinning geometry and the nature of the structure change in going from one individual to another in the "twinned" crystal.

OPTICAL SPECTRUM

The optical spectrum of $NiC_4O_4 \cdot 2H_2O$ was measured using transmitted light and crystals grown in silica gel. The instrument used was a Cary 14 spectrophotometer. Attempts to obtain the spectrum using a powder sample in the form of a KBr pellet or a Nujol mull were unsuccessful due to excessive scattering of light by the powdered crystals. The spectrum was obtained at room temperature from silica gel grown crystals which were placed on a 1 mm quartz plate within a 3 mm diameter circle drilled in a 0.3 mm copper plate which was clipped to the quartz plate. The $NiC_4O_4 \cdot 2H_2O$ crystal cubes were all about 0.2 to 0.3 mm on a side and were held to the quartz plate by the surface tension of a thin film of Nujol and filled the hole in the copper plate completely. An identical combination of quartz and drilled copper plates was placed in the reference beam. The spectrum obtained is given in Figure 19. Four absorptions at 8550, 13800, 14900 and 25700 cm^{-1} are observed. In Table 16 are given the optical absorptions and assignments of the Ni^{++} ion doped in MgO (Low, 1958a,b), the absorption frequencies by Ludi and Schindler (1968) from reflection measurements on powdered $NiC_4O_4 \cdot 2H_2O$, and the present results obtained for silica gel grown $NiC_4O_4 \cdot 2H_2O$ crystals. It is seen that the 10 Dq value obtained in this work is 9550 cm^{-1}, in reasonable agreement with the value detained by Ludi and Schindler.

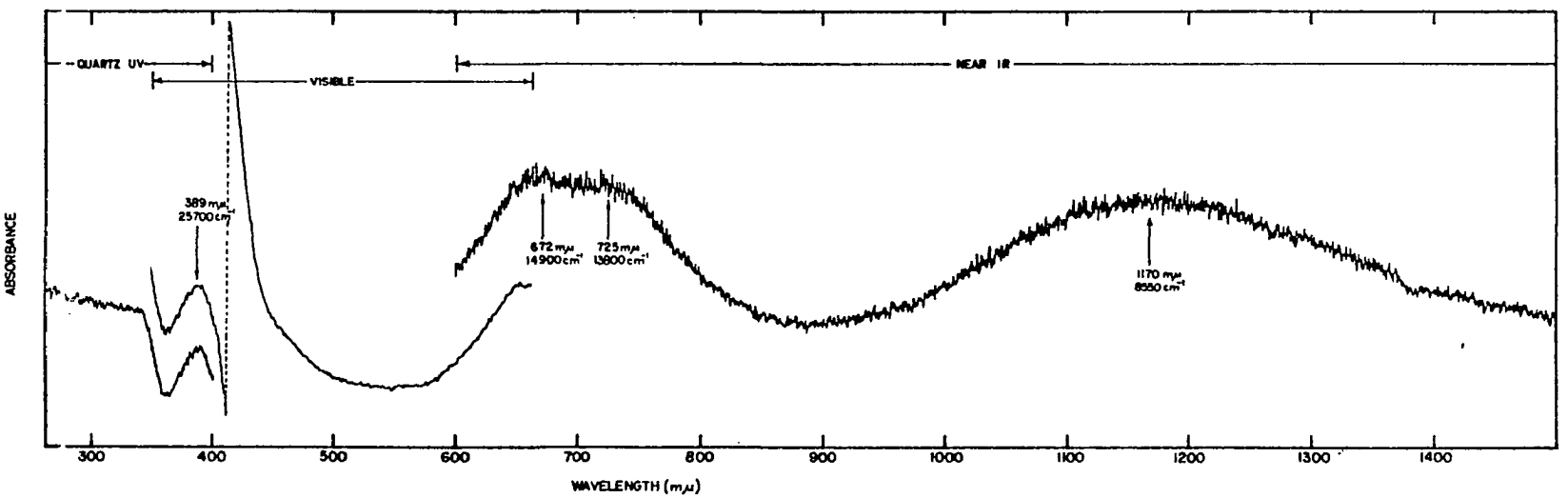

Figure 19. Near IR, visible, and UV absorption spectrum of $NiC_4O_4 \cdot 2H_2O$

Table 16. Assignments for observed absorption frequencies in Ni^{++}:MgO and $NiC_4O_4 \cdot 2H_2O$

Assignment	Experimentally observed absorptions		
	Ni^{++}:MgO (Low, 1958a,b)	$NiC_4O_4 \cdot 2H_2O$ (Ludi and Schindler, 1968)	$NiC_4O_4 \cdot 2H_2O$ (present work)
$^3A_{2g} \rightarrow {}^3T_{2g}$ (10 Dq)	8600 cm^{-1}	8600 cm^{-1}	8550 cm^{-1}
$^3A_{2g} \rightarrow {}^1E_g$	13700	13300	13800
$^3A_{2g} \rightarrow {}^3T_{1g}$	14700	15200	14900
$^3A_{2g} \rightarrow {}^1T_{2g}$	21750	21500 sh[a]	25700
$^3A_{2g} \rightarrow {}^3T_{2g}$	24500	25300	25700
$^3A_{2g} \rightarrow {}^1A_{1g}$	25950		
$^3A_{2g} \rightarrow {}^1T_{1g}$	28300		

[a]sh, shoulder.

The shoulder observed by Ludi and Schindler (1968) at 21,500 cm^{-1} is not seen clearly in this work, although very faint indications of its presence are seen in Figure 19.

A more complete treatment of the Ni^{++}, d^8, ion in an octahedral crystal field has been made by Liehr and Ballhausen (1959) and is discussed in Appendix A.

SUSCEPTIBILITY MEASUREMENTS

Since the magnetic susceptibility measurements made on $NiC_4O_4 \cdot 2H_2O$ by Smentowski (see footnote 1 on page 24) showed large scatter at liquid N_2 temperatures and above, it was decided to remeasure the susceptibility of $NiC_4O_4 \cdot 2H_2O$ to obtain better high temperature data and more closely define the low temperature peak in the susceptibility.

Apparatus and Theory of Measurement

The basis of the susceptibility measurement is the fact that the mutual inductance between two concentric coils is dependent on the permeability of the space inside the coils. The voltages induced in the secondary coil with the sample present and absent (due to the alternating field produced by the primary coil) are measured with an alternating current bridge.

The susceptibility measurements were made on a Hartshorn type mutual inductance bridge (Hartshorn, 1925). The apparatus in several states of modification has been described previously by various authors (Jennings, 1960; Gerstein and Spedding, 1960; Olander, 1966; Maass, 1969; and Rioux, 1969). The most recent account of the apparatus actually used in this work is that by Rioux and is based on a design by Maxwell (1965). A simplified circuit diagram of the

bridge is given in Figure 20. The signal generator feeds an alternating, sinusoidal signal of 45 Hz frequency through the primary circuit, setting up a varying magnetic field in the primaries of the sample coil (see Figure 21) and the external variable mutual inductors. The secondaries of these mutual inductors will develop voltages across them equal to $(j\omega M_s+\rho_s)i_p$ and $(j\omega M_v+\rho_v)i_p$ respectively, where M_s and M_v are the mutual inductances of the sample coils and the external mutual inductor; $\rho_s i_p$ and $\rho_v i_p$ are resistive voltage components in the secondaries due to capacitive effects and eddy current contributions. The external mutual inductor is connected so that the inductive voltage developed in its secondary is 180° out of phase with the inductive voltage developed in the secondary of the sample coils, which can thus be cancelled by adjusting the external mutual inductor. The resistive voltages developed in the secondaries can be nulled by tapping a voltage $R_s i_p$ into the secondary; its polarity can be chosen with the reversing switch to cancel the voltages $\rho_s i_p$ and $\rho_v i_p$. When no signal is observed in the secondary there must be zero voltage drop around the secondary, and

$$(j\omega M_s + \rho_s - j\omega M_v + \rho_v \pm R_s)i_p = 0 \quad , \tag{19}$$

which, on equating real and imaginary parts, yields

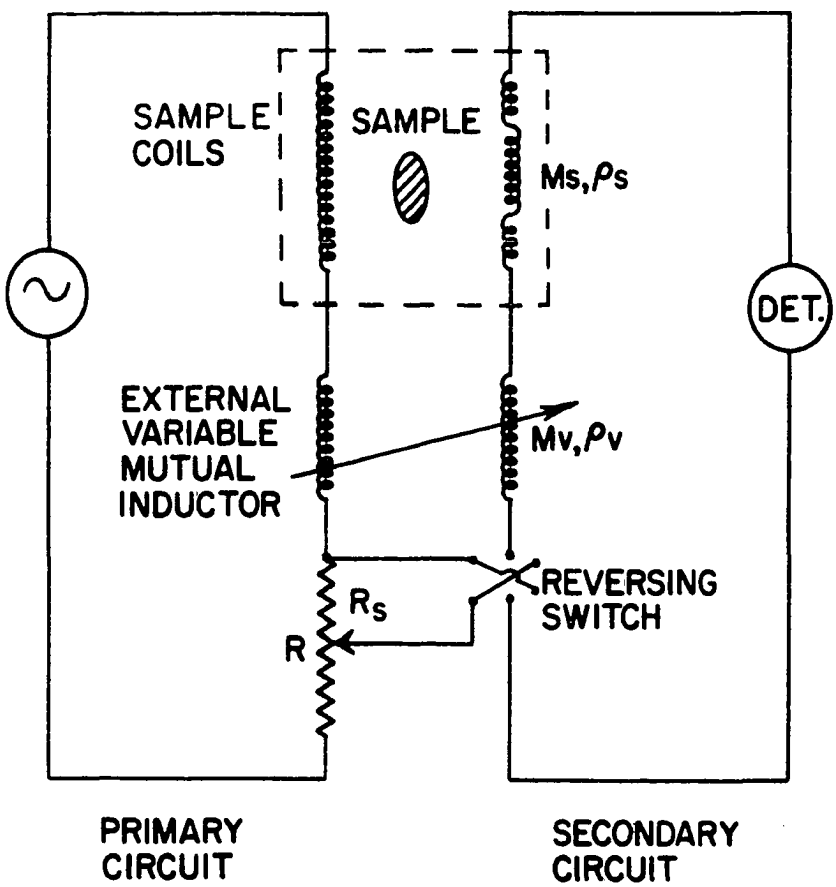

Figure 20. Simplified circuit diagram of the Hartshorn mutual inductance bridge

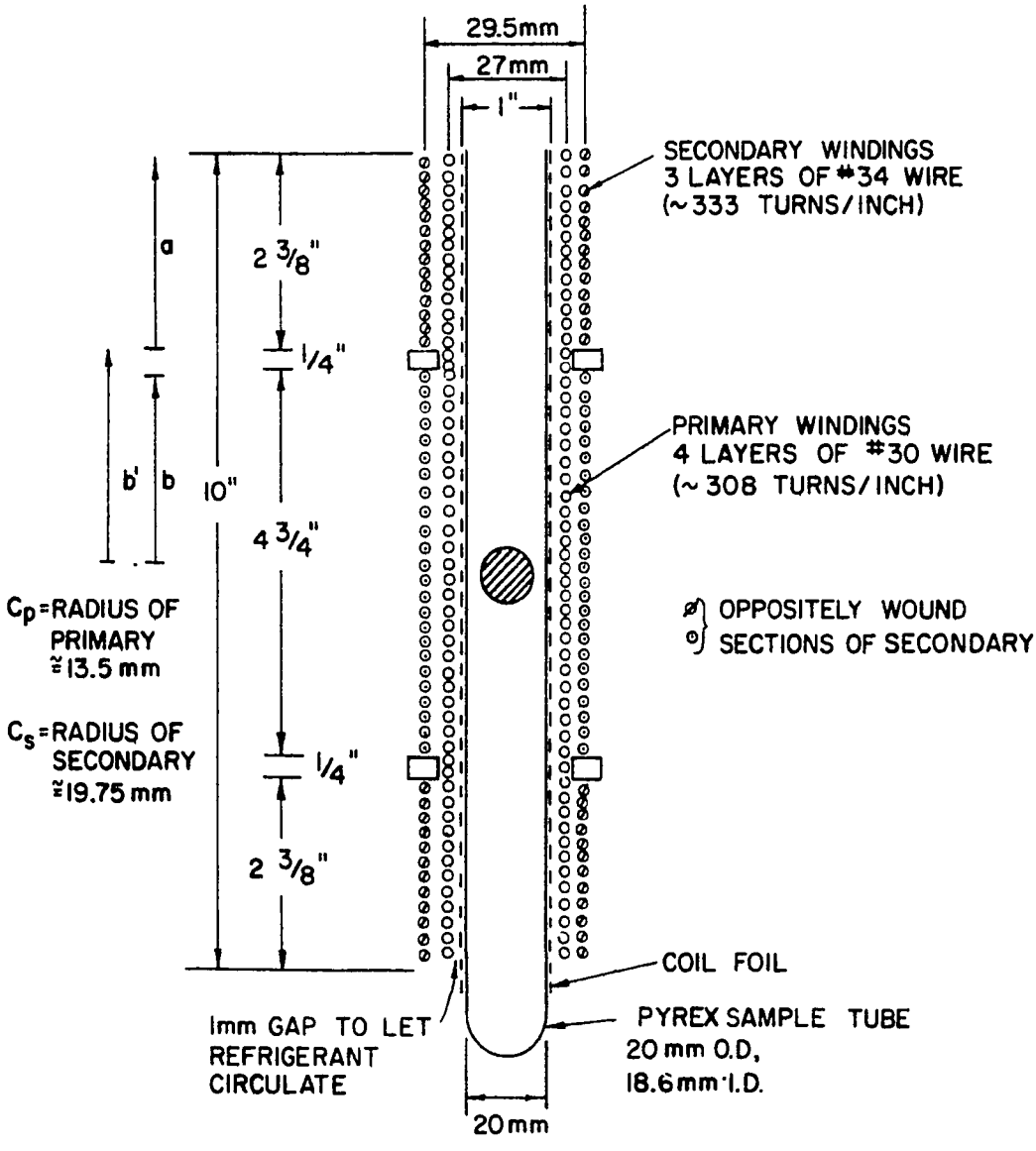

Figure 21. Sample mutual inductance coil

$$M_s = M_v$$
$$R_s = \pm(\rho_s+\rho_v) \tag{20}$$

The design of the sample coil is such that it has nearly zero mutual inductance when there is no sample in the coils. The construction is shown schematically in Figure 21. The primary consists of a ten inch solenoid with a one inch ID; it is composed of four layers of #30 Formvar insulated copper wire. The secondary consists of three sections, each containing three layers of #34 Formvar insulated copper wire; the end sections are wound in a sense opposite to that of the center section and they contain a total of enough turns to give essentially zero mutual inductance between the primary and secondary. If a sample is placed in the secondary with complex susceptibility $\chi=\chi'-j\chi''$, there will be an additional mutual inductance equal to (Gerstein and Spedding, 1960; Abel, et al., 1964; Bleaney and Bleaney, 1967)

$$M = n_s n_p \mu_o \frac{\chi V}{(1+\chi/3)} f_s f_p \tag{21}$$

where n_s and n_p are turns densities of primary and secondary respectively; V is the volume of the sample with volume susceptibility χ; f_s and f_p are constants depending on the dimensions and configuration of the primary and secondary coils respectively. In terms of the dimensions given in

Figure 21 they are

$$f_p = \frac{1}{[1 + (\frac{c_p}{b'+a})^2]^{1/2}} \simeq 0.99$$

$$f_s = \frac{b}{(b^2+c_s^2)^{1/2}} + \frac{b'}{(b'^2+c_s^2)^{1/2}} - \frac{(b'+a)}{((b'+a)^2+c^2)^{1/2}} \simeq 0.92 \qquad (22)$$

Derivation of Equations 21 and 22 assumes the sample is spherical and the external field on it is essentially that at the center of the primary, $n_p f_p i_p$. The numerical values for f_p and f_s are calculated from the approximate dimensions of the sample coils as given in Figure 21. The maximum susceptibility measured in this work was χ_m=0.8 emu/mole, for a sample consisting of N=0.010 moles, occupying a volume of roughly 4cc. Since $\chi V = N\chi_m$, $\chi = N\chi_m/V \simeq 2\times10^{-3}$ emu/cc $\simeq$0.025 MKS/m^3. Therefore $\chi/3 \simeq 0.008$ or less and $1 + \chi/3 \simeq 1$. Equation 21 can then be written as

$$M = \Gamma V\chi = \Gamma N\chi_m = \Gamma N(\chi_m' - j\chi_m'') \qquad (23)$$

where $\Gamma = n_s n_p \mu_o f_s f_p$ is called the coil constant.

The mutual inductance bridge is now used as a null instrument; it is balanced to give zero secondary current both with the sample in and out of the sample coils. The two equations expressing zero voltage drop around the secondary with the sample in and out of the coil are

$$(j\omega M_s + \rho_s + j\omega M_v^{out} + \rho_v \pm R_s^{out})i_p = 0$$

$$(j\omega M_s - j\omega N\Gamma(\chi'-j\chi'') + \rho_s + j\omega M_v^{in} + \rho_v \pm R_s^{in}) = 0 \tag{24}$$

and, taking the difference we have

$$(-j\omega N\Gamma(\chi'-j\chi'') + j\omega\Delta M_v \pm \Delta R_s)i_p = 0$$

$$\Delta M_v = M_v^{in} - M_v^{out} \tag{25}$$

$$\Delta R_s = R_s^{in} - R_s^{out}$$

and

$$\chi' = \frac{\Delta M_v}{N\Gamma}$$

$$\chi'' = \pm \frac{\Delta R_s}{\omega N\Gamma} \tag{26}$$

$$\frac{\chi''}{\chi'} = \pm \frac{\Delta R_s}{\Delta M_v} \cdot \frac{1}{\omega}$$

It is clear that χ' and χ'' can be calculated from the balance settings of M_v and R_s with the sample in and out of the coils, and a knowledge of the coil constant and the frequency of the primary current.

The external variable mutual inductor in the bridge as described by Maass (1969) is a calibrated mutual inductor not

available commercially and difficult to construct. It has been replaced by a commercial decade autotransformer (ratio transformer, ESI "Dekatran" model #DT45) connected across the secondary of a fixed mutual inductor whose primary is part of the primary circuit. The Dekatran is adjusted to tap the desired fraction of inductive voltage from the secondary of the fixed mutual inductor into the secondary circuit. The Dekatran has high impedence and loads the secondary of the fixed mutual inductor very lightly, thus acting as a true voltage divider (Maxwell, 1965).

The circuit diagram of the actual bridge as used is given in Figure 22. The signal generator is an ESI AC generator Detector, model 861A. The power amplifier is a tube type constructed in this laboratory. In series with these in the primary circuit are the primaries of the sample coils, the coarse mutual inductor and the fixed mutual inductance quadrupole coupling coils, and the resistive network. The sample coils have been described above; since it is sometimes difficult to construct a sample coil with zero mutual inductance (in the absence of a sample), a coarse inductor is necessary to bring the bridge to an operating point where the remaining inductive voltage in the secondary of the sample coils can be nulled by the Dekatran. The setting of the external coarse inductor is not changed for any set of "in" and "out" readings. The resistive network

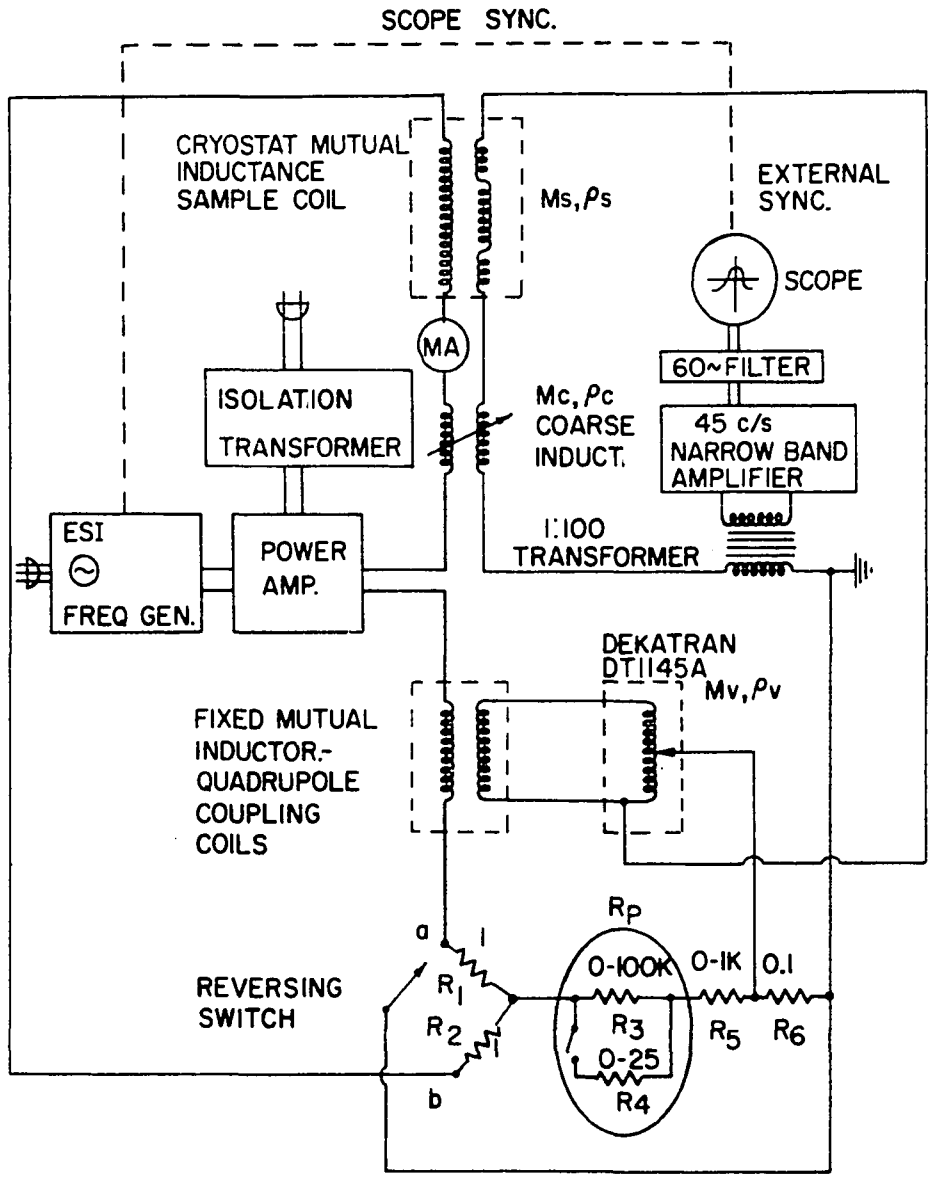

Figure 22. Circuit diagram of Hartshorn mutual inductance bridge as used in the susceptibility measurements on $NiC_4O_4 \cdot 2H_2O$

is designed to allow extremely small resistive voltages to be tapped into the secondary across the 0.1 ohm resistor R_6. The secondary circuit contains the secondaries of the sample coils, coarse mutual inductor, quadrupole coupling coils (in parallel with the Dekatran), plus a 1:100 transformer which couples the secondary circuit to a narrow band amplifier and an oscilloscope. The narrow band amplifier (constructed in this laboratory) is tuned to 45 c/sec; its output is fed through a 60 cycle filter to an oscilloscope which is externally synched with a signal from the signal generator; this allows both in phase and out of phase voltages in the secondary to be detected separately.

The voltage tapped into the secondary across R_6 depends on the setting of the reversing switch.

position a:

$$iR_6 = \frac{dR_1}{d+R_p+R_5+R_1}\, i_p \simeq \frac{dR_1}{R_p+R_5} \text{ where } d = \frac{R_6 R_{sec}}{R_6+R_{sec}} \simeq 0.1\Omega$$

and

$$R_6 \simeq 0.1\Omega,\ R_{sec} \gtrsim 200\Omega,\ R_1 \simeq 1\Omega,\ R_p+R_5 \gtrsim 200\Omega.$$

position b:

$$iR_6 = \frac{dR_2}{d+R_p+R_5+R_1}\, i_p$$

$$\simeq \frac{dR_2}{R_p+R_5}\, i_p \text{ (reversed polarity).}$$

Switching from a to b reverses the polarity of the voltage but its amplitude changes only due to changing R_1 to R_2 which are both nominally one ohm. The voltage across R_6 will be designated

$$iR_6 = \pm\, dR_{1,2}/(R_p+R_5),$$

where $R_{1,2} = R_1$ or R_2 depending on the position of the reversing switch.

The voltage drop around the secondary without the sample in the coils is

$$[j\omega M_s + \rho_s + j\omega M_c + \rho_c + j\omega M_v^{out} + \rho_v \pm \frac{dR_{1,2}}{(R_p+R_5)^{out}}]i_p=0 \tag{27}$$

and with the sample in the coils

$$[j\omega M_s - j\omega N\Gamma(\chi_m'-j\chi_m'') + \rho_s + j\omega M_c + \rho_c + j\omega M_v^{in} + \rho_v \pm \frac{dR_{1,2}}{(R_p+R_5)^{in}}]i_p = 0 \tag{28}$$

The sign of the last term depends on the setting of the reversing switch. Subtracting the two equations gives

$$[-j\omega N\Gamma(\chi_m'-j\chi_m'') + j\omega\Delta M_v \pm dR_{1,2}(\frac{\Delta R}{R^{in}R^{out}})]i_p = 0 \tag{29}$$

where $\Delta M_v = M_v^{in} - M_v^{out}$, $R^{in(out)} = (R_p+R_5)^{in(out)}$ and $\Delta R = R^{in}-R^{out}$. Solving for real and imaginary parts yields

$$\chi'_m = \frac{\Delta M_v}{N\Gamma} \tag{30a}$$

$$\chi''_m = \pm \frac{1}{\omega N\Gamma} \frac{dR_{1,2}\Delta R}{R^{in}_{R}{}^{out}} \tag{30b}$$

The constant Γ is determined by taking in and out readings on a substance of known susceptibility.

The sample coil is mounted on a pyrex coil tube and immersed in two concentric glass dewars as shown in Figure 23. The coils can be cooled to liquid N_2 or liquid He temperatures by direct immersion in these refrigerants in the inner dewar. The inner dewar can be pumped on and liquid He can be pumped down to a temperature of approximately 1.2°K.

The sample is placed into the coil tube via the sample assembly shown in Figure 24(a). The sample container was constructed of bakelite as shown in Figure 24(b). It fits tightly inside a paper heater shell on the outside of which a non inductively wound heater is glued. This sample-heater assembly is suspended by fishline from the upper sample support as shown in Figure 24(a). The unit is movable vertically about 15 inches by sliding the glass tube through the O-ring vacuum coupling attached to the top of the coil tube. The thermocouple and heater leads are led through a rubber hose-hose clamp vacuum wire lead through into the sample space, down the bakelite rod and the fishline. At two points the leads are wound on styrofoam plugs; these

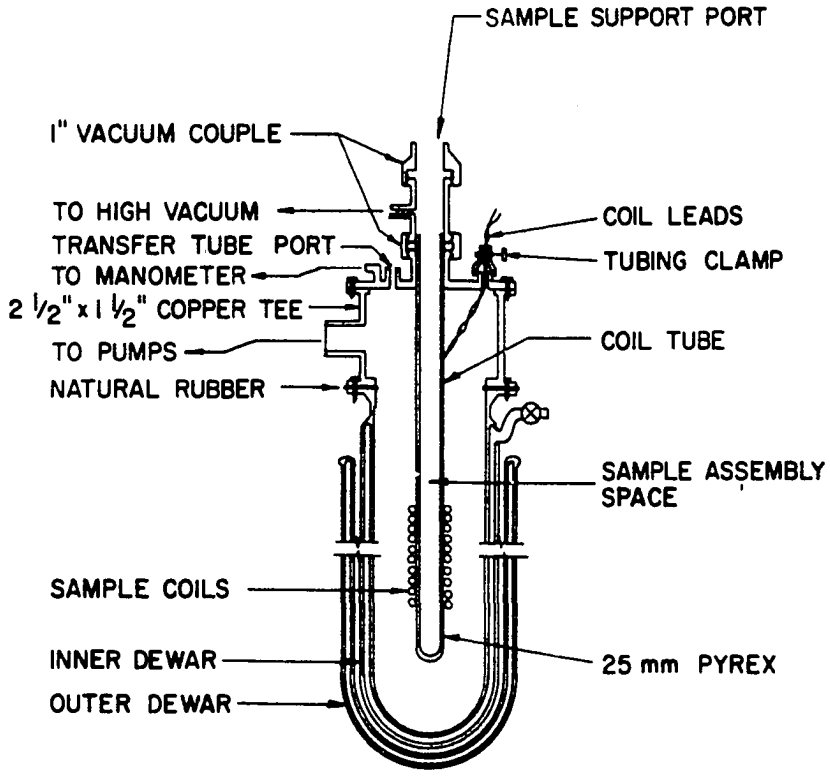

Figure 23. Cryostat and associated equipment

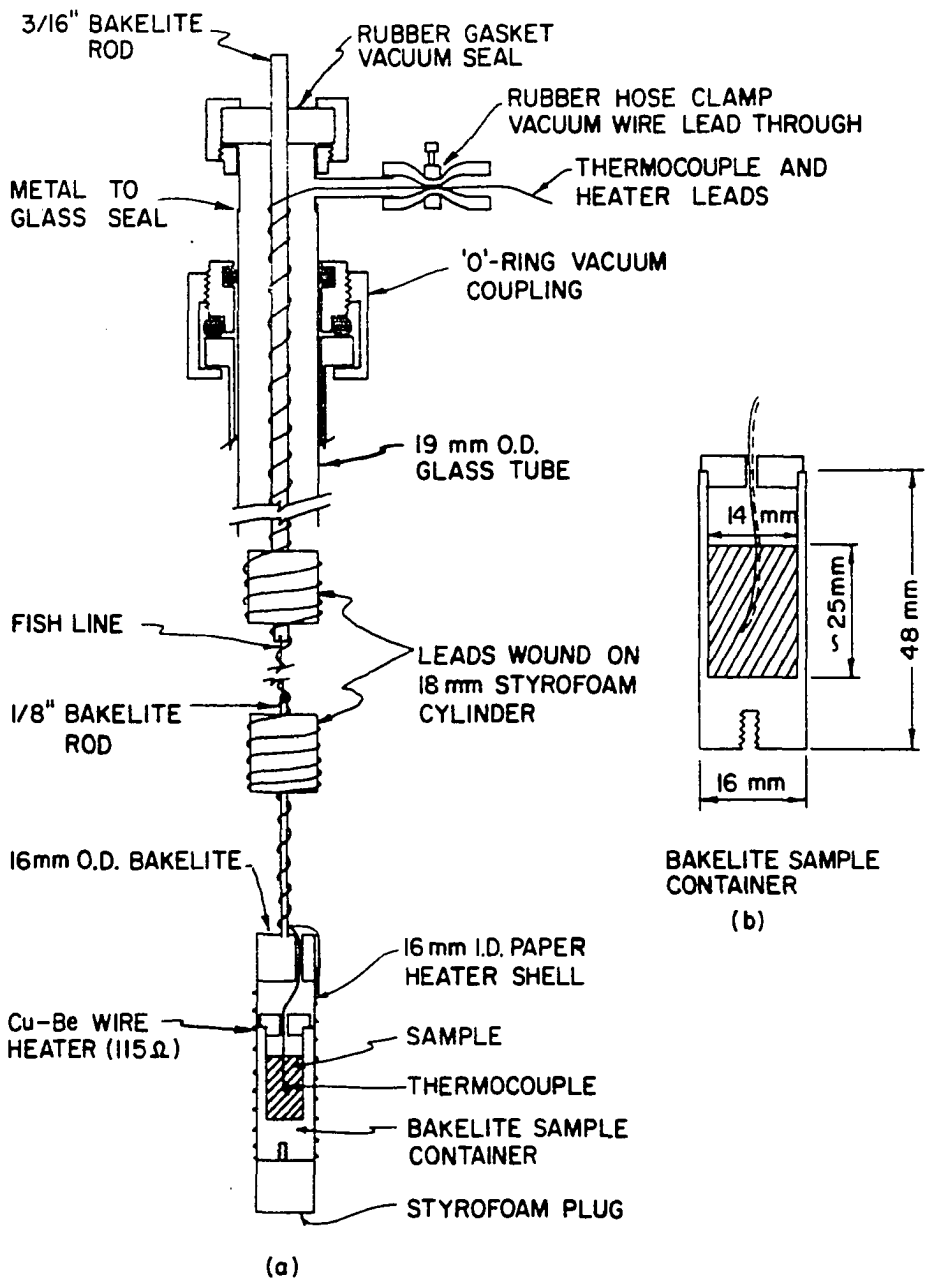

Figure 24. Sample holder assembly (a) sample holder (b) sample container

windings serve to increase the length of wire between the sample and room temperature in order to reduce the amount of heat conducted to the sample along the leads.

The sample in the coil tube is cooled by the liquid N_2 or He surrounding the coil tube via the exchange gas inside the sample space. Temperatures between 1.2-4.2°K were obtained by pumping on the liquid He bath. Temperatures from 4.2-100°K can be obtained by pumping out the sample space and using the heater to heat the sample, with the coils at liquid He temperatures. Temperatures from 78°K to room temperature are obtained using the heater with the coils at liquid N_2 temperature.

The sample coil was originally wound to fit so tightly around the coil tube that refrigerant could not flow between the coil and the coil tube. During measurements at 140°K and above, with the sample coils in liquid N_2 and the sample being heated electrically, it was found that the mutual inductance reading with the sample out of the coils ("out" reading) changed with time after removing the sample from the coils, and the "in" reading changed with time at constant sample temperature after replacing the sample in the coils. Evidently the hot heater next to the inside of the coil tube caused distortions either in the coil tube, which were transmitted mechanically to the sample coil, or in the coil directly by radiated heat. These changes in sample coil

configuration caused changes in mutual inductance not associated with changes in the moment of the sample. The resulting measurements were in error by as much as 50% above 150°K.

To correct this situation a nineteen inch section of the coil tube of 25 mm O.D. was replaced by a tail of 20 mm O.D. pyrex tubing. In order to thermally shield the coil from the heater, a double layer of "coil foil" (Anderson, et al., 1961) was wound and taped about this section, and the sample coil was fastened around the coil foil by means of wooden spacers at the top and bottom of the coil. A gap of about one mm between the coil foil and the sample coil allows free circulation of the refrigerant between the two. The coil foil eliminated radiative heating of the coil which was physically isolated from the coil tube and kept at the bath temperature by refrigerant circulating freely around it. With this arrangement no further problems with "out reading" irreproducibility were observed and measurements to 250°K were obtained.

Temperatures were measured with a No. 36 Au (2 at % Co) versus No. 36 Cu thermocouple referenced at the ice point. The gold-cobalt wire was obtained from the Sigmund Cohn Corp. of Mt. Vernon, New York. The T versus e.m.f. curve for wire drawn from the same bar as the wire used in this work was measured by Powell, Bunch and Corrucini (1961) of the National

Bureau of Standards (Sparks and Powell, 1965). It was assumed that the shape of the e.m.f. curve for the thermocouple used in this experiment was the same and the difference varied linearly with temperature. A calibration point at liquid He (T measured from the vapor pressure) allows one to obtain an e.m.f. vs. T curve. This procedure has previously been found to yield temperatures accurate to 0.5 deg. above 78°K and 0.2 deg between 4.2 and 80°K (Jelinek, 1965). Below 4.2°K vapor pressures over the liquid He bath were measured with mercury and oil manometers; the oil manometer was calibrated versus the mercury manometer. The "1958 He" Scale of Temperatures" was used to convert vapor pressure measurements into temperatures (Brickwedde, van Dijk, Durieux, Clement, and Logan, 1960).

The coils were calibrated with a sample of $GdO_{1.5}$ prepared in this laboratory. Before use it was baked at 800-900°C for 10 hours to decompose any carbonate. A typical spark source mass spectrographic analysis of material from the same batch is in ppm: Mg 15, Cr 10, Si 50, Fe 10, Ta 200, Cu 20, Al 30, Ca 500, Ni 10. Wet chemical analysis on freshly baked material indicates 431 ppm C and 58 ppm F. The susceptibility of $GdO_{1.5}$ used in the calibration is that given by Hacker, Lin and Westrum (1965), who measured the susceptibility from 4-270°K. The susceptibility has been measured also by Brown and Hubbard (1965) and Miller and Jelinek (1968) below

6°K. Examination of these measurements yields the uncertainties attached here to the results of Hacker et al. (1965)

$$\chi_m^{-1} = 2.21\ (\pm 0.01) + 0.1280\ (\pm 0.0018)T \qquad (31a)$$

or

$$\chi_m = \frac{7.814\ (+0.109)}{T + 17.3\ (\pm 0.3)} \qquad (31b)$$

which implies $\mu_{eff} = 7.905\ (\pm 0.055)$ Bohr magnetons and $\theta = -17.3\ (\pm 0.3)$°K since $\chi_m = (N\beta^2/3k)[\mu^2_{eff}/(T-\theta)]$. For a typical calibration the coils used in this work gave $\Delta M_v = 0.042619(\pm 100)$ "turns"[1] for $0.018097(\pm 5)$ moles of $GdO_{1.5}$ at 4.190°K. Using Equations 30a, 30b and 31 one obtains

$$\Gamma = \frac{\Delta M}{N\chi_m} = 6.467(\pm 0.041)\ \frac{\text{turns}}{\text{emu}}\ \text{, coils in liquid He} \qquad (32)$$

for the coil calibration constant when the coils are immersed in liquid He. With the coils in liquid N_2 a different coil constant is expected and a typical value is

$$\Gamma = 6.592(\pm 0.087)\ \frac{\text{turns}}{\text{emu}}\ \text{, coils in liquid } N_2 \qquad (33)$$

---

[1] "Turns" is a term deriving from the use originally of a calibrated mutual inductor with a smallest step of one turn; presently it stands for an arbitrary unit of mutual inductance as read on the Dekatran; the largest decade unit on the Dekatran being 0.1 turn.

The quoted uncertainties in Γ are due to uncertainties in reading ΔM, and uncertainties in N and the susceptibility of $GdO_{1.5}$. Although the uncertainties in Γ are calculated to be around 1% successive determinations of the coil constant have varied by only about 0.5% over half a year.

The calibration discussed above gives Γ in units of turns/emu, and is suitable for calculating χ_m' from a ΔM_v reading using Equation 30a. For calculating χ_m'' from a $\frac{dR_{1,2}}{\omega} \frac{\Delta R}{R_{in}R_{out}}$ reading using Equation 30b, Γ must be in units of Ωsec/emu. Turns are related to Ωsec as follows. From Equations 29, 30a and 30b inductive and resistive voltage differences between in and out readings are

$$V_{ind} = j\omega N\Gamma\chi_m' i_p = j\omega\Delta M_v i_p \tag{34a}$$

$$V_{res} = \omega N\Gamma\chi_m'' i_p = dR_{1,2} \frac{\Delta R}{R_{in}R_{out}} i_p \tag{34b}$$

If the primary current $i_p = i_o e^{i\omega t}$, then magnitudes of peak to peak voltages are

$$|V_{ind.}| = \omega N\Gamma\chi_m' 2i_o = \omega\Delta M_v 2i_o \tag{35a}$$

$$|V_{res.}| = \omega N\Gamma\chi_m'' 2i_o = dR_{1,2} \frac{\Delta R}{R_{in}R_{out}} 2i_o \tag{35b}$$

Experimentally it is found that

$$|V_{ind.}| = 1mv = (2i_o\omega)\cdot(\Delta M_v = 5.29\times10^{-7} \text{ turns}) \tag{36a}$$

$$|V_{res.}| = 1mv = (2i_o dR_{1,2}) \cdot \left(\frac{\Delta R}{R_{in} R_{out}} = 2.80 \times 10^{-7}\ \Omega^{-1}\right) \tag{36b}$$

Dividing (36a) by (36b) yields the relation

$$1 \text{ turn} = \frac{dR_{1,2}}{\omega} \frac{2.80}{5.29}\ \Omega^{-1} \tag{37}$$

Relation 37 can be used to convert Γ in turns/emu to Γ in Ωsec/emu suitable for use in Equation 30b. The values of $dR_{1,2}$ and ω are 0.1816 Ω^2 (for the reversing switch on; all data taken in this mode) and 282.7 sec^{-1} respectively for the apparatus used in this work.

Measurements

Susceptibility measurements were made on samples 2 and 3 listed in Table 1. Two types of measurements were made. In the first type the sample was put into a bakelite sample container and mounted in the sample assembly as shown in Figure 24; this arrangement was used to obtain measurements at any temperature. In the second type of measurement, the sample container, without heater or thermocouple, was simply suspended from nylon fishline in the coil tube without any other support. This arrangement allowed measurements to be made at bath temperatures only. However, it was better suited for field dependent measurements because of the possibility that the heater and thermocouple might contribute to

field dependence. The second arrangement was also convenient for measuring χ_m'' because resistive losses due to eddy currents in thermocouple and heater wires were eliminated.

Measurements on sample 2

Measurements on the preparation labeled as sample 2 in Table 1 were made on a sample of 3.1214g of material. Since this sample was analyzed to contain only 25.37(±0.15)% Ni, it contains 0.01349(±9) moles of Ni. The sample container was constructed from bakelite as shown in Figure 24(b); it weighed 5.9g. The sample was saturated with Dow Corning silicone diffusion pump oil (number 704) to improve heat conduction in the powdered sample. Tests indicated that the bakelite and silicone oil gave very small contributions to the signal at all temperatures. Salinger and Wheatley (1961) have also found that these materials have small susceptibilities. Corrections for the contribution to ΔM by the sample assembly were made. Some of these were due in part to inductive pickup from the heater and thermocouple wires. The results obtained for sample number 2 are given in Tables 17 and 18. Table 17 lists the results obtained by using sample support arrangement type 1. Runs 1-4 were made with the coils in liquid He, the sample being heated electrically. Temperatures were measured with the thermocouple discussed previously except for the initial points at bath temperatures. The temperatures of these points were

Table 17. Molar susceptibility of $NiC_4O_4 \cdot 2H_2O$. Sample wt.=3.1214g (0.01349 moles of Ni) labeled sample #2 in Table 1 (25.37% Ni)

T(°K)	χ_m' ($\frac{emu}{mole}$)	$\chi_m'^{-1}$ ($\frac{mole}{emu}$)	$\frac{\chi_m'(T-\theta)}{(\frac{emu°K}{mole})}$	T(°K)	χ_m' ($\frac{emu}{mole}$)	$\chi_m'^{-1}$ ($\frac{mole}{emu}$)	$\frac{\chi_m'(T-\theta)}{(\frac{emu°K}{mole})}$
	Run 1			14.80	0.0588	17.00	1.286
4.175	0.1143	8.750	1.284	16.24	0.0551	18.13	1.285
4.51	0.1123	8.903	1.300	17.59	0.0519	19.28	1.278
4.73	0.1102	9.075	1.298	19.35	0.0488	20.5	1.289
5.04	0.1064	9.402	1.286	21.07	0.0457	21.9	1.284
5.95	0.0984	10.16	1.280	22.56	0.0433	23.1	1.282
6.64	0.0935	10.69	1.280	24.13	0.0410	24.4	1.280
7.51	0.0884	11.31	1.288	28.67	0.0370	27.0	1.322
8.28	0.0840	11.90	1.288	29.08	0.0365	27.4	1.319
9.43	0.0778	12.85	1.283	32.22	0.0331	30.2	1.299
11.24	0.0698	14.33	1.277	34.90	0.0305	32.8	1.281
12.64	0.0646	15.49	1.272	37.65	0.0287	34.8	1.284
14.26	0.0597	16.76	1.272	40.17	0.0273	36.6	1.290
17.07	0.0527	18.99	1.270	41.90	0.0263	38.0	1.288
	Run 2			44.44	0.0250	40.0	1.286
				47.68	0.0234	42.8	1.280
4.175	0.1139	8.778	1.280	50.07	0.0224	44.6	1.280
4.175	0.1139	8.782	1.279	53.68	0.0210	47.6	1.275
4.60	0.1111	8.998	1.295	57.07	0.0199	50.3	1.276
5.07	0.1076	9.296	1.305	60.04	0.0190	52.7	1.273
5.42	0.1042	9.598	1.300	62.02	0.0184	54.4	1.271
6.71	0.0946	10.57	1.303	46.65	0.0241	41.5	1.294
7.67	0.0882	11.34	1.299	50.65	0.0222	45.1	1.280
9.33	0.0795	12.58	1.303	53.81	0.0210	47.6	1.28
11.70	0.0688	14.53	1.291	56.89	0.0199	50.2	1.27
13.16	0.0637	15.71	1.287	59.90	0.0189	52.8	1.27
				65.90	0.0174	57.6	1.27

Table 17 (Continued)

T(°K)	χ_m' ($\frac{emu}{mole}$)	$\chi_m'^{-1}$ ($\frac{mole}{emu}$)	$\frac{\chi_m'(T-\theta)}{(\frac{emu°K}{mole})}$	T(°K)	χ_m' ($\frac{emu}{mole}$)	$\chi_m'^{-1}$ ($\frac{mole}{emu}$)	$\frac{\chi_m'(T-\theta)}{(\frac{emu°K}{mole})}$
67.64	0.0170	58.7	1.27			Run 4	
70.45	0.0162	61.5	1.26	4.191	0.1137	8.794	1.279
73.23	0.0159	63.0	1.28	4.10	0.1137	8.796	1.269
75.97	0.0154	64.9	1.28	4.76	0.1045	9.569	1.235
78.68	0.0149	67.0	1.28	6.50	0.0925	10.81	1.254
82.94	0.0143	70.1	1.28	8.27	0.0824	12.14	1.262
85.59	0.0138	72.4	1.28	12.39	0.0652	15.34	1.268
88.21	0.0136	73.6	1.29	17.34	0.0520	19.25	1.268
89.45	0.0133	75.2	1.28	16.84	0.0532	18.82	1.270
89.82	0.0135	73.9	1.31	21.23	0.0445	22.49	1.258
		Run 3		20.55	0.0452	22.14	1.247
4.21	0.1138	8.786	1.282	27.34	0.0370	27.0	1.27
4.21	0.1138	8.788	1.282			Run 5	
4.27	0.1139	8.788	1.291	76.98	0.0153	65.5	1.284
4.02	0.1140	8.769	1.263	77.12	0.0152	65.9	1.277
5.00	0.1043	9.59	1.257	77.19	0.0153	65.2	1.292
8.49	0.0815	12.26	1.257	77.33	0.0153	65.4	1.291
15.07	0.0575	17.40	1.272	105.73	0.0114	88.0	1.282
27.51	0.0370	27.1	1.28	105.39	0.0113	88.4	1.272
33.77	0.0323	31.0	1.32	127.73	0.0095	105.	1.29
33.69	0.0322	31.1	1.31	126.93	0.0096	104.	1.28
41.75	0.0265	37.7	1.29	152.21	0.0080	125.	1.27
45.26	0.0247	40.6	1.29	151.63	0.0079	127.	1.25
50.29	0.0225	44.4	1.29	176.71	0.0068	147.	1.25
50.03	0.0227	44.1	1.30	175.43	0.0071	141.	1.30
56.04	0.0204	48.9	1.29	203.41	0.0065	154.	1.36
63.94	0.0184	54.4	1.30	201.09	0.0065	154.	1.35

Table 17 (Continued)

T(°K)	χ'_m ($\frac{emu}{mole}$)	χ'^{-1}_m ($\frac{mole}{emu}$)	$\frac{\chi'_m(T-\theta)}{(\frac{emu°K}{mole})}$	T(°K)	χ'_m ($\frac{emu}{mole}$)	χ'^{-1}_m ($\frac{mole}{emu}$)	$\frac{\chi'_m(T-\theta)}{(\frac{emu°K}{mole})}$
221.56	0.0058	173.	1.32			Run 7	
219.69	0.0057	174.	1.30	77.12	0.0152	65.6	1.283
246.44	0.0052	192.	1.32	77.12	0.0150	66.6	1.265
243.32	0.0051	197.	1.27	77.25	0.0152	65.7	1.283
240.36	0.0052	192.	1.29	77.28	0.0152	66.0	1.278
		Run 6		122.75	0.0099	101.	1.28
				122.63	0.0097	103.	1.26
77.04	0.0152	65.8	1.278	173.21	0.0073	137.	1.32
77.10	0.0153	65.5	1.284	172.88	0.0071	140.	1.28
76.99	0.0152	65.6	1.281	201.73	0.0064	157.	1.33
77.07	0.0153	65.5	1.284	200.05	0.0064	157.	1.32
80.14	0.0148	67.6	1.291	219.93	0.0058	172.	1.32
85.33	0.0139	71.9	1.284	218.85	0.0059	170.	1.33
90.62	0.0131	76.6	1.275	232.36	0.0057	177.	1.36
90.64	0.0130	76.8	1.272	232.00	0.0054	186.	1.29
98.28	0.0122	82.3	1.280	238.86	0.0052	192.	1.28
108.91	0.0109	91.6	1.266	238.68	0.0052	192.	1.28
118.10	0.0101	99.0	1.264	251.27	0.0050	202.	1.28
117.92	0.0101	98.8	1.265	250.51	0.0050	202.	1.28
130.62	0.0091	110.	1.25				
146.43	0.0083	121.	1.27			Run 8	
156.98	0.0076	131.	1.25	4.182	0.1142	8.760	1.283
170.47	0.0072	140.	1.27	4.182	0.1141	8.762	1.282
186.24	0.0069	145.	1.33	4.182	0.1140	8.772	1.281
185.70	0.0068	148.	1.30	4.072	0.1152	8.679	1.282
195.94	0.0065	155.	1.31	3.838	0.1179	8.479	1.285
207.81	0.0062	162.	1.33	3.555	0.1212	8.248	1.286

Table 17 (Continued)

T(°K)	χ'_m ($\frac{emu}{mole}$)	χ'^{-1}_m ($\frac{mole}{emu}$)	$\frac{\chi'_m(T-\theta)}{(\frac{emu°K}{mole})}$	T(°K)	χ'_m ($\frac{emu}{mole}$)	χ'^{-1}_m ($\frac{mole}{emu}$)	$\frac{\chi'_m(T-\theta)}{(\frac{emu°K}{mole})}$
3.320	0.1246	8.026	1.293	1.464	0.2364	4.230	2.014
3.038	0.1291	7.748	1.303	1.464	0.2364	4.230	2.014
2.810	0.1327	7.534	1.327				
2.563	0.1380	7.247	1.327		Run 10		
2.158	0.1500	6.668	1.382	4.191	0.1127	8.873	1.268
2.121	0.1514	6.604	1.390	4.191	0.1115	8.969	1.254
2.067	0.1544	6.476	1.409	3.303	0.1218	8.214	1.261
2.004	0.1571	6.366	1.423	2.530	0.1348	7.417	1.291
1.923	0.1719	5.816	1.544	2.481	0.1357	7.370	1.294
1.860	0.1984	5.041	1.769	2.090	0.1484	6.740	1.357
				1.964	0.1561	6.408	1.408
	Run 9			1.976	0.1547	6.464	1.397
4.189	0.1141	8.766	1.283				
4.189	0.1142	8.755	1.284		Run 11		
3.567	0.1214	8.237	1.290	4.191	0.1128	8.868	1.268
2.865	0.1318	7.588	1.308	4.191	0.1127	8.875	1.267
2.893	0.1312	7.620	1.306	2.724	0.1326	7.539	1.297
4.183	0.1142	8.756	1.284	2.323	0.1413	7.078	1.325
4.183	0.1140	8.773	1.281	2.313	0.1413	7.076	1.324
2.523	0.1383	7.233	1.324	2.278	0.1425	7.018	1.330
1.895	0.1828	5.470	1.637	2.025	0.1528	6.544	1.388
1.806	0.2074	4.821	1.838	1.956	0.1600	6.249	1.442
1.753	0.2154	4.643	1.897	1.892	0.1801	5.551	1.612
1.676	0.2349	4.257	2.051	1.774	0.2086	4.793	1.842
1.638	0.2602	3.844	2.262	1.645	0.2711	3.689	2.359
1.542	0.2723	3.672	2.342	1.542	0.2735	3.656	2.352
1.464	0.2341	4.272	1.994				

Table 17 (Continued)

T(°K)	χ'_m ($\frac{emu}{mole}$)	χ'^{-1}_m ($\frac{mole}{emu}$)	$\frac{\chi'_m(T-\theta)}{(\frac{emu°K}{mole})}$
1.473	0.2447	4.087	2.087
1.443	0.2038	4.908	1.732
1.224	0.1600	6.251	1.325
1.394	0.2090	4.784	1.766
1.541	0.2699	3.705	2.321
1.554	0.2762	3.621	2.378
1.556	0.2769	3.612	2.384
1.589	0.2814	3.553	2.433
1.612	0.2734	3.657	2.370
1.632	0.2604	3.840	2.262
1.686	0.2331	4.290	2.038

obtained from vapor pressure measurements. Runs 8-11 were made with the coils in the liquid He bath in thermal contact with the sample via He exchange gas in the sample space. The temperature of the bath was lowered by pumping; the temperature was controlled by manually operating a throttle valve to control the pumping speed. The lowest pressure attained was about 0.7 mm Hg at a bath temperature of about 1.22°K. The primary current was 100 ma for Run 1, 30 ma and 50 ma for Run 2 and 50 ma for the remainder of the runs. These currents correspond to fields of approximately 21.3, 6.4 and 10.6 Oe at maximum (see Appendix B). The frequency was 45 Hz. No field dependence was observed above 4.2°K.

Table 18 lists the results of measurements made as a function of field on sample 2. These were type 2 measurements without heater and thermocouple; therefore, χ_m'' was also obtained. These measurements were made at 30, 50, 100 and 150 ma, corresponding to fields of 6.1, 10.2, 20.4 and 30.6 Oe at maximum (see Appendix B). The experimental points above 4.2°K are given in Figure 25 as a plot of $1/\chi_m'$ versus T. The results below 4.2°K are given in Figure 26. Both χ_m' and χ_m'' are plotted. The $\chi_m'^{-1}$ versus T curve is linear down to 4.2°K obeying a Curie-Weiss law and exhibiting paramagnetic behavior. As expected χ_m' was found to be field independent in this region and χ_m'' was found to be very small as indicated by the results in Table 2. Figure 26 indicates that there

Table 18. Field dependent susceptibility of $NiC_4O_4 \cdot 2H_2O$. Sample wt.=3.124g; labeled sample 2 in Table 1 (25.37% Ni); no thermocouple or heater assembly were used

T(°K)	χ'_m ($\frac{emu}{mole}$)	χ''_m ($\frac{emu}{mole}$)
i_p=30 ma; H=6.4 Oe		
4.203	0.1132	0.447×10^{-3}
4.203	0.1130	0.450
4.189	0.1132	0.455
4.194	0.1181	0.429
2.822	0.1307	0.480
2.216	0.1441	0.480
2.209	0.1448	0.480
2.158	0.1470	0.547
2.035	0.1517	0.549
1.884	0.1766	3.522
1.788	0.2080	6.86
1.694	0.2256	7.39
1.659	0.2385	8.21
1.652	0.2420	8.52
1.644	0.2470	8.96
1.631	0.2533	9.74
1.610	0.2662	11.83
1.595	0.2752	13.57
1.575	0.2841	15.62
1.561	0.2857	16.17
1.553	0.2845	15.97
1.540	0.2805	15.17
1.524	0.2725	13.48
1.487	0.2547	9.86
1.443	0.2374	7.48
1.388	0.2118	5.58
1.270	0.1667	1.400
1.234	0.1608	1.165
i_p=50 ma; H=10.6 O_e		
77.18	0.0150	0.165×10^{-3}
77.18	0.0150	0
77.17	0.0150	0
77.17	0.0150	0
4.196	0.1132	0.461×10^{-3}
4.196	0.1131	0.450
i_p=100 ma; H=21.3 Oe		
77.21	0.0146	0.060×10^{-3}
77.21	0.0146	0.119
77.21	0.0147	0.116
77.21	0.0146	0.116
4.198	0.1130	0.405
4.197	0.1131	0.403
4.196	0.1129	0.424
4.196	0.1130	0.384
3.891	0.1164	0.424
3.843	0.1170	0.424
3.419	0.1221	0.485
2.983	0.1285	0.445
2.970	0.1287	0.447
2.615	0.1352	0.538
2.603	0.1353	0.518
4.201	0.1131	0.459
4.201	0.1130	0.472
3.021	0.1279	0.524
2.578	0.1357	0.565
2.348	0.1416	0.565
4.199	0.1130	0.652
1.981	0.1550	0.645
1.967	0.1563	-
1.943	0.1588	0.816
1.856	0.1825	5.22
1.822	0.1941	8.21
1.681	0.2261	10.33
1.658	0.2349	11.40
1.594	0.2682	18.95
1.582	0.2755	21.96
1.567	0.2786	23.25
1.560	0.2800	24.00

Table 18 (Continued)

T(°K)	χ_m' ($\frac{emu}{mole}$)	χ_m'' ($\frac{emu}{mole}$)	T(°K)	χ_m' ($\frac{emu}{mole}$)	χ_m'' ($\frac{emu}{mole}$)
1.546	0.2800	24.52×10^{-3}	2.816	0.1309	0.342×10^{-3}
1.548	0.2803	25.21	2.380	0.1398	0.426
1.508	0.2662	21.06	2.149	0.1476	0.406
1.482	0.2560	18.08	2.043	0.1518	0.465
1.486	0.2538	17.40	1.900	0.1664	1.671
1.456	0.2435	14.98	1.902	0.1657	1.545
1.454	0.2424	14.84	1.806	0.1964	9.08
1.453	0.2432	-	1.709	0.2131	9.69
1.385	0.2136	13.14	1.661	0.2304	11.29
			1.645	0.2367	11.92
i_p=150 ma; H=31.9 Oe			1.634	0.2419	12.26
4.197	0.1130	0.447×10^{-3}	1.617	0.2495	13.76
4.196	0.1130	0.447	1.598	0.2593	16.06
4.191	0.1132	0.343	1.564	0.2739	22.53
4.191	0.1132	0.343	1.552	0.2758	23.82
3.860	0.1163	0.398	1.537	0.2747	24.10
3.435	0.1219	0.377	1.480	0.2615	20.15
			1.434	0.2324	13.23
			1.379	0.2126	13.31
			1.259	0.1636	1.294

is a transition to an ordered magnetic state at about 1.56°K. The direction of the deviation of the susceptibility from Curie-Weiss behavior indicates that the ordered state is ferromagnetic. The existence of magnetic losses as measured by χ_m'' correlates with this indication. There is a shoulder on the high temperature side of the peaks in both χ_m' and χ_m''. The shoulder is centered roughly at 1.8°K. As can be seen from Figure 26 there is only a very small field dependence in χ_m'. The field dependence in χ_m'' is more pronounced. The χ_m'' points plotted for 50 ma were taken with a type 1 sample

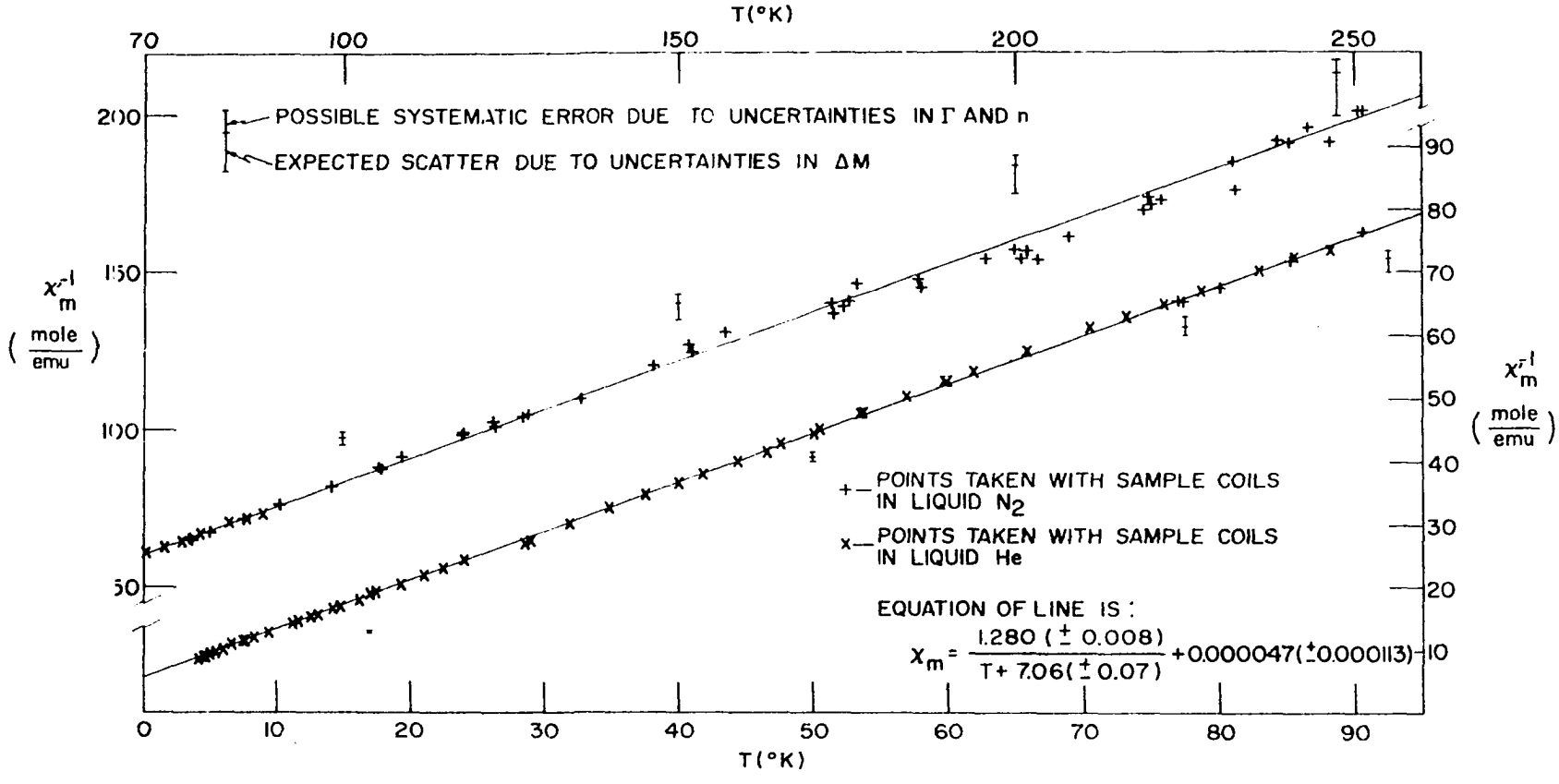

Figure 25. Molar susceptibility of $NiC_4O_4 \cdot 2H_2O$, sample 2, above 4.2°K

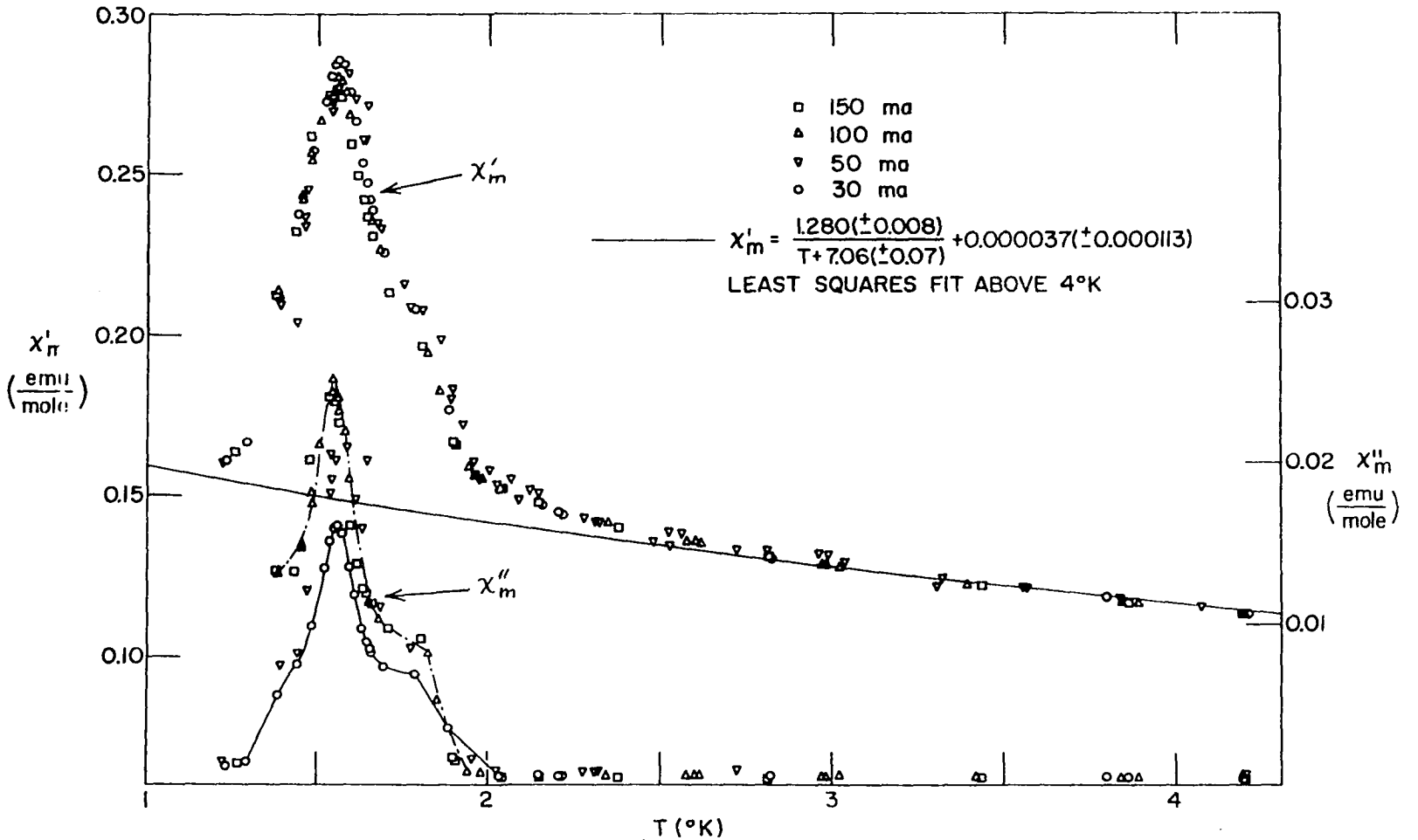

Figure 26. Molar susceptibility of $NiC_4O_4 \cdot 2H_2O$, sample 2, below 4.2°K

arrangement including heater and thermocouple.

Measurements on sample 3

Only type 1 measurements were made on sample 3, containing 27.79(±0.15)% Ni. Two samples were measured; sample 3a weighed 2.2298g (0.010555(±59) moles of Ni^{++}) and sample 3b weighed 0.7934g (0.003756(±26) moles of Ni^{++}). Both samples were run in the same bakelite sample container weighing 5.37g and with 1.31g and 0.785g of silicone oil, respectively, saturating the samples. Points were taken at liquid nitrogen temperatures at 50 ma and at liquid He temperatures at 100 ma. The experimental results are given in Table 19. Figure 27 shows the behavior of χ_m' and χ_m'' below 4.2°K. As can be seen, both χ_m' and χ_m'' exhibit two peaks at 1.68°K and 2.05°K. The peaks indicate two magnetic transitions in sample 3. Further, both peaks in χ_m' and χ_m'' are larger in magnitude and occur at higher temperatures than the peak observed for sample 2. In this temperature range, the susceptibility behavior of the two samples thus seems to be quite different. The small shoulder at 1.8°K observed in χ_m' and χ_m'' of sample 2, however (see Figure 26), could be considered as indicative of the same type of double peak behavior exhibited by sample 3.

Table 19. Molar susceptibility of $NiC_4O_4 \cdot 2H_2O$, sample #3.
Sample 3a, 2.2298g (0.010555 moles of Ni).
Sample 3b, 0.7852g (0.003756 moles of Ni)

T(°K)	χ_m' ($\frac{emu}{mole}$)	χ_m'' ($\frac{emu}{mole}$)	T(°K)	χ_m' ($\frac{emu}{mole}$)	χ_m'' ($\frac{emu}{mole}$)
	Sample 3a				
77.12	0.0150	0.048×10^{-3}	1.738	0.6737	93.42×10^{-3}
77.12	0.0149	0.048	1.732	0.7036	87.44
77.16	0.0151	0.029		Sample 3b	
77.16	0.0149	0.052			
77.16	0.0150	0.064	77.04	0.0155	0.0221×10^{-3}
4.190	0.1094	0.433	77.04	0.0153	0.0288
4.190	0.1094	0.368	77.04	0.0154	0.0
4.191	0.1093	0.380	77.04	0.0153	0.0
4.190	0.1093	0.513	4.178	0.1094	0.707
4.190	0.1093	0.369	4.178	0.1100	0.628
3.518	0.1168	0.469	2.392	0.1376	0.702
3.500	0.1168	0.350	2.148	0.1514	0.784
2.914	0.1258	0.436	2.115	0.1634	0.972
2.342	0.1374	0.262	2.104	0.1785	1.255
2.012	0.3719	128.3	2.094	0.2050	4.30
2.023	0.3827	130.0	2.082	0.2818	15.05
1.851	0.2687	40.93	2.064	0.3876	45.75
4.192	0.1096	0.432	2.048	0.4331	109.2
4.192	0.1095	0.480	2.018	0.4130	145.9
4.192	0.1095	0.435	2.004	0.3766	126.2
4.192	0.1095	0.353	1.973	0.3369	104.8
3.580	0.1176	0.496	1.954	0.3070	83.65
2.640	0.1298	0.453	1.933	0.2854	64.43
2.297	0.1390	0.411	1.910	0.2712	46.45
1.970	0.3143	90.52	1.869	0.2651	38.41
2.152	0.1477	0.456	1.838	0.2745	32.20
2.114	0.1564	0.480	1.822	0.2887	32.20
2.079	0.2634	11.18	1.774	0.4351	52.00
2.050	0.4394	105.1	1.750	0.7162	105.7
2.061	0.3922	128.3	1.678	0.7907	137.6
1.991	0.3557	114.0	1.650	0.7878	164.4
1.972	0.3250	96.27	1.659	0.7860	152.9
1.921	0.2740	54.42	1.683	0.7791	133.4
1.881	0.2644	44.96	1.598	0.7569	153.4
1.852	0.2693	41.44	1.535	0.7098	152.3
1.817	0.2996	41.85	1.443	0.6386	147.9
1.785	0.3760	51.93	1.379	0.5920	143.8
			1.248	0.5059	133.1

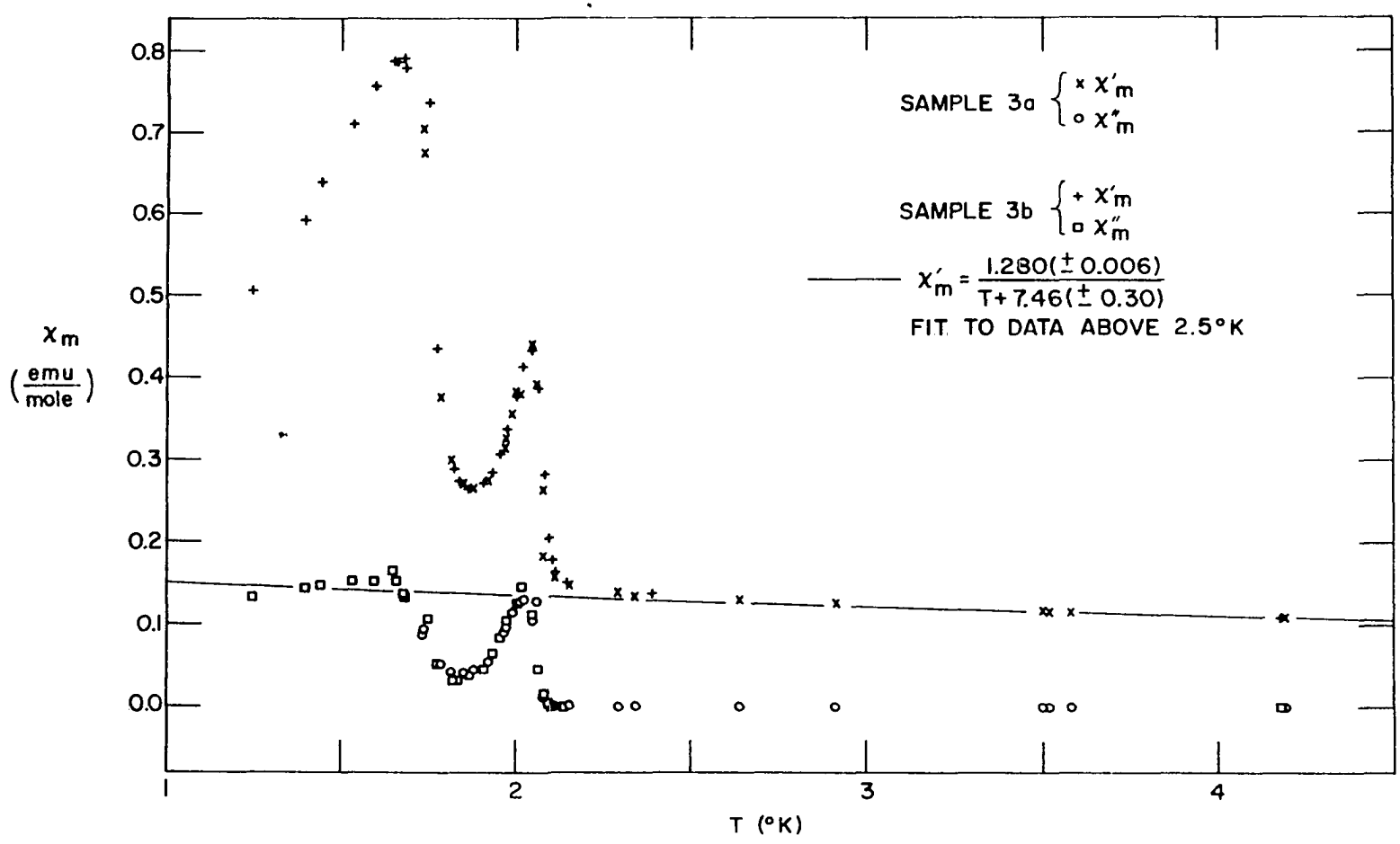

Figure 27. Molar susceptibility of $NiC_4O_4 \cdot 2H_2O$, sample 3, below 4.2°K

Data analysis

If the susceptibility of the two samples follows Curie-Weiss law behavior above 4.2°K, then

$$\chi_m = \frac{C}{T-\theta} \quad . \tag{38}$$

where C is the Curie constant and θ is called the Weiss constant. $\chi_m=\chi_m'$, since $\chi_m''=0$ in the paramagnetic region at the low frequencies employed in this work. The reciprocal susceptibility will then be a linear function of T:

$$\chi_m^{-1} = -\frac{\theta}{C} + \frac{1}{C} T \tag{39}$$

A linear least squares fit of the experimental data in the paramagnetic region to Equation 39 gave χ_m^{-1} = 5.99(0.20) + 0.7681(0.0020) T for sample 2 and χ_m^{-1} = 5.83(0.20) + 0.7814(0.0039) T for sample 3. The resulting values for C and θ are given in Table 20. The uncertainties in rounded brackets are standard deviations derived from the scatter of the experimental points about the line of best fit.

On theoretical grounds, as discussed in Appendix A, however, one expects the susceptibility of octahedrally coordinated nickel to be of the form

$$\chi_m = \frac{C}{T-\theta} + \alpha \tag{40}$$

To determine, C, θ and α, a nonlinear least squares program was written and used to fit the high temperature data for

Table 20. Results of high temperature data analysis (data for $T \geq 4.2°K$)

		Sample 2		Sample 3	
Result of fit to $\chi_m = \frac{C}{T-\theta}$	$C(\frac{emu\ deg}{mole})$	1.302	(0.003) [±0.027]	1.280	(0.006) [±0.027]
	θ(deg)	-7.80	(0.28) [±0.27]	-7.46	(0.30) [±0.27]
Result of fit to $\chi_m = \frac{C}{T-\theta} + \alpha$	$C(\frac{emu\ deg}{mole})$	1.280	(0.008) [±0.027]	-	-
	θ(deg)	-7.06	(0.07) [±0.27]		
	$\alpha(\frac{emu}{mole})$	0.37	(1.13)x10^{-4}		

sample 2 to Equation 40. Young (1962) and Deming (1943) were used as a guide in writing the program. The results for sample 2 are given in Table 20. The values for C and θ differ somewhat from those obtained in the fit of the data to Equation 39. A fit of the data for sample 3 to Equation 40 is not possible since only a few points at liquid He and liquid N_2 temperatures are available. A linear fit was made however and the results are given in Table 20. The values of C for the two samples obtained from the linear fit differ by only 1.7%, indicating essentially the same effective moment for both samples. The value of C obtained from a linear fit of the data for sample 3 is exactly equal to the value of C obtained for sample 2 in the nonlinear fit; this

result is probably accidental. However, for sample 2 the results of the nonlinear fit will be used and for sample 3 the results of the linear fit will be used, since in both cases those are the best results available.

Uncertainties

The uncertainties quoted in Table 20 in the rounded brackets are standard deviations calculated from the scatter of the experimental points about the line of best fit. This scatter is due to errors in reading ΔM_v and T. Although the accuracy of the thermocouple temperature measurements is about 0.5 degree, this error is systematic, and a series of successive temperature measurements is expected to yield values uniformly low or high with scatter of about 0.05 degree. That is, it is the case that $\delta T/T << \delta(\Delta M)/\Delta M$, where δT and δM are possible reading errors in one temperature or ΔM measurement. One can thus assume that T is measured "exactly" and that the experimental scatter is due to reading errors in the determination of ΔM_v. Estimated uncertainties in reading ΔM_v lead to errors in χ_m of 0.15% at 1.5°K, 0.41% at 4.2°K, 2.2% at 77.1°K and 6.8% at 250°K. The expected scatter in the experimental points due to these errors is indicated in Figure 25. As can be seen, the actual scatter of the points is somewhat less than expected throughout most of the temperature range.

In addition to the random type errors discussed above a

systematic error due to uncertainties in Γ and N could be included in the observed χ_m's. This will be a systematic error because the same Γ and N are used in calculating all χ_m's. Assuming the uncertainties in Γ and N quoted previously, the possible systematic error in χ_m was calculated to be 1.42% in the range where the coils are in liquid He and 2.1% in the range where they are in liquid N_2. The size of this possible error has also been indicated in Figure 25. If one assumes the susceptibility to follow Equation 39 the additional uncertainties in C and θ due to this possible systematic error are easily estimated graphically to be ± 0.027 and ± 0.27 respectively; one can assume that these additional uncertainties in C and θ will be approximately the same if χ_m versus T is assumed to obey Equation 40. It is not possible in this case to estimate the error in α simply, but since α essentially represents curvature in the nearly straight line of $1/\chi_m$ versus T it should not be changed much by a systematic type of error in χ_m^{-1}. The possible systematic errors in C and θ are given in square brackets in Table 20. The relationships are such that if the systematic error in C is positive it is also positive in θ.

Susceptibility Measurements: Discussion of Results

At temperatures above 4.2°K the measured susceptibility for sample 2 could be represented by the equation

$$\chi_m = \frac{1.280(\pm 0.035)}{T+7.06(\pm 0.34)} + 0.37(1.13)\times 10^{-4} \qquad (41)$$

From this relation the diamagnetic contribution of about -0.75×10^{-4} emu/mole must be subtracted (Selwood, 1956; West and Niu, 1963a). The paramagnetic contribution is then given by

$$\chi_m = \frac{1.280(\pm 0.035)}{T+7.06(\pm 0.34)} + 1.12(1.13)\times 10^{-4} \qquad (42)$$

In the crystal field approximation one expects octahedrally coordinated Ni^{++} ions to have a paramagnetic susceptibility (as given in Appendix A)

$$\chi_m = \frac{8N\mu_B^2}{3kT}\left(1 - \frac{4\lambda}{10Dq}\right)^2 + \frac{8N\mu_B^2}{10Dq} \qquad (43)$$

where $g = 2\left(1 - \frac{4\lambda}{10Dq}\right)$ and $p_{eff} = g[S(S+1)]^{1/2}$. From the susceptibility data (Equation 42) one calculates $g=2.262(\pm 0.031)$ and $p_{eff}=3.20(\pm 0.04)$. The effective number of Bohr magnetons is in good agreement with the value obtained by West and Niu (see Table 1), but is lower than the value derived from the data of Smentowski and Gerstein (see Table 2).

The value of 10Dq measured via the optical spectrum is 8550 cm^{-1} (see the section on the optical spectrum). This value allows one to calculate a value for λ of $-280(\pm 30)$ cm^{-1},

which is 86% of the free ion value of -324 cm^{-1} (Moore, 1952; Shenstone, 1954). Similar reductions in the spin orbit coupling parameters have been found for other transition metal ions in coordination complexes. In particular, for Ni^{++} ions coordinated by six H_2O molecules (roughly octahedrally) some typical measured spin orbit coupling parameters are: -281 cm_{-1} in α-$NiSO_4 \cdot 6H_2O$ (Fisher and Hornung, 1968); -250 to -270 cm^{-1} in several Tutton salts of prototype formula $K_2Ni(SO_4)_2 \cdot 7H_2O$ (Owen, 1955a,b; Griffiths and Owen, 1952); and -242 cm^{-1} for Ni^{++} doped in MgO (Low, 1958a,b). The measured spin orbit coupling parameter is called the effective spin orbit coupling parameter.

This reduction in the spin orbit coupling parameter has usually been explained with use of the molecular orbital theory, a brief discussion of which is given in Appendix A. The expression for the g-factor obtained from the M.O. theory is

$$g = 2(1-4N_\sigma k\ \lambda/10Dq) \qquad (44)$$

where N_σ and k have the definitions given in Appendix A. The effective spin orbit coupling parameter measured is set equal to $N_\sigma\ k\ \lambda_o$,

$$\lambda_{eff} = N_\sigma\ k_\sigma\ \lambda_o \qquad (45)$$

where λ_o is the free ion spin orbit coupling parameter. The ratio of λ_{eff} to λ_o is about 0.864 and we set

$$N_\sigma\ k \simeq 0.864 \qquad (46)$$

Assuming $N_\sigma \simeq 1$ and using Equation A72 we find that the fraction of unpaired electron density transferred to each oxygen atom is about 9%. A similar calculation by Owen and Thornley (1966) yields an unpaired spin density of 3.8% (k=0.88) on the F^- ion in the NiF_6^{-4} complex. The lower value was obtained because π-bonding was included in their calculations. It is likely that π-bonding is important in $NiC_4O_4 \cdot 2H_2O$ also, but is not easily incorporated in a M.O. treatment of the complex.

The above calculation of the unpaired spin transfer to the oxygen atom in $NiC_4O_4 \cdot 2H_2O$ is subject to a number of approximations given above and in Appendix A.

The theoretical expression for the temperature independent paramagnetic susceptibility (Equation 43) yields a value of 2.43×10^{-4} emu/mole while the measured value is $1.07(1.13) \times 10^{-4}$ emu/mole. From the large standard deviation in the measured value, all of which is due to the experimental scatter in the data, all one can say is that the two values agree to within two standard deviations of the measured value.

The Weiss constant (see Appendix A) obtained from the experimental data is $-7.06(\pm 0.34)$°K, which if due to magnetic interactions, would predict that they are antiferromagnetic. However, the susceptibility of both samples exhibit peaks characteristic of ferromagnetic ordering at temperatures ≤ 2°K.

Susceptibility behavior identical to the Curie-Weiss

law can be obtained for a Ni^{++} complex if the zero-field ground state manifold of the ion is split (see Appendix A) by spin orbit coupling. However, no meaningful results concerning the zero field splitting can be obtained from the powder data; to extract any information about zero field splittings from the "Weiss constant" would require single crystal data.

The original interest in $NiC_4O_4 \cdot 2H_2O$ came from the expectation of observing one-dimensional magnetic interactions via susceptibility measurements since the structure as originally proposed by West and Niu (1963a) was a linear coordination polymer in which Ni^{++} ions are linked by squarate ions as shown in Figure 4(a). The possibility of superexchange between the Ni^{++} ions via the π-molecular orbitals of the squarate ion indicated that exchange interactions would most likely be antiferromagnetic (Kanamori, 1959; Anderson, 1963). Although the structure was found not to be a linear coordination polymer, as discussed in the section on the structural work, any magnetic superexchange interactions are still expected to go through the squarate ion π-orbitals leading to antiferromagnetic interactions.

The low temperature susceptibility results, however, indicate that $NiC_4O_4 \cdot 2H_2O$ orders ferromagnetically at temperatures less than 2°K. The exact ordering temperature of sample #2 is 1.56°K. Sample #3 exhibits two peaks at 2.05°K and 1.68°K. Sample #2 also shows a shoulder on the

high temperature side of the peak at 1.56°. The shoulder is centered at about 1.8°K (see Figures 26 and 27). Therefore it seems that both samples qualitatively exhibit the same type of double peak behavior at lower temperatures. Both peaks in sample #3 are characteristic of ferromagnetic ordering, while in sample #2 the larger peak is also characteristic of ferromagnetic ordering. The small shoulder in χ_m for sample #2 is not well resolved and no conclusions about it can be reached. This double peak behavior might be due to an impurity in the sample or to the ferromagnetic ordering of two magnetic sublattices in the sample.

It would be of great interest to measure the susceptibility of a single crystal of $NiC_4O_4 \cdot 2H_2O$ in order to resolve the ambiguities in the interpretation of the powder magnetic susceptibility measured in this sample.

PARAMAGNETIC RESONANCE

Attempts were made to obtain the electron spin resonance spectrum of the Ni^{++} ion in $NiC_4O_4 \cdot 2H_2O$ (Carrington and McLachlan, 1967; Low, 1958a,b,1960; Bleaney and Stevens, 1953). The instrument used was a Strand model 602B, X band ($h\nu \simeq 0.32$ cm^{-1}) electron paramagnetic resonance spectrometer combined with a 12" Magnion electromagnet. The magnet was capable of a maximum field of about 12 kOe. Cavities available were a Strand cylindrical TE_{011} cavity and a Varian rectangular TE_{102} cavity. Cold Finger type liquid N_2 and liquid He dewars (constructed in this laboratory) were available for low temperature measurements. The lowest temperature attainable with the liquid He dewar is estimated to be approximately 15°K.

A search for a resonance signal was made using powdered $NiC_4O_4 \cdot 2H_2O$ and "twinned" crystal cubes as large as 0.5 mm on a side. Also, samples of $ZnC_4O_4 \cdot 2H_2O$ doped with 1-3% Ni^{++} (both powder and "twinned" crystal samples) were investigated at room temperature, liquid N_2 temperatures and at 15°K. No signal was observed in any of these experiments. Since experimental conditions were such that an absorption as wide as 500 Oe should have given signals at least 5 times the noise, it is concluded that the zero field splitting of the ground state spin triplet must be large enough so that a 12

kOe DC field is insufficient to produce transitions induced by the energy quanta available with the X band spectrometer. Zero field splitting and variation of the energy levels as a function of an applied magnetic field is discussed in Appendix A.

An attempt to obtain the electron spin resonance of Ni^{++} in $NiC_4O_4 \cdot 2H_2O$ using K or Q band spectrometers would therefore be very fruitful in determining the zero field splitting and g factors of the ion and thus elucidating the actual symmetry of the crystal field about the Ni ion and giving a check on the g factor derived from the susceptibility measurements.

The best results would be obtained from single crystals, however, and at present no technique has been found to grow single crystals large enough for electron paramagnetic resonance work. Experiments on "twinned" crystals would face some of the same problems found in the structural work and would require exact knowledge of the twinning mode to yield meaningful results.

SUGGESTIONS FOR FURTHER WORK

The results of this investigation have been summarized in the various sections and some suggestions for further work have been given. The major need is for the production of single crystals to allow a straight forward structural determination without the ambiguities introduced by the twinning found in the crystals grown in this work. Such single crystals might most easily be obtained by further efforts to obtain them by breaking "twinned" crystals. Single crystals large enough for susceptibility and electron paramagnetic resonance measurements can not be obtained in this way and a technique to grow large single crystals of $NiC_4O_4 \cdot 2H_2O$ is needed.

It would also be of interest to determine the structure of $CuC_4O_4 \cdot 2H_2O$ which was found by West and Niu (1963a) to have a different powder pattern and hence different structure than $NiC_4O_4 \cdot 2H_2O$. The differences in the structure of the Mn, Zn and Cu croconate salts have been discussed in the Literature Review section. Such a tetragonal distortion of the coordination about the Cu^{++} ion is typical [compare for example the structures of $CsNiCl_3$ (Stucky, D'Agostino, and McPherson, 1966) and $CsCuCl_3$ (Schlueter, Jacobson and Rundle, 1968)] and it would be interesting to determine the change in structure in going from Ni^{++} to Cu^{++} squarate.

Finally, it would be desirable to make heat capacity measurements on Ni squarate samples below 4.2°K in the region

of the magnetic transitions to obtain some measure of the entropy associated with the transitions. Such capability has recently been achieved in this group with the completion of a ^{3}He calorimeter (Keller, 1970).

LITERATURE CITED

Abel, W. R., A. C. Anderson, and J. C. Wheatley, 1964, Rev. Sci. Instr., 35, 444.

Abragam, A., and M. H. L. Pryce, 1951, Proc. Roy. Soc. (London), A205, 135.

Anderson, A. C., G. L. Salinger, and J. C. Wheatley, 1961, Rev. Sci. Instr. 32, 1110.

Anderson, P. W., 1959, Phys. Rev., 115, 2.

Anderson, P. W., 1963,"Theory of Exchange in Insulators," in Solid St. Phys., Vol. 2, F. Seitz and D. Turnbull, Eds., Academic Press, New York, N.Y., p. 99.

Baenziger, N. C., J. J. Hegenbarth, and D. C. Williams, 1963, J. Am. Chem. Soc., 85, 1539.

Baenziger, N. C., and J. J. Hegenbarth, 1964, J. Am. Chem. Soc., 86, 3250.

Baenziger, N. C., and D. G. Williams, 1966, J. Am. Chem. Soc., 88, 689.

Ballhausen, C. J., 1962, Ligand Field Theory, McGraw-Hill Book Company, Inc., New York, N.Y.

Bethe, H. A., 1929, Ann. Physik, 3, 133.

Bleaney, B., and K. W. H. Stevens, 1953, Repts. Prog. Phys., 16, 108.

Bleaney, B. I., and B. Bleaney, 1957, Electricity and Magnetism, Oxford University Press, London.

Bloss, F. D., 1961, An Introduction to the Methods of Optical Crystallography, Holt, Rinehart and Winston, New York, N.Y.

Brickwedde, F. G., H. van Dijk, M. Durieux, J. R. Clement and J. K. Logan, 1960, J. Res. Nat. Bur. Stand., 64A, 4.

Brown, R. E., and W. M. Hubbard, 1965,"The Magnetic Susceptibility of Rare Earth Oxides Below 4.2°K",in Book 4 of the Conference Preprints, Fifth Rare-Earth Research Conference, Ames, Iowa.

Buerger, M. J., 1959, Vector Space and its Application in Crystal Structure Investigation, John Wiley and Sons, Inc., New York, N.Y.

Buerger, M. J., 1960, Crystal Structure Analysis, 1st ed., John Wiley and Sons, Inc., New York, N.Y.

Buerger, M. J., 1964, The Precession Method, John Wiley and Sons, Inc., New York, N.Y.

Bunn, C. W., 1946, Chemical Crystallography, 1st ed., Oxford University Press, London.

Burbank, R. D., 1952, Rev. Sci. Instr., 23, 321.

Busing, W. R., and H. A. Levy, 1957, Acta. Cryst., 10, 180.

Busing, W. R., K. O. Martin, and H. A. Levy, 1962, A FORTRAN Crystallographic Least Squares Program, Oak Ridge National Laboratory Report ORNL-TM-305 [Oak Ridge National Laboratory, Tennessee].

Busing, W. R., K. O. Martin, and H. A. Levy, 1964, A FORTRAN Crystallographic Function and Error Program, Oak Ridge National Laboratory Report ORNL-TM-306 [Oak Ridge National Laboratory, Tennessee].

Carrington, A., and A. D. McLachlan, 1967, Introduction to Magnetic Resonance, Harper and Row, New York, N.Y.

Cohen, S., J. R. Lacher and J. D. Park, 1959, J. Am. Chem. Soc., 81, 3480.

Condon, E. U., and G. H. Shortley, 1951, Theory of Atomic Spectra, Cambridge University Press, New York, N.Y.

Cotton, A. F., 1963, Chemical Applications of Group Theory, John Wiley and Sons, Inc., New York, N.Y.,

Deming, W. E., 1943, Statistical Adjustment of Data, John Wiley and Sons, Inc., New York, N.Y.

Eyring, H., J. Walter, and G. E. Kimball, 1944, Quantum Chemistry, John Wiley and Sons, Inc., New York, N.Y.

Figgis, B. N., 1966, Introduction to Ligand Fields, John Wiley and Sons, Inc., New York, N.Y.

Fisher, R. A., and E. W. Hornung, 1968, J. Chem. Phys., 48, 4284.

Furnas, T. C., Jr., 1957, Single Crystal Orienter Instruction Manual, General Electric Co., Milwaukee, Wisconsin.

Gehring, D. G., 1969, Magnetic Susceptibilities of Dimethylammonium Trichlorocuprate(II) and tetramethylammonium Trichloronickelate(II). Unpublished M.S. thesis, Library, Iowa State University of Science and Technology, Ames, Iowa.

Gerstein, B. C., and F. H. Spedding, 1960, Heat Capacity and Magnetic Susceptibility of Thulium Ethylsulfate, U.S. Atomic Energy Commission Report IS-331 (Ames Laboratory, Iowa State University of Science and Technology, Ames, Iowa).

Glick, M. D., and L. F. Dahl, 1966, Inorg. Chem., 5, 289.

Glick, M. D., G. L. Downs and L. F. Dahl, 1964, Inorg. Chem., 3, 1712.

Grenville-Wells, H. J., and S. C. Abrahams, 1952, Rev. Sci. Instr. 23, 328.

Griffith, J. S., 1961, The Theory of Transition Metal Ions, Cambridge University Press, New York, N.Y.

Griffiths, J. H. E., and J. Owen, 1952, Proc. Roy. Soc. (London), A213, 459.

Hacker, H., Jr., M. S. Lin, and E. F. Westrum, Jr., 1965, "Magnetic susceptibility of Several Rare Earth Oxides", in Rare Earth Research III, L. Eyring, Ed., Gordon and Breach, New York, N.Y., p. 93.

Hall, T. P. P., W. Hayes, R. W. H. Stevenson and J. Wilkens, 1963, J. Chem. Phys. 38, 1977; 39, 35.

Hansen, H. P., F. Herman, J. D. Lea, and S. Skillman, 1964, Acta. Cryst., 17, 1040.

Hartshorn, L., 1925, J. Sci. Instr., 2, 145.

Henish, H. K., J. Dennis, and J. I. Hanoka, 1965, J. Phys. Chem. Solids, 26, 493.

Hochstrasser, R. M., 1966, Molecular Aspects of Symmetry, W. A. Benjamin, Inc., New York, N.Y.

Hughes, E. W., 1941, J. Am. Chem. Soc., 63, 1737.

International Tables for X-Ray Crystallography, 1952, Vol. I, N. F. M. Henry and K. Lonsdale, Eds., The Kynoch Press, Birmingham, England.

International Tables for X-Ray Crystallography, 1959, Vol. II, J. S. Kaspar and K. Lonsdale, Eds., The Kynoch Press, Birmingham, England.

International Tables for X-Ray Crystallography, 1962, Vol. III, C. H. McGillavray, G. D. Rieck, and K. Lonsdale, Eds., The Kynoch Press, Birmingham, England.

Ito, M., and R. West, 1963, J. Am. Chem. Soc., 85, 2580.

Jelinek, F. J., 1965, Thermal Hysteresis and Initial Susceptibility Investigation of Magnetic Transitions in Several Rare Earth Metals, Unpublished M.S. thesis, Library, Iowa State University of Science and Technology, Ames, Iowa.

Jennings, L. D., 1960, Rev. Sci. Instr., 31, 1269.

Kanamori, J., 1959, J. Phys. Chem. Solids, 10, 87.

Karle, I. L., Britts and S. Bremmer, 1964, Acta. Cryst., 17, 1506.

Keller, D. A., 1970, The Electronic Heat Capacity of ReO_3, Unpublished Ph.D. thesis, Library, Iowa State University of Science and Technology, Ames, Iowa.

Knox, K., R. G. Shulman and S. Sugano, 1963, Phys. Rev., 130, 512.

Liehr, A. D., and C. J. Ballhausen, 1959, Ann. Phys., 6, 134.

Low, W., 1958a, Ann. N.Y. Acad. Sci., 72, 69.

Low, W., 1958b, Phys. Rev., 109, 247.

Low, W., 1960, Paramagnetic Resonance in Solids, Academic Press Inc., New York, N.Y.

Ludi, A., and P. Schindler, 1968, Angew. Chem. Internat. Ed., 7, 638.

Maahs, G., and P. Hegenberg, 1966, Angew. Chem. Internat. Edit., 5, 888.

Maass, G. J., B. C. Gerstein, and R. D. Willett, 1967, J. Chem. Phys., 46, 401.

Maass, G. J., 1969, Magnetism and Bonding in Potassium Trichlorocuprate(II). Unpublished Ph.D. thesis, Library, Iowa State University of Science and Technology, Ames, Iowa.

Macintyre, W. M., and M. S. Werkema, 1964, J. Chem. Phys., 42, 3563.

Maxwell, E., 1965, Rev. Sci. Instr., 36, 553.

Miller, A. E., and F. J. Jelinek, 1968, Low Temperature Magnetic Behavior of Several Oxides of Gadolinium, Unpublished paper, Dept. of Metallurgy, University of Notre Dame, South Bend, Indiana.

Misetich, A. A., and T. Buch, 1964, J. Chem. Phys., 41, 2524.

Moore, C. E., 1952, Nat. Bur. Standards (U.S.) Circ., 467, Vol. 2.

Morrish, A. H., 1965, The Physical Principles of Magnetism, John Wiley and Sons, Inc., New York, N.Y.

Mullin, C. J., J. M. Keller, C. L. Hammer and R. H. Good, Jr., 1966, Annals of Physics, 37, 55.

Nakomoto, K., 1963, Infrared Spectra of Inorganic and Coordination Compounds, John Wiley and Sons, Inc., New York, N.Y.

Olander, F., 1966, Frequency Dependence of the Magnetization of Holmium in the Neighborhood of the Ferromagnetic Ordering Temperature; Unpublished M.S. thesis, Library, Iowa State University of Science and Technology, Ames, Iowa.

Owen, J., and K. W. H. Stevens, 1953, Nature, 171, 836.

Owen, J., 1955a, Proc. Roy. Soc., A227, 183.

Owen, J., 1955b, Discussions Faraday Soc., (London), 19, 127.

Owen, J., and J. M. H. Thornley, 1966, Repts. Prog. Physics, 29, 675.

Park, J. D., S. Cohen, and J. R. Lacher, 1962, J. Am. Chem. Soc., 84, 2919.

Patterson, A. L., 1935, Z. Krist., A90, 517.

Powell, R. L., M. D. Bunch and R. J. Corrucini, 1961, Cryogenics, 1, 139.

Pryce, M. H. L., 1950, Proc. Phys. Soc. (London), A63, 25.

Rao, C. N. R., 1963, Chemical Applications of I.R. Spectroscopy, Academic Press, New York, N.Y., 1963.

Rioux, F. J., 1969, Single Crystal Susceptibility Study of One-dimensional Antiferromagnetic Interactions in $CsCuCl_3$. Unpublished Ph.D. thesis, Library, Iowa State University of Science and Technology, Ames, Iowa.

Rioux, F. J., and B. C. Gerstein, 1970, J. Chem. Phys., 53, 1789.

Robertson, J. M., 1953, Organic Crystals and Molecules, Cornell University Press, Ithaca, New York, N.Y.

Rodgers, J., and R. A. Jacobson, 1969, ALF: A general Fourier program in PL1 for Triclinic, Monoclinic and Orthorhombic Space Groups. U.S. Atomic Energy Commission Report IS-107 [Ames Laboratory, Ames, Iowa].

Salinger, G. L., and J. C. Wheatley, 1961, Rev. Sci. Instr., 32, 872.

Schlueter, A. W., R. A. Jacobson and R. E. Rundle, 1968, Inorg. Chem., 5, 277.

Selwood, P. W., 1956, Magnetochemistry, 2nd ed. Interscience Publishers, New York, N.Y.

Shenstone, A. G. J., 1954, J. Opt. Soc. Amer., 44, 749.

Silverstein, R. M., and G. C. Bassler, 1967, Spectrometric Identification of Organic Compounds, John Wiley and Sons, Inc., New York, N.Y.

Skujins, S., J. Delderfield and A. C. Webb, 1968, Tetrahedron, 24, 4805.

Slater, J. C., 1964, J. Chem. Phys., 41, 3199.

Slater, J. C., 1965, Quantum Theory of Molecules and Solids, Vol. II, McGraw-Hill Book Company, New York, N.Y.

Smart, J. S., 1966, Effective Field Theories of Magnetism, W. B. Sannders, Philadelphia, Pa.

Smith, J., B. C. Gerstein, S. H. Liu, and G. Stucky, 1970, J. Chem. Phys., 53, 481.

Sparks, L. L. and R. L. Powell, 1965, Available Low Temperature Thermocouple Information and Services, National Bureau of Standards Report No. 8750 [National Bureau of Standards, Boulder Laboratories, Boulder, Col.]

Sprenger, H. E., and W. Ziegenbein, 1968, Angew. Chem. Internat. Edit., 7, 530.

Stevens, K. W. H., 1953, Proc. Roy. Soc. (London), A219, 542.

Stout, G. H., and L. H. Jensen, 1968, X-Ray Structure Determination, 1st ed., The Macmillan Company, New York, N.Y.

Stout, J. W., and B. Hadley, 1964, J. Chem. Phys., 40, 55.

Stucky, G., S. D' Agostino, and G. McPherson, 1966, J. Am. Chem. Soc., 88, 4828.

Sugano, S., and R. G. Shulman, 1963, Phys. Rev., 130, 517.

Takehara, A., and M. Yokoi, 1958, Shinshu Daigoku Sen Igakuba Kenkyû Hôkoku, 7, 108. Original not available, abstracted in Chem. Abstr., 54, 1015a (1960).

Tinkham, M., 1956, Proc. Roy. Soc. (London), A236, 535.

Van Vleck, J. H., 1932, Electric and Magnetic Susceptibilities, Oxford University Press, New York, N.Y.

Van Vleck, J. H., 1935a. J. Chem. Phys. 3, 807.

Van Vleck, J. H., 1935b, J. Chem. Phys., 3, 803.

Van Vleck, J. H., and A. Sherman, 1935, Rev. Mod. Phys., 7, 167.

Vogel, R. E., and C. P. Kempter, 1959, A Mathematical Technique for Precision Determination of Lattice Constants, Los Alamos Scientific Laboratory Report LA-2317 [Los Alamos Scientific Laboratory, Los Alamos, N.M.]

Vogel, R. E., and C. P. Kempter, 1961, Acta. Cryst., 14, 1130.

Waser, J., 1951a, Rev. Sci. Instr., 22, 563.

Waser, J., 1951b, Rev. Sci. Instr., 22, 567.

Watanabe, H., 1966, Operator Methods in Ligand Field Theory, Prentice Hall, Inc., Englewood Cliffs, N.J.

West, R., and H. Y. Niu, 1962, J. Am. Chem. Soc., 84, 1324.

West, R., and D. L. Powell, 1963, J. Am. Chem. Soc., 85, 2577.

West, R., and H. Y. Niu, 1963a, J. Am. Chem. Soc., 85, 2589.

West, R., and H. Y. Niu, 1963b, J. Am. Chem. Soc., 85, 2586.

West, R., H. Y. Niu, D. L. Powell, and M. V. Evans, 1960, J. Am. Chem. Soc., 82, 6204.

Wong, Chi-Hsiang, R. E. Marsh and V. Schoemaker, 1964, Acta. Cryst., 17, 131.

Yamada, K., N. Mizuno, and Y. Hirata, 1958, Bull. Chem. Soc. Japan, 31, 543.

Young, H. D., 1962, Statistical Treatment of Experimental Data, McGraw-Hill Book Co., Inc., New York, N.Y.

ACKNOWLEDGMENTS

I wish to express my thanks to Dr. B. C. Gerstein for suggesting this research project and for his help, guidance and encouragement during the course of this work.

I am grateful for many helpful discussions with Dr. W. A. Taylor concerning this work.

Finally, I wish to thank the staff of the Ames Laboratory for their help, especially the analytical groups for making the sample analyses, and the groups involved in X-ray structure work for consultation and assistance in the X-ray investigation.

APPENDIX A: CRYSTAL FIELD AND MOLECULAR ORBITAL THEORY OF THE d^8 Ni^{+2} ION WITH OCTAHEDRAL COORDINATION

The purpose of this section is to very briefly consider the crystal field and molecular orbital theories for the octahedrally coordinated Ni^{++} (d^8) ion and to derive an energy level scheme which can be used to discuss the spectroscopic and magnetic measurements made in this work. The basic theory is discussed extensively in numerous books and articles. The most useful references have been Theory of Atomic Spectra by Condon and Shortley (1951), Ligand Field Theory by Ballhausen (1962), Introduction to Ligand Fields by Figgis (1966), Operator Methods in Ligand Field Theory by Watanabe (1966) and Quantum Chemistry by Eyring, Walter and Kimball (1944).

The theory of crystal fields was first developed by Bethe (1929), who investigated the effect of the symmetry and strength of a crystalline field on the electronic energy levels of free ions placed in the field. Since then the theory has found application in describing the bonding in transition metal complexes in solution and crystals, and the experimental results of heat capacity, magnetic susceptibility, electron spin resonance and absorption spectroscopy measurements have been explained with its help. The analysis of some of the results of these experiments require the use of molecular orbital theory, which is a more general theory of bonding but

contains the crystal field theory as a special case Ballhausen, 1962).

The Free Ion

The discussion of the treatment of the free ion will follow Condon and Shortley (1951), Eyring, Walter and Kimball (1944) and Griffith (1961). The electronic wavefunctions and energies of a many electron ion are the solutions of Schroedingers equation using the approximate, nonrelativistic Hamiltonian

$$H = -\frac{\hbar^2}{2m}\sum_i \nabla_i^2 - \sum_i \frac{Ze^2}{r_i} + \sum_{j>i} \frac{e^2}{r_{ij}} + \sum_i \xi(r_i)\hat{\ell}_i \cdot \hat{s}_i \qquad (A1)$$

The terms are listed in order of decreasing energy. In the solution of this problem the Hamiltonian above is first approximated by the central field Hamiltonian

$$H_c = -\frac{\hbar^2}{2m}\sum_i \nabla_i^2 + \sum_i U(r_i) \qquad (A2)$$

where $U(r_i)$ is spherically symmetrical and consists of the nuclear attraction terms and most of the electronic repulsions; the repulsions acting on electron i are approximated as a spherical charge distribution due to the other electrons. H_c is a sum of one electron Hamiltonians and yields as solutions wavefunctions very similar to the hydrogenic wave functions; i.e., the wavefunctions are

products of angular and radial parts. The angular functions are the familiar spherical harmonics, $Y_{\ell m}(\theta,\phi)$; the radial parts are very similar to the hydrogenic radial functions and the familiar orbitals s, p, d, f, g, h and quantum numbers (n, ℓ, m_ℓ, m_s) are retained. Configurations are written and closed shells are ignored. For partially filled shells, such as d^2 for example, properly antisymmetrized many electron wavefunctions are written by use of the Slater determinant formalism and the effect of $V_{pert} = H_o - H_c$ on these states is calculated by perturbation theory.

$$V_{pert} = \sum_i \left(-\frac{Ze^2}{r_i} - U(r_i)\right) + \sum_{i>j} \frac{e^2}{r_{ij}} + \sum_i \xi(r_i)\hat{\ell}_i \cdot \hat{s}_i \qquad \text{(A3)}$$

This procedure results in new wavefunctions characterized by total orbital angular momentum $L=\Sigma\ell_i$, $M_L=\Sigma(m_\ell)_i$, total spin angular momentum $S = \sum_i s_i$, $M_S = \sum_i (m_s)_i$, and total angular momentum J=L+S, L+S-1,... L-S. The procedure for obtaining these functions and their energies is exhaustively treated by Condon and Shortley (1951). For a single d electron, ignoring the closed shells, one obtains the term $^2D_{5/2,3/2}$, in standard notation (i.e., L=2; S=1/2; J=5/2, 3/2). For two d electrons, d^2, one obtains the terms and electrostatic repulsion energies given in Table 21 in terms of the Condon-Shortley parameters F_0, F_2 and F_4, where

$$F_k = \frac{e^2}{D_k} \int_0^\infty \int_0^\infty \frac{r_<^k}{r_>^{k+1}} [R_1(d)]^2 r_1^2 dr_1^2 [R_2(d)]^2 r_2^2 d_2,$$

with $D_0 = 1$, $D_2 = 49$, and $D_4 = 441$. For hydrogenic radial functions one obtains $F_2 = 203Z$ and $F_4 = 14.7Z$ in cm^{-1}. Usually, however, the F_k are evaluated from experimental spectra. For Ni^{++}, d^8, (considered in the hole formalism) experimentally one finds $F_2 \simeq 1710$ cm^{-1} and $F_4 \simeq 132$ cm^{-1} (Shenstone, 1954).

The spin orbit coupling term in the Hamiltonian (term 4 in $V_{pert.}$) will split the two triplet terms according to their J values. For ^3F, J = 4, 3, 2 and for ^3P, J = 2, 1, 0. For a particular term the splitting is given by

$$\Delta E_{J,J-1} = \lambda J \tag{A4}$$

where $\lambda = \frac{\xi_{3d}}{2}$ for d^2 and $\lambda = -\frac{\xi_{3d}}{2}$ for d^8. The splittings for d^2 and d^8 are given in Table 21. For the free ion Ni^{++} the spin orbit coupling parameter is $\xi_{3d}=648$ cm^{-1}, and $\lambda = -324$ cm^{-1} (Moore, 1952). These levels can be further split by a magnetic field. The operator connected with this splitting (the Zeeman effect) is, for a field in the z direction,

$$H_z = \mu_B(L_z+2S_z)H_z = \mu_B(J_z+S_z)H_z \tag{A5}$$

and the energy levels are

$$E_z = \mu_B H_z M_J g \tag{A6}$$

where

$$g = 1 + \frac{J(J+1)-L(L+1)+S(S+1)}{2J(J+1)} \qquad (A7)$$

a schematic diagram of the energy levels is given in Figure 28.

Table 21. Term energies of configuration $d^8(Ni^{++})$ due to interelectronic repulsion and spin orbit splittings for the free ion

Term	Electron repulsion energies in terms of Condon-Shortley parameters	Spin orbit splittings
$^1S_0$	$F_0 + 14F_2 + 126F_4$	
$^1G_4$	$F_0 + 4F_2 + F_4$	
$^3P_0$	$F_0 + 7F_2 - 84F_4$	-2λ
$^3P_1$	"	$-\lambda$
$^3P_2$	"	λ
$^1D_2$	$F_0 - 3F_2 + 36F_4$	
$^3F_2$	$F_0 - 8F_2 - 9F_4$	-4λ
$^3F_3$	"	$-\lambda$
$^3F_4$	"	3λ

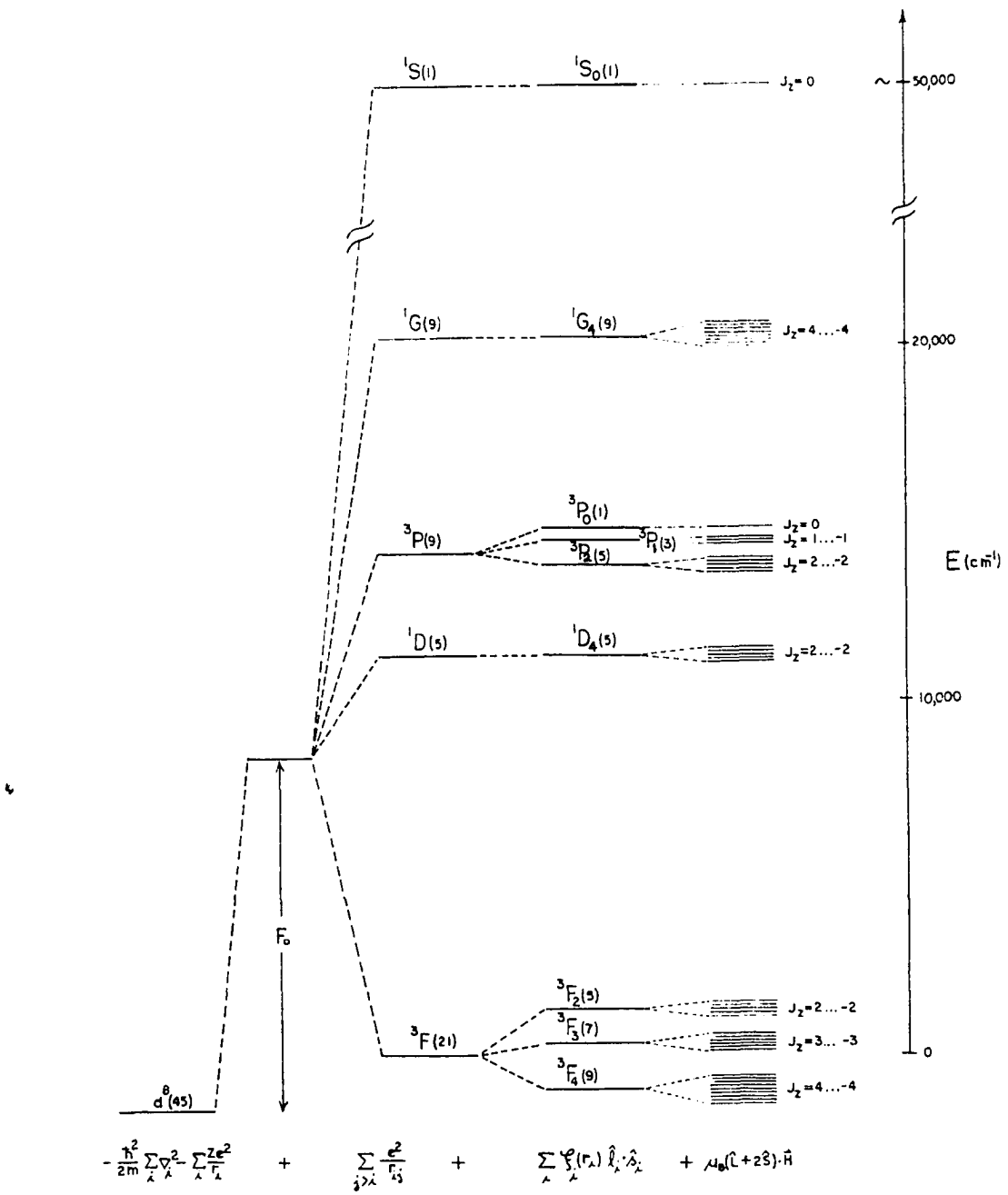

Figure 28. The Ni^{++} (d^8) free ion energy levels. Only the term splittings and spin orbit splittings are to scale. The Zeeman splittings are on the order of 10^{-4} cm^{-1}/gauss

The magnetic moment of N free, noninteracting ions with energy levels characterized by energies in A6 and J, M_J values as discussed will be (Morrish, 1965)

$$M = N\frac{\sum_{-J}^{+J} M_J g\mu_B e^{M_J g\mu_B H/kT}}{\sum_{-J}^{+J} e^{M_J g\mu_B H/kT}} \qquad \text{(A8)}$$

For multiplets such that $E_{J'}-E_J >> kT$ (i.e., all atoms considered to be in ground state) or, since $M_J g\mu_B H/kT \leq 10^{-2}$, (A8) reduces to

$$M = Ng\mu_B \frac{\sum_{-J}^{J} M_J(1 + M_J g\mu_B H/kT)}{\sum_{-J}^{J} (1+M_J g\mu_B H/kT)} \qquad \text{(A9)}$$

Terms like $\sum_{-J}^{J} M_J = 0$, $\sum_{-J}^{J} 1 = 2J+1$ and $\sum_{-J}^{J} M_J^2 = \frac{J(J+1)(2J+1)}{3}$,

so that

$$M = \frac{Ng^2 J(J+1)\mu_B^2 H}{3kT}$$

and, the susceptibility is given by

$$\chi = \frac{Ng^2 J(J+1)\mu_B^2}{3kT} = \frac{N\mu^2}{3kT} = \frac{N p_{eff}^2 \mu_B^2}{3kT} \qquad \text{(A10)}$$

where $\mu = p_{eff}\mu_B$ and $p_{eff} = g[J(J+1)]^{1/2}$. Equation (A10) is known as Curie's Law, $\chi=\frac{C}{T}$, with $C=\frac{N\mu^2}{3K}$.

If the separations between levels are comparable to kT,

the whole manifold with J=|L+S|,...|L-S| will be populated and one obtains for the susceptibility a sum over terms such as A10, each term attenuated by the Boltzman factor.

$$\chi = N \frac{\sum_{J=|L-S|}^{|L+S|} \{[g_J^2 \mu_B^2 J(J+1)/3kT] e^{-E(J)/kT}}{\sum_{J=|L-S|}^{|L+S|} (2J+1) e^{-E(J)/kT}} \qquad \text{(A11)}$$

For a gaseous free Ni^{++} ion the ground term is ^3F with a J manifold of J=4,3,2. The spin orbit energies are 3λ, $-\lambda$ and -4λ respectively where $\lambda = -324$ cm^{-1}. Therefore the J=4 and J=3 levels are separated by 1296 cm^{-1} (1860°K) and the ratio of population will be 0.002 at 300°K, so that the susceptibility should be given to a good approximation by A10.

$$\chi(Ni^{++}d^8, \text{ free ion}) = \frac{N \mu_B^2}{3kT} 20 \simeq \frac{2.5}{T}$$

where J=4, g=1.25 and $p_{eff} = 5.59$ (A12)

The Crystal Field Approximation

In this approximation the ligands surrounding a transition metal ion are considered as point charges or point dipoles which create an electric field about the central ion. The effect of this electrostatic potential on the energy levels of the central ion is then calculated making use of perturbation theory. In particular, in this work the main interest lies in the effect of an octahedral ligand field on

the energy levels of the Ni^{++} ion which has the d^8 configuration. First it is instructive to look at the effect of an octahedral field on a single d electron.

The crystalline field is treated as a perturbation on the free ion wavefunctions. The strength of the crystalline field relative to the various terms in the free ion Hamiltonian (A1) results in three different modes of treatment. The three cases are:

1. $V < \xi(r)\hat{\ell}\cdot\hat{s}$, rare earth complexes

2. $\xi(r)\hat{\ell}\cdot\hat{s} < V < e^2/r_{ij}$, complexes of first transition group

3. $e^2/r_{ij} < V$, complexes of second and third transition groups (covalent complexes)

Octahedral Ni^{++} complexes are usually somewhere between cases 2 and 3, called the weak and strong field cases respectively. In the weak field treatment, since $V < \frac{e^2}{r_{ij}}$, one considers the effect of the crystalline potential as a perturbation on the free ion states while in the strong field case, where $V > \frac{e^2}{r_{ij}}$, basis functions diagonal in H_c and V are formed and electronic interactions between electrons are considered as a perturbation on these ground states. At intermediate field strengths one may use either formalism. In this discussion the strong field approach will be used. That is, the wavefunctions used as a starting point are the ones obtained from the Hamiltonian

$$H_0 = -\frac{\hbar^2}{2m}\sum_i \nabla_i^2 - \sum \frac{Ze^2}{r_i} \qquad \text{(A13)}$$

The solutions of this Hamiltonian for the first transition series will be the 3d hydrogenic wave functions if one ignores closed shells. If we have the configuration d^1 (d^1) as in Sc^{++}, we have one electron to be placed in one of five degenerate d orbitals (excluding the radial functions)

$$d_{\pm 2} = Y_{2,\pm 2} = \sqrt{3/8}\ (x \pm iy)^2\ (\sqrt{5/4\pi}\ \frac{1}{r^2})$$

$$d_{\pm 1} = Y_{2,\pm 1} = \sqrt{3/8}\ (x \pm iy)^2\ (\sqrt{5/4\pi}\ \frac{1}{r^2}) \qquad \text{(A14)}$$

$$d_0 = Y_{2,0} = \mp\ 3/2\ (x \pm iy)z\ (\sqrt{5/4\pi}\ \frac{1}{r^2})$$

The form of the potential field at a central ion obtained from placing negative charges about the ion in the form of an octahedron is (Watanabe, 1966)

$$V_O = \frac{6Ze}{a} + (\frac{49}{18})^{\frac{1}{2}}(2\pi)^{\frac{1}{2}}(\frac{Zer^4}{a^5})[Y_{4,0} + (\frac{5}{14})^{\frac{1}{2}}(Y_{4,4} + Y_{4,\bar{4}})] \qquad \text{(A15)}$$

where Z is the charge on the ligands, a is the distance of the ligands from the central ion, and the $Y_{\ell,m}$'s are the spherical harmonics. The form of V_O is obtained by expanding the potential as a series of normalized spherical harmonics. The potential must transform like the irreducible representation ("irrep") A_{1g} (be invariant) under all operations

of the group O_h (Cotton, 1963; Hochstrasser, 1966). This eliminates all terms except those with n=4ℓ, m=0,±4k; Terms with n>4 are eliminated because the direct product of two d orbital sets spans no representations of the rotation group of order higher than 4. The first term in A15 will raise the energy of an electron in any wavefunction given in A14 equally by an amount 6ze/a, while the angular part will split the energy levels of the five d functions. Degenerate perturbation theory yields the energies and associated eigenstates

$$\left.\begin{array}{lll} E = -4Dq & (xz) = -\frac{1}{\sqrt{2}}(d_1 - d_{\bar{1}}) & \\ & (xy) = \frac{1}{i\sqrt{2}}(d_2 - d_{\bar{2}}) & \} d_\varepsilon (t_{2g}) \\ & (yz) = -\frac{1}{i\sqrt{2}}(d_1 + d_{\bar{1}}) & \end{array}\right. \qquad \text{(A16)}$$

$$\left.\begin{array}{lll} E = 6Dq & (z^2) = d_0 & \\ & (x^2-y^2) = \frac{1}{\sqrt{2}}(d_2 + d_{\bar{2}}) & \} d_\gamma (e_g) \end{array}\right. \qquad \text{(A17)}$$

where

$$D = 35ze/4a^5 \text{ and } q = \bar{r}^4 = \int_0^\infty R^*_{3,2}\, r^4\, R_{3,2}\, r^2 dr$$

The symbols t_{2g} and e_g applied to the two groups of orbitals are descriptive of the transformation properties of the two groups of wavefunctions in octahedral symmetry. The two groups of energy levels are separated by 10Dq, the

t_{2g} levels being the lower. Into these energy levels the d electrons are fed. For d^1 we get the configuration $(t_{2g})^1$ and since there are no interelectronic interactions with one electron the energy levels of the system are as given in A16 and A17.

If we have more than one d electron various configurations are possible. In the case of d^8 we have the possible configurations $t_{2g}^6 e_g^2$, $t_{2g}^5 e_g^3$, and $t_{2g}^4 e_g^4$ in order of increasing energy; or, considering two electron holes in a filled d shell, we obtain the configurations e_g^2, $t_{2g}e_g$ and t_{2g}^2 in increasing energy. All possible wavefunctions can be classified according to their symmetry properties in the symmetry group O_h or the double group O'. The irreps of the orbital parts of the wavefunctions are given in Table 22 with their energies; a left superscript indicates the spin function associated with the orbital function. The Γ_i are Bethe's (1929) notation for irreps in the octahedral double group O', and are given in parentheses to indicate the irreps spanned by the total spin-orbit functions for the configurations indicated (Ballhausen, 1962). For holes, Dq is negative and e_g^2 is lowest in energy. The transformation properties of the spin functions $[\frac{1}{\sqrt{2}}(\alpha\beta-\beta\alpha);\ S=0\ M_S=0]$ and $[\alpha\alpha, \frac{1}{\sqrt{2}}(\alpha\beta+\beta\alpha), \beta\beta;\ S=1,\ M_S=\pm1,0]$ are like the A_1' (Γ_1) and $T_1'(\Gamma_4)$ irreps of O' respectively. For the singlet states (S=0) in Table 22 the total spin-orbit wavefunction will

Table 22. Irreps of the double group O' spanned by configurations e_g^2, $t_{2g}\,e_g$ and t_{2g}^2

Configuration	Irreps spanned in O'	Crystal field energy
e_g^2	$^3A_2'(\Gamma_5) + {}^1A_1'(\Gamma_1) + {}^1E_2'(\Gamma_3)$	12Dq
$t_{2g}e_g$	$^3T_2'(\Gamma_1+\Gamma_3+\Gamma_4+\Gamma_5)+{}^3T_1'(\Gamma_2+\Gamma_3+\Gamma_4+\Gamma_5)$	
	$+{}^1T_2'(\Gamma_5)+{}^1T_1'(\Gamma_4)$	2Dq
t_{2g}^2	$^3T_1'(\Gamma_1+\Gamma_3+\Gamma_4+\Gamma_5)+{}^1T_2'(\Gamma_5)+{}^1A_1'(\Gamma_1)+{}^1E_1'(\Gamma_3)$	

transform like the orbit wavefunction above. For the triplet states the spin-orbit functions will transform like (in the double group O'; Ballhausen, 1962)

$$
\begin{aligned}
e_g^2\,, \quad & {}^3A_2' = T_1'(\Gamma_4)\,x\,A_2'(\Gamma_2) \rightarrow T_2'(\Gamma_5) \\
t_{2g}e_g, \quad & {}^3T_2' = T_1'(\Gamma_4)\,x\,T_2'(\Gamma_5) \\
& \rightarrow A_2'(\Gamma_2)+E_1'(\Gamma_3)+T_1'(\Gamma_4)+T_2'(\Gamma_5) \\
t_{2g}e_g, \quad & {}^3T_1' = T_1'(\Gamma_4)\,x\,T_1'(\Gamma_4) \\
& \rightarrow A_1'(\Gamma_1)+E_1'(\Gamma_3)+T_1'(\Gamma_4)+T_2'(\Gamma_5) \\
t_{2g}^2\,, \quad & {}^3T_1' = \quad " \qquad\qquad "
\end{aligned}
\tag{A18}
$$

One sees that there are four excited states with wave-

functions transforming like the ground state function $\Gamma_5(^3A_{2g},e_g^2)$; the explicit form of the ground state wavefunction is

$$\Gamma_5^{1,2,3}(^3A_{2g},e_g^2) = \begin{cases} \theta_1 = |(x^2-y^2)(z^2)|\alpha\alpha \\ \theta_2 = |(x^2-y^2)(z^2)\frac{(\alpha\beta+\beta\alpha)}{\sqrt{2}} \\ \theta_3 = |(x^2-y^2)(z^2)|\beta\beta \end{cases} \quad \text{(A19)}$$

where a convenient short hand notation is used to write the wavefunctions. The "holes" are always understood to be in order 1,2 in the form $|a(1)b(2)|$ which is meant to represent the diagonal terms of a Slater determinant,

$$|ab| = \frac{1}{\sqrt{2}}\begin{vmatrix} a(1) & b(1) \\ a(2) & b(2) \end{vmatrix} . \quad \text{(A20)}$$

The wavefunction of the lowest excited state that transforms like $\Gamma_5(^3A_{2g},e_g^2)$ is

$$\Gamma_5^{1,2,3}({}^3T_{2g}, t_{2g}e_g) = \begin{cases} \phi_1 = \frac{1}{4\sqrt{2}}\{(|(xz)(z^2)|+\sqrt{3}|(xz)(x^2-y^2)| \\ \quad -i|(yz)(z^2)|+i\sqrt{3}|(yz)(x^2-y^2)|)(\alpha\beta+\beta\alpha) \\ \quad +4i|(xy)(z^2)|\alpha\alpha\} \\ \phi_2 = \frac{1}{4}\{(|(xz)(z^2)|+\sqrt{3}|(xz)(x^2-y^2)|)(\beta\beta-\alpha\alpha) \\ \quad -i(|(yz)(z^2)|-\sqrt{3}|(yz)(x^2-y^2)|)(\beta\beta+\alpha\alpha)\} \\ \phi_3 = -\frac{1}{4\sqrt{2}}\{(|(xz)(z^2)|+\sqrt{3}|(xz)(x^2-y^2)| \\ \quad +i|(yz)(z^2)|-i\sqrt{3}|(yz)(x^2-y^2)|)(\alpha\beta+\beta\alpha) \\ \quad +4i|(xy)(z^2)|\beta\beta\} \end{cases} \quad \text{(A21)}$$

The rest of the functions can be similarly constructed. The electrostatic interaction $(\frac{e^2}{r_{ij}})$ and spin orbit coupling $(\hat{L}\cdot\hat{S})$ Hamiltonians will now be diagonal in these symmetry classified wavefunctions (Hochstrasser, 1966). The energy levels associated with these symmetry adapted wavefunctions have been calculated for each Γ_i(i=1,2,3,4,5) by Liehr and Ballhausen (1959). The energy matrix for the Hamiltonian

$$H = \sum_i(-\frac{\hbar^2}{2m}\nabla_i^2-\frac{Ze^2}{r_i}) + V_0 + \sum_{j>i}\frac{e^2}{r_{ij}} + \sum_i \xi(r_i)\hat{\ell}_i\cdot\hat{s}_i \quad \text{(A22-A23)}$$

for the wavefunctions transforming like Γ_5, for example, is given in Table 23a.

Table 23a. Matrix elements of the Hamiltonian given in (A22-A23) with the wavefunctions transforming like Γ_5 in O'

$^3A_{2g}(e_g^2)$	$^3T_{2g}(t_{2g}e_g)$	$^3T_{1g}(t_{2g}e_g)$	$^1T_{2g}(t_{2g}e_g)$	$^3T_{1g}(t_{2g}^2)$	$^1T_{2g}(t_{2g}^2)$
$-8F_2-9F_4+12Dq$	$2\sqrt{2}\ \lambda$	0	2λ	0	0
	$-8F_2-9F_4+2Dq-\frac{1}{2}\lambda$	$\frac{\sqrt{3}}{2}\lambda$	$-\frac{\sqrt{2}}{2}\lambda$	$-\sqrt{3}\lambda$	$\sqrt{6}\lambda$
		$4F_2-69F_4+2Dq+\frac{1}{2}\lambda$	$-\frac{\sqrt{6}}{2}\lambda$	$6F_2-30F_4+\lambda$	$\sqrt{2}\lambda$
			$21F_4+2Dq$	$-\sqrt{6}\lambda$	$2\sqrt{3}\ (F_2-5F_4)$
				$-5F_2-24F_4-8Dq-\lambda$	$\sqrt{2}\lambda$
					F_2+16F_4-8Dq

The eigenvalues of these matrices are functions of F_2, F_4, Dq and λ. Liehr and Ballhausen solved the matrix given in Table 23a and the matrices corresponding to Γ_1, Γ_2, Γ_3 and Γ_4 for their eigenvalues by numerical methods, for the best estimated experimental values of λ and $F_4(F_2 = 14F_4)$ as a function of Dq. They present the results as a plot of the energy levels of the various states as a function of Dq, and compare the absorption spectrum of Ni^{++} ions doped in MgO obtained by Low (1958a,b) with the predicted transition energies at Dq = $-850\ cm^{-1}$ for $\lambda = -275\ cm^{-1}$ and $F_4 = 90\ cm^{-1}$ $(F_2=14F_2)$, finding excellent agreement (see Table 23b).

As can be seen from Table 23b, the ground state function $\Gamma_5^{1,2,3}(^3A_{2g}, e_g^2)$ couples under the spin orbit interaction to $\Gamma_5^{1,2,3}(^3T_{2g}, t_{2g}e_g)$ and $\Gamma_5^{1,2,3}(^1T_{2g}, t_{2g}e_g)$. This interaction will mix in some of the excited state functions into the ground state; the correct ground state wave function to first order in λ is (Eyring, et al., 1944)

$$\begin{aligned}\phi(\Gamma_5^n) &= \Gamma_5^n(^3A_{2g}, e_g^2) - \frac{2\sqrt{2}\lambda}{|10Dq|}\,\Gamma_5^n(^3T_{2g}, t_{2g}e_g) \\ &\quad - \frac{2\lambda}{|8F_2+30F_4-10Dq|}\,\Gamma_5^n(^1T_{2g}, t_{2g}e_g) \\ &\simeq \Gamma_5^n(^3A_{2g}, e_g^2) + 0.107\,\Gamma_5^n(^3T_{2g}, t_{2g}e_g) \\ &\quad + 0.030\,\Gamma_5^n(^1T_{2g}, t_{2g}e_g)\end{aligned} \tag{A24}$$

Table 23b. Transition assignments for the Ni^{++}:MgO spectrum (Low, 1958a,b) as obtained by Liehr and Ballhausen (1959)

Absorptions observed by Low (1958a,b) (cm^{-1})	Spectral transition assignments by Liehr and Ballhausen (1959)	Predicted transition energies[a] (cm^{-1})
8600	$^3\Gamma_5(^3A_{2g},e_g^2) \rightarrow {}^{3,1}\Gamma_3(^3T_{2g},t_{2g}e_g[^1E_g,e_g^2])$	8500(10Dq)
	$^3\Gamma_4(^3T_{2g},t_{2g}e_g)$	
	$^3\Gamma_5(^3T_{2g},t_{2g}e_g)$	
	$^3\Gamma_2(^3T_{2g},t_{2g}e_g)$	
13700	$^3\Gamma_5(^3A_{2g},e_g^2) \rightarrow {}^{3,1}\Gamma_1(^3T_{1g},t_{2g}e_g[^1A_{1g},e_g^2])$	13,500
	$^3\Gamma_4(^3T_{1g},t_{2g}e_g)$	
14700	$^3\Gamma_5(^3A_{2g},e_g^2) \rightarrow {}^3\Gamma_5(^3T_{1g},t_{2g}e_g)$	14,500
	${}^{3,1}\Gamma_3(^3T_{1g},t_{2g}e_g;{}^3T_{2g},t_{2g}e_g;[^1E_g,e_g^2])$	

[a]Assuming Dq=-850 cm^{-1}, λ=-275 cm^{-1} and F_4=90 cm^{-1} (F_2=14F_4).

Table 23b (Continued)

Absorptions observed by Low (1958a,b) (cm^{-1})	Spectral transition assignments by Liehr and Ballhausen (1959)	Predicted transition energies (cm^{-1})
21750	$^3\Gamma_5(^3A_{2g},e_g^2) \rightarrow {}^1\Gamma_1([^1A_{1g},e_g^2],{}^3T_{1g},t_{2g}e_g;{}^3T_{1g},t_{2g}^2)$	20,500
	$^1\Gamma_5([^1T_{2g},t_{2g}e_g])$	
24500	$^3\Gamma_3(^3T_{1g},t_{2g}^2)$	24,000
	$^3\Gamma_5(^3T_{1g},t_{2g}^2)$	
	$^{3,1}\Gamma_4(^3T_{1g},t_{2g}^2;[^1T_{1g},t_{2g}e_g])$	
	$^3\Gamma_1(^3T_{1g},t_{2g}^2)$	
25950	$^3\Gamma_5(^3A_{2g},e_g^2) \rightarrow {}^{1,3}\Gamma_4([^1T_{1g},t_{2g}e_g];{}^3T_{1g},t_{2g}^2)$	24,700
28300	does not fit into energy level scheme	
34500	$^3\Gamma_5(^3A_{2g},e_g^2) \rightarrow {}^1\Gamma_3([^1E_g,t_{2g}^2])$	31,300
	$^1\Gamma_5([^1T_{2g},t_{2g}^2])$	

If one applies a magnetic field to the Ni^{++} ion the ground state will be split. The Hamiltonian is given in A5. The matrix elements of the Zeeman operator with the $^3A_{2g}$ ground state wavefunctions (excluding the $^3T_{2g}$ and $^1T_{1g}$ contributions) as given in A19 are (taking the field in the z direction)

$$\begin{aligned} \langle\theta_1|H_z|\theta_1\rangle &= 2H_z & M_s &= +1 \\ \langle\theta_2|H_z|\theta_2\rangle &= 0 & M_s &= 0 \\ \langle\theta_3|H_z|\theta_3\rangle &= -2H_z & M_s &= -1 \end{aligned} \tag{A25}$$

and, assuming, for transitions between these levels (as in an E.P.R. spectrometer, selection rule $\Delta M_s = \pm 1,0$)

$$h\nu = g_k \mu_B H_k \quad , \quad k=\text{a particular direction with respect to molecular geometry} \tag{A26}$$

one obtains $g_z=g_x=g_y=2$, because all directions are equivalent in octahedral symmetry.

If the corrected wavefunctions given in A24 are used, the matrix elements to first order in λ are

$$\begin{aligned} \langle\phi(\Gamma_5{}^1)|H_z|\phi(\Gamma_5{}^1)\rangle &= (2 - \frac{8\lambda}{10Dq})\ \mu_B H_z \\ \langle\phi(\Gamma_5{}^2)|H_z|\phi(\Gamma_5{}^2)\rangle &= 0 \\ \langle\phi(\Gamma_5{}^2)|H_z|\phi(\Gamma_5{}^3)\rangle &= -(2 - \frac{8\lambda}{10Dq})\ \mu_B H_z \end{aligned} \tag{A27}$$

leading to a g value of $g_z=2-\frac{8\lambda}{10Dq}$, correct to first order in λ.

Magnetic Susceptibility: Van Vleck's Equation

Van Vleck (1932) has developed a general theory of the magnetic susceptibility for a system with zero order wave-functions ψ_i^0 and energies E_i^0 acted on by the Hamiltonian given in (A5). The susceptibility for the direction S=x,y,z, is

$$\chi_s = N \frac{\sum_i \left[\frac{(E_s^{(1)ii})^2}{kT} - 2E_s^{(2)i}\right] e^{-E_i^0/kT}}{\sum_i e^{-E_i^0/kT}} \qquad \text{(A28)}$$

where

$$E_s^{(1)ii} = \langle \psi_i^0 | \mu_B (L_s + 2S_s) | \psi_i^0 \rangle \text{ , low frequency contribution}$$

$$E_s^{(2)i} = \sum_j \frac{\langle \psi_i^0 | \mu_B (L_s + 2S_s) \psi_j^0 \rangle \langle \psi_j^0 | \mu_B (L_s + 2S_s) | \psi_i^0 \rangle}{E_i - E_j} \text{ ,}$$

high frequency term.

Applying this to octahedrally coordinated nickel we have from (A27) and ignoring the second order terms,

$$\chi_z = N\mu_B^2 \left(2\frac{[2 - \frac{8\lambda}{10Dq}]^2}{kT}\right) \frac{e^{-0/kT}}{3e^{-0/kT}} \qquad \text{(A29)}$$

$$\chi_z = \frac{8N\mu_B^2}{3kT} \left(1 - \frac{4\lambda}{10Dq}\right)^2$$

In an octahedral environment all directions are equivalent and $\chi_z = \chi_x = \chi_y$. Also $g_z = g_x = g_y = 2\left(1 - \frac{4\lambda}{10Dq}\right)$ and

$p_{eff}^2 = g^2 S(S+1) = 2g^2$ with an effective spin of 1, so that

$$\chi_z = \frac{N\, p_{eff}^2\, \mu_B^2}{3kT} \qquad \text{(A30)}$$

The magnetic moment of the Ni has been reduced from the free ion value of 5.59 μ_B to approximately 3.18 μ_B for the $Ni(H_2O)_6^{+2}$ complexes in Ni^{++} Tutton salts (Griffiths and Owen, 1952). This reduction is the well known quenching of the orbital angular momentum of the d electrons by the crystal field. If it were not for the small admixture (via spin-orbit coupling) of the excited state $\Gamma_5(^3T_{2g}, t_{2g}e_g)$ into the orbitally nondegenerate ground state the orbital moment would be completely quenched leaving the spin only moment of 2.83 μ_B.

The second order terms in (A28) will give rise to a temperature independent paramagnetic susceptibility. The orbital ground state is essentially $|(x^2-y^2)(z^2)|$ times a spin function, and because of orthogonality it is only the orbital angular momentum operator L_z which contributes to $E_z^{(2)i}$. Operating with L_z on the orbital function gives

$$L_z|(x^2-y^2)(z^2)| = 2i|(xy)(z^2)| \qquad \text{(A31)}$$

Now the space function $|(xy)(z^2)|$ belongs to the $^3T_{2g}$ state which is 10Dq above the ground state see (A24, A21).

Therefore, considering the three ground state energy levels ($M_s=\pm1,0$), one obtains

$$N\frac{\sum_i -2E_2^{(2)} i_e^{-E_i^0/kT}}{\sum_i e^{-E_i^0/kT}} = N\frac{-2}{3}\left[\frac{3\mu_B^2(2i)(-2i)}{-10Dq}\right] = \frac{8N\mu_B^2}{10Dq} \quad (A32)$$

The total susceptibility is then

$$\chi_z = \frac{8N\mu_B^2}{3kT}\left(1-\frac{4\lambda}{10Dq}\right)^2 + \frac{8N\mu_B^2}{10Dq} = \chi_x = \chi_y = \chi_{av.} \quad (A33)$$

When the susceptibility of a Ni^{++} salt is measured there is also a contribution to the measured temperature independent part due to the diamagnetism of all elements in the compound.

For a $Ni(H_2O)_6^{++}$ complex then ($\lambda=-270\ cm^{-1}$, $Dq=850\ cm^{-1}$) one would expect a susceptibility of (using A33)

$$\chi \approx \frac{1.27}{T} + 2.43\times10^{-5} \quad (A34)$$

Zero Field Splitting

If the field on an ion has an axial or lower symmetry component it will split levels which are orbitally degenerate in O_h symmetry. In the case of Ni^{++}, d^8, the $\Gamma_5^n(^3A_{2g},e_g^2)$ ground state would not be split by an axial crystalline field, but by virtue of the small components of the excited states $\Gamma_5^n(^3T_{2g},t_{2g}e_g)$ and $\Gamma_5^n(^1T_{2g},t_{2g}e_g)$ mixed into the ground

state via the spin orbit coupling, small splittings will be observed in the ground state. The magnetic susceptibility will now be different at temperatures where kT is comparable to the zero field splitting of the ground state and the susceptibility will depend on the angle the applied measuring field makes with the axial direction of the axial field component.

This problem, for the case of an ion which has an orbitally nondegenerate, singlet ground state (without considering the spin-orbit coupling) has been treated elegantly by Pryce (1950). The effect of the spin orbit coupling and of the applied field H on the ground state is considered using the perturbation Hamiltonian

$$H_{ZF} = \lambda \hat{L} \cdot \hat{S} + \mu_B \bar{H} \cdot (\hat{L} + 2\hat{S}) \qquad \text{(A35)}$$

In this treatment the usual operator representation is employed for $\hat{L}$, but no representation is chosen for $\hat{S}$, and instead of obtaining the change in the energy levels due to the perturbation, one obtains an expression called the spin-Hamiltonian (Abragam and Pryce, 1951) which gives the energy levels as a function of $\hat{S}$. The energy levels correct to second order in λ and μ_B are the eigenvalues of a Hamiltonian involving only the spin variables

$$H_{SH} = E_0 + 2\mu_B(\delta_{ij} - \lambda\Lambda_{ij}) S_i H_j - \lambda^2 \Lambda_{ij} S_i S_j - \mu_B^2 \Lambda_{ij} H_i H_j \qquad \text{(A36)}$$

where the tensor coordinates i,j=x,y,z and the summation convention is assumed; the external field is $\bar{H}=\hat{i}H_x+\hat{j}H_y+\hat{k}H_z$ and Λ_{ij} is given by

$$\Lambda_{ij} = \sum_{n\neq 0} \frac{\langle 0|L_i|n\rangle\langle n|L_j|0\rangle}{(E_n-E_0)} \tag{A37}$$

The indices 0,...n,... refer to the orbital levels, zero being the lowest, an orbital singlet. The first term in (A36), E_0, is the unperturbed energy; the second term, $2\mu_B(\delta_{ij}-\lambda\Lambda_{ij})S_iH_j$, is the magnetic energy of a spin system with a g-factor represented by the tensor

$$g_{ij} = 2(\delta_{ij}-\lambda\Lambda_{ij}) \quad . \tag{A38}$$

The third term, $-\lambda^2\Lambda_{ij}S_iS_j$ is the second order contribution of the spin-orbit coupling. If Λ_{ij} is isotropic as in octahedral fields, it merely represents an equal downward shift of all 2S+1 levels; if not, as in axial fields or fields of lower symmetry, there is in addition a splitting of the levels, even in the absence of a magnetic field. The last term, $-\mu_B^2\Lambda_{ij}H_iH_j$, is spin independent, quadratic in H and corresponds to a temperature independent paramagnetic susceptibility (i.e., it corresponds to the term containing $E_s^{(2)i}$ in (A28).

In general all the elements Λ_{ij} and g_{ij} will be non-zero, but if the coordinate axes are chosen to be the

principle axes of the tensor Λ_{ij} (that is the principle axes of the symmetry of the crystal field) then $\Lambda_{xx}=\Lambda_x$, $\Lambda_{yy}=\Lambda_y$, $\Lambda_{zz}=\Lambda_z$ and $g_{xx}=g_x$, $g_{yy}=g_y$, $g_{zz}=g_z$, all other terms being zero. If the crystalline field is axial and z is taken parallel to the field axis, then $\Lambda_z=\Lambda_{\parallel}$, $\Lambda_x=\Lambda_y=\Lambda_{\perp}$ and $g_z=g_{\parallel}$ and $g_x=g_y=g_{\perp}$; if the field is octahedral $\Lambda_x=\Lambda_y=\Lambda_z$ and $g_x=g_y=g_z$.

Consider the term $-\lambda^2\Lambda_{ij}S_iS_j$ in H_{SH}, which remains even at zero magnetic field, and is the term that causes zero field splitting of the ground state spin multiplet. In fields of symmetry lower than axial the spin Hamiltonian becomes

$$H_{SH}= \mu_B(g_xS_xH_x+g_yS_yH_y+g_zS_zH_z) + DS_z^2+E(S_x^2-S_y^2) \quad \text{(A39)}$$

where

$$D = -\lambda^2(\Lambda_z- \tfrac{1}{2}(\Lambda_x+\Lambda_y))$$
$$E = -\frac{\lambda^2}{2}(\Lambda_x-\Lambda_y) \quad \text{(A40)}$$

Certain terms which shift all levels in the ground manifold equally have been dropped from (A39). The terms remaining split the ground manifold.

The energy levels can now be calculated using as wavefunctions effective spin, S=1, functions

$$|1\rangle \quad M_s=+1$$
$$|0\rangle \quad M_s=0 \quad \text{(A41)}$$
$$|\bar{1}\rangle \quad M_s=-1$$

The energy levels for fields in the z, x, and y directions are

$$
\begin{aligned}
H||z \qquad & E_{\pm}^{z} = D \pm [\, \mu_B^2 g_z^2 H_z^2 + E^2 \,]^{1/2} \\
& E_0^{z} = 0 \\
H||x \qquad & E_0^{x} = D - E \\
& E_{\pm}^{x} = \frac{D+E}{2} \pm [\, (\tfrac{D+E}{2})^2 + g_x^2 \mu_B^2 H_x^2 \,]^{1/2} \\
H||y \qquad & E_0^{y} = D + E \\
& E_{\pm}^{y} = \frac{D-E}{2} \pm [\, (\tfrac{D-E}{2})^2 + \mu_B^2 g_y^2 H_y^2 \,]^{1/2}
\end{aligned}
\tag{A42}
$$

at zero field all three cases reduce to $E=0,\ D \pm E$. The behavior of the energy levels as a function of field is given in Figure 29. The figure is drawn for the case of $\alpha NiSO_4 \cdot 6H_2O$ where D=6.85°K and E=0.41°K (Stout and Hadley, 1964).

Paramagnetic spin resonance transitions may take place among the levels plotted in Figure 29, with the selection rule $\Delta S = \pm 1, 0$. However, since zero field splittings for Ni^{+2} coordinated by six water molecules are generally large (D=-1 to -3 cm^{-1} and E=-0.1 to 1 cm^{-1} for Ni^{+2} Tutton salts; Griffiths and Owen, 1952), it will usually require very high fields to bring the levels close enough for transitions to take place in an X-band spectrometer ($h\nu \approx 0.32\ cm^{-1} \simeq .46°K$).

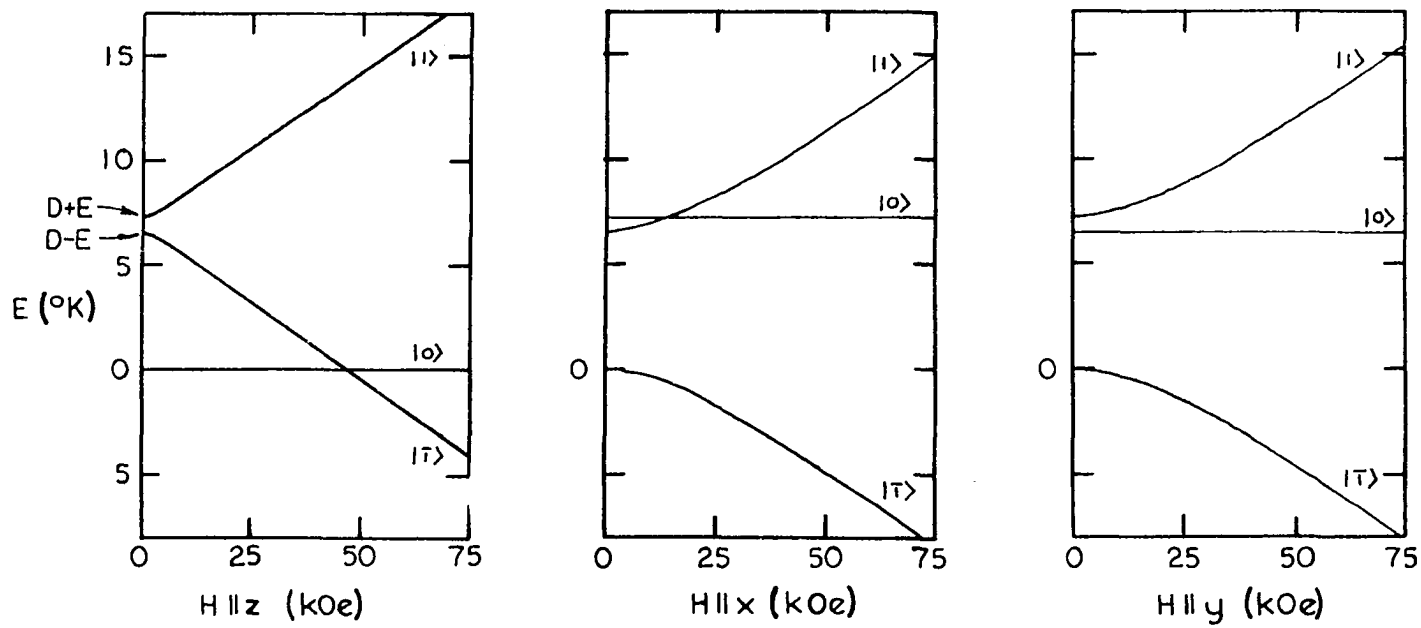

Figure 29. Variation of the energy levels of the ground manifold of Ni^{++} d^8 in an orthorhombic field

More moderate fields are required for K and Q band spectrometers ($h\nu \simeq 0.6$ cm^{-1} and 1 cm^{-1} respectively).

The formulas for the susceptibilities in the x,y, and z directions are

$$\chi_x = \frac{2N\mu_B^2 g_x^2}{Qk(D-E)}\left[1-\exp\left(-\frac{D-E}{T}\right)\right] + \frac{N\mu_B^2}{\lambda}(2-g_x)$$

$$\chi_y = \frac{2N\mu_B^2 g_y^2}{Qk(D+E)}\left[1-\exp\left(-\frac{D+E}{T}\right)\right] + \frac{N\mu_B^2}{\lambda}(2-g_y) \qquad \text{(A43)}$$

$$\chi_z = \frac{2N\mu_B^2 g_z^2}{Qk(2E)}\left[\exp\left(-\frac{D-E}{T}\right)-\exp\left(-\frac{D+E}{T}\right)\right] + \frac{N\mu_B^2}{\lambda}(2-g_z)$$

where $Q = 1 + \exp\left(-\frac{D-E}{T}\right)+\exp\left(-\frac{D+E}{T}\right)$ is the partition function, D and E are in units of °K. At temperatures such that T>>D,E, these expressions reduce to

$$\chi_x \simeq \frac{2N\mu_B^2 g_x^2}{3k}\left(\frac{1}{T-\frac{D+3E}{6}}\right) + \frac{N\mu_B^2}{\lambda}(2-g_x)$$

$$\chi_y \simeq \frac{2N\mu_B^2 g_y^2}{3k}\left(\frac{1}{T-\frac{D-3E}{6}}\right) + \frac{N\mu_B^2}{\lambda}(2-g_y) \qquad \text{(A44)}$$

$$\chi_z \simeq \frac{2N\mu_B^2 g_z^2}{3k}\left(\frac{1}{T+\frac{2D}{6}}\right) + \frac{N\mu_B}{\lambda}(2-g_z)$$

The calculated susceptibilities are given in Figure 30 for $\alpha NiSO_4 \cdot 6H_2O$. From (A44) one sees that a susceptibility in the form of a Curie-Weiss law (Equation A45) can be obtained from a compound with zero field splitting.

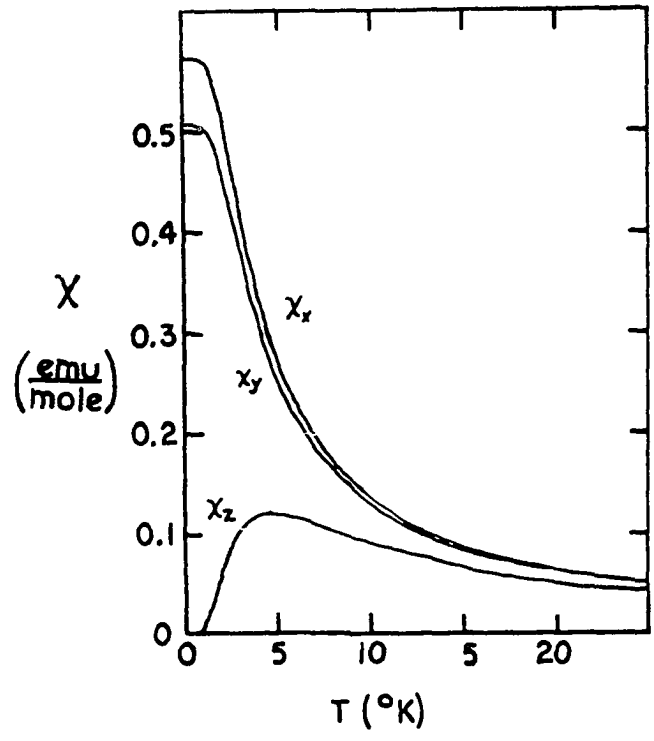

Figure 30. Susceptibility of a Ni^{+2} ion in an orthorhombic crystal field (D=6.85°K, E=0.41°K)

In a condensed system magnetic ions will interact either through dipole fields or through the mechanism of super-exchange (Smart, 1966; Anderson, 1959; 1963). The simplest theory that takes account of these interactions is the Weiss molecular field theory in which all interactions are lumped into an effective field at every ion proportional to the average net magnetic moment of the crystal. The result of this theory is a modification of the Curie law for the magnetic susceptibility of a paramagnet called the Curie-Weiss law,

$$\chi = \frac{C}{T-\theta} , \qquad \text{(A45)}$$

where θ is called the paramagnetic Curie temperature or the Weiss constant.

In terms of a model in which only nearest neighbor interactions are considered and the interactions between two ions with spins S_i and S_j are taken as the Heisenberg exchange interaction,

$$H_{ex} = -2J\Sigma\hat{S}_i \cdot S_j , \qquad \text{(A46-A49)}$$

(J being the exchange constant), the formula for θ is

$$\theta = 2ZJS(S+1)/3k , \qquad \text{(A50)}$$

where Z in the number of nearest neighbors (Smart, 1966). Crystals with ferromagnetic exchange interactions will have

positive θ values and crystals with antiferromagnetic exchange will have negative θ values.

Molecular Orbital Theory

In the molecular orbital theory (MO theory) the structural unit for the electronic wavefunctions of a transition metal complex is a unit such as $(NiF_6)^{-4}$, for example. That is, wavefunctions for the valence electrons (both the transition metal and ligand valence electrons) are constructed as linear combinations of atomic orbitals (LCAO's), the atomic orbitals (AO's) being, for example, the Ni 3d (and 4S) and the F 2p and 2s orbitals. The linear combinations of these AO's are called molecular orbitals or MO's (LCAOMO's). Electrons placed in these orbitals then have some probability of being found on a ligand atom and their probability of being found on the metal atom is reduced.

Although the crystal field theory is very successful as a semiempirical theory in explaining the behavior of the d electrons in complexes of 3d transition series atoms, certain experimental evidence which could not be explained adequately by the crystal field theory resulted in the general recognition of the MO theory as being superior. The main experimental results which were better explained by the MO theory were:

1. Reduced orbital contribution to the magnetic moment or the apparent reduction of the spin orbit coupling interaction (Stevens, 1953; Owen, 1955a,b; Low, 1958a,b; Griffiths and Owen, 1952)
2. Reduction of F_2 and F_4 in the complexes from the free ion values (Owen 1955a,b; Knox, Shulman and Sugano, 1963).
3. Hyperfine interaction between the magnetic electrons and the ligand nuclei (Owen and Stevens, 1953; Tinkham, 1956).
4. Reduction of the hyperfine interaction between the magnetic electrons and the transition metal nucleus (Watanabe, 1966).

The MO theory is successful in explaining all of these experimental results. The theory was first developed by Van Vleck (1935a, 1935b) and Van Vleck and Sherman (1935), and was applied to explain the spin orbit coupling parameter reduction and the reduction of the term separations (reduction in F_2 and F_4) by Stevens (1953) and Owen (1955a,b). The showed that the mixing of ligand p-orbitals with metal 3d functions had the effect of lowering all matrix elements and particularly matrix elements of L_z by a factor k (the orbital reduction factor), smaller than unity.

More concrete evidence of the essential correctness of the MO theory was supplied by the experimental observation of ligand nucleus hyperfine interactions with the magnetic

electrons in paramagnetic resonance experiments on Ir^{+4} ions diluted in the diamagnetic salt $(NH_4)_2(PtCl_6)$ (Owen and Stevens, 1953), indicating that the Ir^{+4} d electrons did indeed spend some time on the chlorine atoms.

A short discussion of the MO theory as applicable to $(NiF_6)^{-4}$ will now be given. The general presentation of Owen and Thornley (1966) will be followed. The AO orbitals to be used in constructing the LCAOMO's are the Ni^{++} 3d orbitals and the 2s and 2p orbitals of the F^- ions. Since it is desirable to work with symmetry adapted wavefunctions the d orbitals are classified according to their transformation properties in the group O_h as in the crystal field theory (see A16 and A17); two groups of orbitals, e_g and t_{2g} are obtained

$$e_g: \quad d_{z^2} = d_0 \qquad\qquad t_{2g}: \quad d_{xz} = -\frac{1}{\sqrt{2}}(d_1 - d_{\bar{1}}) \tag{A51}$$

$$d_{x^2-y^2} = \frac{1}{\sqrt{2}}(d + d_{\bar{2}}) \qquad\qquad d_{xy} = \frac{1}{i\sqrt{2}}(d_2 - d_{\bar{2}})$$

$$d_{yz} = -\frac{1}{i\sqrt{2}}(d_1 + d_{\bar{1}})$$

The F-orbitals consist of six 2s and eighteen 2p orbitals. The coordinate system that will be used to label the functions is given in Figure 31. For example, the p orbital on F_1^- which is pointing along the F_1^- -Ni^{++} vector is labeled x_1, with its positive lobe pointing away from the Ni^{++} ion; the other two p orbitals on F_1^- are labeled

y_1 and z_1 with their positive lobes pointing in the direction of the arrows indicated in Figure 31. All F^- s and p orbitals with rotational symmetry about the F^--Ni^{+2} axes can participate in σ bonding. Linear combinations of the p and s orbitals which transform as the irreps of the octahedral group are constructed by standard group theoretical techniques (Cotton, 1963; Hochstrasser, 1966). Three sets of σ-type linear combinations transforming like a_{1g}, e_g and t_{1u} are obtained:

$$p\sigma a_{1g}=(\tfrac{1}{6})^{\frac{1}{2}}\{-x_1-y_2-z_3+x_4+y_5+z_6\} \qquad s\sigma a_{1g}=(\tfrac{1}{6})^{\frac{1}{2}}\{s_1+s_2+s_3+s_4+s_5+s_6\}$$

$$p\sigma e_g(z^2)=(\tfrac{1}{12})^{\frac{1}{2}}\{x_1+y_2-x_4-y_5-2z_3-2z_6\} \qquad s\sigma e_g(z^2)=(\tfrac{1}{12})^{\frac{1}{2}}\{-s_1-s_2-s_4-s_5+2s_3+2s_6\}$$

$$p\sigma e_g(x^2-y^2)=\tfrac{1}{2}\{-x_1+y_2+x_4-y_5\} \qquad s\sigma e_g(x^2-y^2)=\tfrac{1}{2}\{s_1-s_2+s_4-s_5\}$$

$$p\sigma t_{1u}(x)=(\tfrac{1}{2})^{\frac{1}{2}}\{-x_1-x_4\} \qquad s\sigma t_{1u}(x)=(\tfrac{1}{2})^{\frac{1}{2}}\{s_1-s_4\} \qquad \text{A52)}$$

$$p\sigma t_{1u}(y)=(\tfrac{1}{2})^{\frac{1}{2}}\{-y_2-y_5\} \qquad s\sigma t_{1u}(y)=(\tfrac{1}{2})^{\frac{1}{2}}\{s_2-s_4\}$$

$$p\sigma t_{1u}(z)=(\tfrac{1}{2})^{\frac{1}{2}}\{-z_3-z_6\} \qquad s\sigma t_{1u}(z)=(\tfrac{1}{2})^{\frac{1}{2}}\{s_3-s_6\}$$

Of these only the e_g set will be used to form σLCAOMO's the 3d e_g orbitals of the Ni ion. The other two sets of orbitals transforming like a_{1g} and t_{1u} could be used to

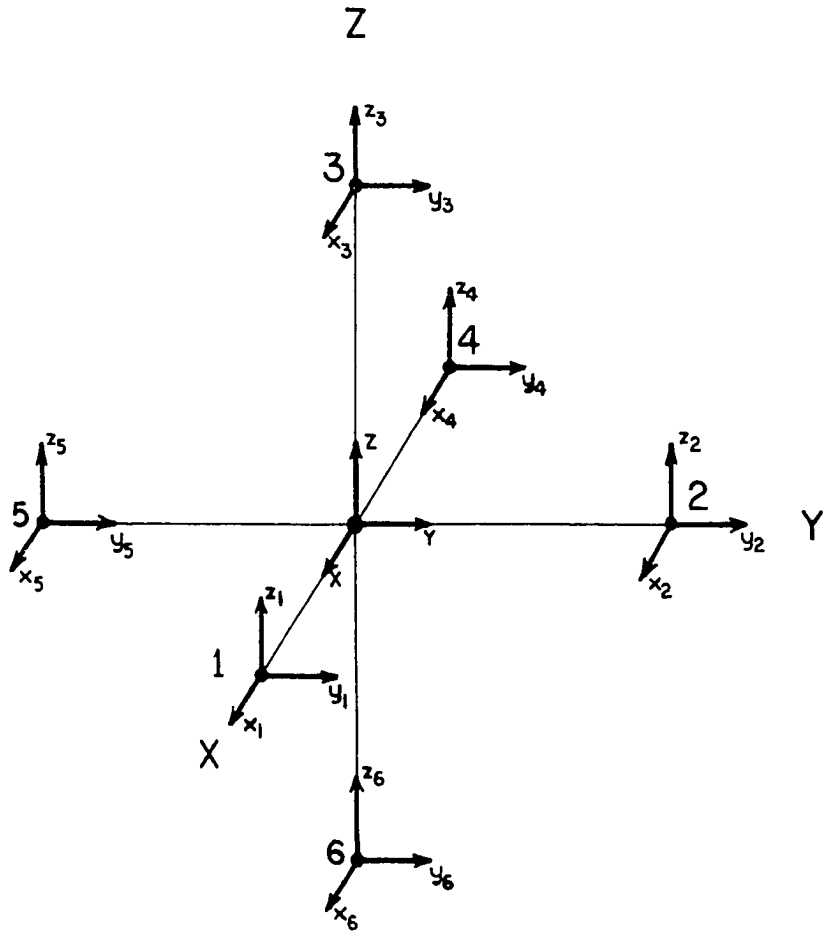

Figure 31. Coordinate system used in MO theory of $Ni^{+2}(L^{-n})_6$

form σLCAOMO's with the empty 4s and 4p orbitals of the Ni^{++} ion; although such participation of these higher energy orbitals of the Ni^{++} ion is conceivable their energies are somewhat higher than the 2p orbitals resulting in small participation and they will be neglected in this treatment. The a_{1g} and t_{1u} σ combinations will therefore be regarded as non-bonding.

The sets of π-type linear combinations are t_{1g}, t_{1u}, t_{2g} and t_{2u}. Again, only the t_{2g} set will be used to form π LCAOMO's with the t_{2g} orbitals of the Ni^{++} ion. The t_{2g} π ligand combinations are:

$$\begin{aligned} p\pi\ t_{2g}(xz) &= \tfrac{1}{2}\{z_2+y_3-z_5-y_6\} \\ p\pi\ t_{2g}(yz) &= \tfrac{1}{2}\{z_1+x_3-z_4-x_6\} \\ p\pi\ t_{2g}(xy) &= \tfrac{1}{2}\{y_1+x_2-y_4-x_5\} \end{aligned} \qquad \text{(A53)}$$

The linear combinations transforming like t_{1g}, t_{1u} and t_{2u} are considered to be nonbonding; they are tabulated by Watanabe (1966).

Symmetry classified ligand and d orbitals can now be combined to give bonding and antibonding orbitals. The admixture is controlled by the octahedral potential of seven positive charges, and the coefficients of admixture should in principle be calculated by solving the secular determinant which has nonvanishing matrix elements only between the 3d and

symmetry-classified ligand orbitals that belong to the same label of the same irreducible representation. That is, the 3d $t_{2g}(xz)$ orbital for example, has matrix elements only with the pπ $t_{2g}(xz)$ orbital, and the eigenfunctions of the secular matrix are linear combinations of the 3d and symmetry classified ligand orbitals that have nonvanishing matrix elements with the potential. The secular matrix for the 3d $t_{2g}(xz)$ and pπ $t_{2g}(xz)$ orbitals can be written as

$$\begin{array}{cc} 3d\ t_{2g}(xz) & p\pi\ t_{2g}(xz) \\ \begin{bmatrix} E_{3d}-V_d & V_{pd} \\ V_{dp} & E_{2p}-V_p \end{bmatrix} & \end{array} \quad , \tag{A54}$$

where E_{3d} is the energy of the single 3d electron in the free ion and E_{2p} is the energy of the single 2p electron in the free ion F^-. The Hamiltonian operator used in (A54) is

$$H = -\frac{\hbar^2}{2m}\nabla^2 - \frac{Z_0 e^2}{r_0} - \sum_{i=1}^{6}\frac{Ze^2}{r_i} \tag{A55}$$

where the sum is over the ligands, Z_0 is the effective charge of the central ion core and Z is the effective charge of the F^- ion. The matrix elements are

$$\langle 3d\ t_{2g}(xz)|H|3d\ t_{2g}(xz)\rangle = E_{3d} - \langle 3d\ t_{2g}(xz)|\sum_i \frac{Ze^2}{r_i}|3d\ t_{2g}(xz)\rangle$$

$$= E_{3d} - V_d$$

$$\langle p\pi\ t_{2g}(xz)|H|p\pi\ t_{2g}(xz)\rangle = E_{2p} - \langle p\pi\ t_{2g}(xz)|\frac{Z_0e^2}{r_0}|p\pi\ t_{2g}(xz)\rangle$$

$$-\langle y_1|\sum_i \frac{Ze^2}{r_i}|y_1\rangle = E_{2p} - V_p$$

$$\langle 3d\ t_{2g}(xz)|H|p\pi\ t_{2g}(xz)\rangle = E_{2p}\ S_\pi - \langle 3d\ t_{2g}(xz)|\sum_{i(\neq 1)} \frac{Ze^2}{r_i}|y_1\rangle$$

$$-\langle 3d\ t_{2g}(xz)|\frac{Z_0e^2}{r_0}|p\pi\ t_{2g}(xz)\rangle = V_{dp}$$

$$= E_{3d}S_\pi$$

$$-\langle p\pi\ t_{2g}(xz)|\sum_i \frac{Ze^2}{r_i}|3d\ t_{2g}(xz)\rangle$$

$$= V_{pd} \qquad \text{(A56)}$$

S_π is the group overlap integral $\langle p\pi\ t_{2g}(xz)|3d\ t_{2g}(xz)\rangle$. The formal solution of A54 is

$$\varepsilon = \frac{1}{2}[(E_{3d}-V_d+E_{2p}-V_p) \pm \{([E_{3d}-V_d]-[E_{2p}-V_p])^2+4V_{dp}^2\}^{\frac{1}{2}}] \qquad \text{(A57)}$$

If $E_{3d}-V_d > E_{2p}-V_p$, then

$$\varepsilon_> > (E_{3d}-V_d) > (E_{2p}-V_p) > \varepsilon_< \qquad \text{(A58)}$$

where $\varepsilon_>$ and $\varepsilon_<$ are the larger and smaller of the two eigenvalues of the secular matrix. The wavefunctions corresponding to $\varepsilon_>$ and $\varepsilon_<$ can be obtained as linear combinations of 3d $t_{2g}(xz)$ and pπ $t_{2g}(xz)$, the admixture of the two being a function of the matrix elements. The higher energy LCAOMO is called an antibonding orbital and the lower energy LCAOMO is called a bonding orbital. The antibonding orbital will consist mainly of the 3d $t_{2g}(xz)$ orbital with a small admixture of the pπ $t_{2g}(xz)$ orbital, and the bonding orbital will consist mainly of the pπ $t_{2g}(xz)$ orbital with a small admixture of the 3d $t_{2g}(xz)$ orbital. The energy levels are indicated schematically in Figure 32(a) and the formula for the two functions is given. If fewer than four electrons are placed in the molecular orbitals there is a net stabilization when the bond is formed; if four electrons are placed in the molecular orbitals, no net stabilization occurs.

This procedure is performed for every pair of central ion and ligand orbitals belonging to the same label of the same irrep. The qualitative energy level diagram obtained is given in Figure 32(b). In the cluster NiF_6^{-4} there are 56 electrons in the valence shells, 34 of these are placed in the nonbonding ligand orbitals and 22 are placed in the MO's, the last two going into the antibonding e_g^a MO. The LCAOMO functions of the two upper antibonding levels are

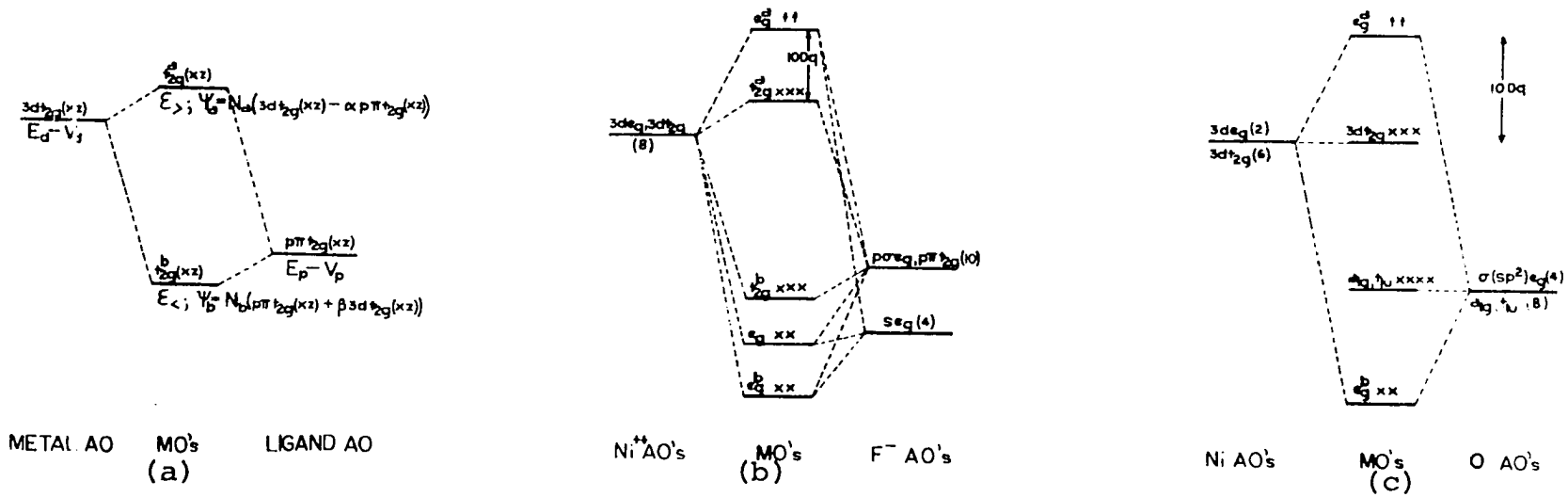

Figure 32. Molecular orbital energy level diagrams ((a) energy level diagrams for bonding and antibonding orbital formed from the $edt_{2g}(xz)$ metal orbital and the $p\pi t_{2g}(xz)$ ligand orbital; (b) energy level diagram for molecular orbitals of the NiF_6^{-4} cluster in octahedral symmetry, including π-bonding; (c) energy level diagram for the molecular orbitals of the NiO_6 cluster in $NiC_4O_4 \cdot 2H_2O$)

$$e_g^a(x^2-y^2) = N_\sigma[d_{x^2-y^2} - \tfrac{1}{2}\alpha_\sigma(-x_1+x_4+y_5-y_5)]$$
$$e_g^a(z^2) = N_\sigma[d_{z^2} - \tfrac{1}{\sqrt{12}}\alpha_\sigma(-2z_3+2z_6+x_1-x_4+y_2-y_5)] \quad \text{(A59)}$$

neglecting the contribution of the ligand s orbitals for simplicity, and

$$t_{2g}^a(xy) = N_\pi[d_{xy} - \tfrac{1}{2}\alpha_\pi(y_1-y_4+x_2-x_5)]$$
$$t_{2g}^a(yz) = N_\pi[d_{yz} - \tfrac{1}{2}\alpha_\pi(z_2-z_5+y_3-y_6)] \quad \text{(A60)}$$
$$t_{2g}^a(zx) = N_\pi[d_{zx} - \tfrac{1}{2}\alpha_\pi(x_3-x_6+z_1-z_4)]$$

A transition between these two levels corresponds to the energy difference 10Dq in crystal field theory.

In the case of the Ni^{++} ion in $NiC_4O_4 \cdot 2H_2O$, the Ni^{++} ion is coordinated by four squarate oxygens in a plane, with two water oxygens completing roughly octahedral coordination by occupying the remaining trans apexes. One may consider the σ type orbitals on the oxygen atoms to be sp^2 hybrids in the case of the squarate oxygens or roughly sp^3 hybrids in the case of the water molecules, occupied by lone pairs in each case. The only π orbitals that could participate in the bonding are the molecular π orbitals of the whole squarate ion. Although these orbitals must be the main path of any superexchange between neighboring Ni^{++} ions in the structure (Anderson, 1959, 1963), they cannot be

simply introduced into the MO theory. Therefore the coordination about the Ni^{++} ion in $NiC_4O_4 \cdot 2H_2O$ will be considered to consist of six oxygen ions each of which has a σp and a σs orbital participating in the bonding to the central ion and any π bonding will be neglected. The MO energy level scheme will then be as given in Figure 31. Each O atom contributes 2 electrons and the Ni^{+2} ion contributes eight electrons, or a total of 20 electrons. These are placed in the energy levels as shown in Figure 32(c).

The transition 3d $t_{2g} \rightarrow e_g^a$ corresponds to the $^3A_{2g} \rightarrow {}^3T_{2g}$ transition in the crystal field theory and 10Dq is taken as the energy difference between these two levels. The wavefunctions of the two unpaired spins (or holes) are

$$\begin{aligned} e_g^a(x^2-y^2) &= N_\sigma\{d_{x^2-y^2} - \tfrac{1}{2}\alpha_\sigma(-x_1+x_4+y_2-y_5) \\ &\quad - \tfrac{1}{2}\alpha_s(x_1+s_4-s_2-s_5)\} \\ e_g^a(z^2) &= N_\sigma\{d_{z^2} - \frac{1}{\sqrt{12}}\alpha_\sigma(-2z_3+2z_6+x_1-x_4+y_2-y_5) \\ &\quad - \frac{1}{\sqrt{12}}\sigma_s(2s_3+2s_6-s_1-s_2-s_4-s_5)\} \end{aligned} \tag{A61}$$

where

$$\begin{aligned} N_\sigma^{-2} &= 1-4\alpha_\sigma S_\sigma - 4\alpha_s S_s + \alpha_\sigma^2 + \alpha_s^2 \\ S_\sigma &= -\langle d_{x^2-y^2}|x_1\rangle, \quad S_s = \langle d_{x^2-y^2}|s_1\rangle \end{aligned} \tag{A62}$$

One may now construct ground state and excited state two

electron (hole) wavefunctions as linear combinations of Slater determinants exactly as already illustrated for the crystal field approximation; the one electron wavefunctions will be the e_g^a antibonding MO's given in (A61), while the t_{2g} functions will be the $3dt_{2g}$ functions of the Ni^{++} ion. The ground state 2 electron wavefunction will be

$$\Gamma_5^{1,2,3}({}^3A_{2g},(e_g^a)^2)= \begin{array}{l} |e_g^a(x^2-y^2)e_g^a(z^2)|\alpha\alpha \\ |e_g^a(x^2-y^2)e_g^a(z^2)|\frac{(\alpha\beta+\beta\alpha)}{\sqrt{2}} \\ |e_g^a(x^2-y^2)e_g^a(z^2)|\beta\beta \end{array} \quad \text{(A63)}$$

and the excited state $\Gamma_5^{1,2,3}({}^3t_{2g},t_{2g}e_g^2)$ is

$$\begin{aligned} \Gamma_5^1({}^3T_{2g},t_{2g},e_g^a) = \frac{1}{4\sqrt{2}}\{ & (|d_{xz}e_g^a(z^2)|+\sqrt{3}|d_{xz}e_g^a(x^2-y^2)| \\ & -i|d_{yz}e_g^a(z^2)| \\ & +i\sqrt{3}|d_{yz}e_g^a(x^2-y^2)|)(\alpha\beta+\beta\alpha) \\ & +4i|d_{xy}e_g^a(z^2)|\alpha\alpha\} \end{aligned}$$

$$\Gamma_5^2({}^3T_{2g}, t_{2g}e_g^a) = \frac{1}{4}\{(|d_{xz}e_g^a(z^2)|+\sqrt{3}|d_{xz}e_g^a(x^2-y^2)|)(\beta\beta-\alpha\alpha)$$

$$-i(|d_{yz}e_g^a(z^2)|$$

$$-\sqrt{3}|d_{yz}e_g^a(x^2-y^2)|)(\beta\beta+\alpha\alpha)\}$$

$$\Gamma_5^3({}^3T_{2g}, t_{2g}e_g^2) = -\frac{1}{4\sqrt{2}}\{(|d_{xz}e_g^a(z^2)|+\sqrt{2}|d_{xz}e_g^a(x^2-y^2)|$$

$$+i|d_{yz}e_g^a(z^2)|$$

$$-i\sqrt{3}|d_{yz}e_g^a(x^2-y^2)|)(\alpha\beta+\beta\alpha)$$

$$+4i|d_{xy}e_g^a(z^2)|\beta\beta\} \qquad \text{(A64)}$$

The other excited state wavefunctions can also be constructed in this manner.

The matrix elements of the spin orbit coupling Hamiltonian $\sum_i \xi_d \hat{\ell}_i \cdot \hat{s}_i$ between wavefunctions transforming identically under group O_h are then calculated and the first order corrections to the ground state wavefunctions are obtained.

Only the admixture of the $\Gamma_5^n(^3T_{2g}, t_{2g}e_g^a)$ state is calculated since the admixture of the $\Gamma_5^n(^1T_{2g}, t_{2g}e_g^a)$ will not give a contribution to the g factor.

The expression for the spin-orbit coupling Hamiltonian for a complex in the molecular orbital theory should be (Misetich and Buch, 1964).

$$H_{so} = \sum_i [\xi_d(r_i)\hat{\ell}_i \cdot \hat{s}_i + \sum_L \xi_L(r_{iL})\hat{\ell}_{iL} \cdot \hat{s}_{iL}] \qquad \text{(A65)}$$

where $\xi_{d,L}(r_i) = \frac{\hbar^2}{2m^2c^2} \frac{1}{r} \frac{\partial U_{d,L}(r_i)}{\partial r}$, where $U_{d,L}(r_i)$ is the potential in which the electrons move. That is, there should be a contribution to the spin orbit coupling from the unpaired electrons on the ligand ion. However, since $\xi \propto \frac{Z}{r^3}$ the approximation that $\xi_d(r_i)\hat{\ell}_i \cdot \hat{s}_i$ acts only on electrons in the d part of the LCAO (ignoring electrons in the overlap region and on the ligands) is very good; in addition, Misetich and Buch (1964) find that in the case of the NiF_6^{-4} complex, the part $\sum_L \xi_L(r_{iL})\hat{\ell}_{iL} \cdot \hat{s}_{iL}$ of H_{so} contributes only 1.7% of the total, and this part will be neglected in the present discussion. This will leave only the part

$$H'_{so} = \sum_i \xi_d(r_i)\hat{\ell}_i \cdot \hat{s}_i \qquad \text{(A66)}$$

which is taken to operate on the d function part of the MO's only. The matrix elements of H'_{so} between $\Gamma_5^n(^3A_{2g}, (e_g^a)^2)$

and $\Gamma_5^n(^3T_{2g}, t_{2g}e_g^a)$ are then given by

$$\langle\Gamma_5^n[^3A_{2g}, (e_g^a)^2]\,|H'_{so}|\,\Gamma_5^n[(^3T_{2g}, t_{2g}e_g^a]\rangle = -2\sqrt{2}\,N_\sigma\lambda \qquad (A67)$$

and the corrected ground state wavefunctions are

$$\Gamma_5^n = \Gamma_5^n[^3A_{2g}, (e_g^a)^2] - \frac{2\sqrt{2}\,N_\sigma\lambda}{|10Dq|}\,\Gamma_5^n(^3T_{2g}, t_{2g}e_g^a) \qquad (A68)$$

The matrix elements of the Zeeman Hamiltonian (see Equation A5 are now calculated with the field taken in the z-direction. The matrix elements are

$$\langle\Gamma_5^1|\mu_B H_z(L_z+2S_z)|\Gamma_5^1\rangle = \mu_B H_z(2-\frac{8N_\sigma k\lambda}{10Dq})$$

$$\langle\Gamma_5^2|\mu_B H_z(L_z+2S_z)|\Gamma_5^2\rangle = 0 \qquad (A69)$$

$$\Gamma_5^3|\mu_B H_z(L_z+2S_z)|\Gamma_5^3\rangle = -\mu_B H_z(2-\frac{8N_\sigma k\lambda}{10Dq})$$

where $k=\langle e_g^2(x^2-y^2)\,|\ell_z|\,d_{xy}\rangle/\langle d_{x^2-y^2}|\ell_z|\,d_{xy}\rangle = N_\sigma(1-2\alpha_\sigma S_\sigma - 2\alpha_s S_s)$ is known as the orbital reduction factor. The method for calculating the matrix elements in (A69) has been discussed by Owen and Thornley (1966) and Misetich and Buch (1964). If one assumes the ligand orbital admixtures in (A61) to be small, then k can be approximated as

$$k \simeq 1 - \frac{1}{2}N_\sigma(\alpha_\sigma^2+\alpha_s^2) \qquad (A70)$$

If one places one electron in each of the e_g^a molecular orbitals the fraction of electron in any ligand orbital will

be given by

$$f_L = \frac{1}{3} N_\sigma^2 (\alpha_\sigma^2 + \alpha_\varepsilon^2) \tag{A71}$$

and k becomes, if one takes $N_\sigma \simeq 1$,

$$k \simeq 1 - \frac{3}{2} f_L \tag{A72}$$

The g factor is now given by

$$g = \langle \Gamma_5^1 | L_z + 2S_z | \Gamma_5^1 \rangle - \langle \Gamma_5^2 | L_z + 2S_z | \Gamma_5^2 \rangle$$

$$= \langle \Gamma_5^2 | L_z + 2S_z | \Gamma_5^2 \rangle - \langle \Gamma_5^3 | L + 2S_z | \Gamma_5^3 \rangle \tag{A73}$$

and from (A69) we have

$$g = 2 - \frac{8 N_\sigma k \lambda_o}{10Dq} \tag{A74}$$

where λ_o is the free ion spin orbit coupling constant. The effective spin orbit coupling constant is

$$\lambda_{eff} = N_\sigma k \lambda_o \tag{A75}$$

this is the spin orbit coupling constant measured in the susceptibility measurements on $NiC_4O_4 \cdot 2H_2O$. $N_\sigma k$ can be estimated by taking the ratio λ_{eff}/λ_o.

Misetich and Buch (1964) have treated the complex NiF_6^{-4} in the manner discussed above including π bonding and the ligand contribution to the spin orbit coupling Hamiltonian.

They use numerical values of the normalization constants, mixing coefficients and overlap integrals obtained from the theoretical calculations of Sugano and Schulman (1963); the value of 10Dq was that measured by Knox et al. (1963) in $KMgF_3:Ni^{++}$; the free ion spin orbit coupling parameters were adjusted to values corresponding to the charges on the ions in the complex. The calculated g value of 2.273 was in excellent agreement with the measured value of 2.28 (Hall et al. 1963).

APPENDIX B: FIELD CALCULATION FOR THE PRIMARY SAMPLE COIL

The primary sample coil is 25.4 cm long and consists of 4 layers of #30 Formvar covered Cu wire. The average diameter is 1.35 cm and the turns density is 121.0 turns/cm. The field at the center of a long solenoid is given by Bleaney and Bleaney, 1957)

$$H = n \frac{1}{[1+(\frac{a}{b})^2]^{1/2}} i_p = (150.6 \frac{Oe}{amp}) i_p \qquad (A76)$$

where n is the turns density, a and b are the radius and half length of the coil. The current measured on the bridge is the r.m.s. maximum current. Therefore, to obtain the maximum current one must multiply by 1.414, and the maximum field for a measured current i_p is

$$H_{max} = (212.9 \frac{Oe}{amp}) i_p .$$

The maximum and minimum fields used in this work were 31.9 and 6.4 Oe at currents of 150 and 30 ma respectively.